

POLITECNICO DI TORINO

Collegio di Ingegneria Chimica e dei Materiali

Master of Science Course

in Materials Engineering

**Doped reduced graphene oxide as catalyst
for the reduction reaction of oxygen and
carbon dioxide**



Tutors

prof. Giancarlo Cicero

dr. Nadia Garino

dr. Adriano Sacco

Candidate

Luciano Fabrizio

Dicembre 2019

Index

List of abbreviation and symbols	III
Riassunto in italiano	V
Abstract	XXVII
1. Introduction	1
2. Carbocatalysis	3
2.1 Graphene	3
2.1.1 Synthesis	5
2.2 Graphene Oxide (GO)	6
2.2.1 Synthesis	6
2.2.2 Structure	7
2.2.3 Properties	10
2.3 Reduced Graphene Oxide (rGO)	10
2.3.1 Chemical reduction	12
2.3.2 Thermal reduction	13
2.3.3 Microwave reduction	14
2.3.4 Electrochemical reduction	15
2.3.5 Reduction mechanism	15
3. Oxygen Reduction Reaction (ORR) and applications	19
3.1 Oxygen Reduction Reaction (ORR)	20
3.2 Catalysts	21
4. CO ₂ Reduction Reaction (CO ₂ RR)	27
4.1 Catalysts	30
4.2 Other parameters	32
5. Materials and methods	33
5.1 Samples preparation	33
5.2 Physical, morphological and chemical characterization	35
5.3 ORR characterization	35
5.3.1 Electrode preparation	35
5.3.2 Electrochemical measurements	37
5.4 CO ₂ RR characterization	40

5.4.1 Electrode preparation	41
5.4.2 Cell preparation	41
5.4.3 Chronoamperometry	42
5.4.4 Gas Chromatography	42
5.4.5 High Performance Liquid Chromatography	44
6. Results and discussion	45
6.1 Physical, morphological and chemical characterization	45
6.1.1 Field Emission Scanning Electron Microscopy (FESEM)	45
6.1.2 Transmission Electron Microscopy (TEM)	45
6.1.3 X-ray Photoelectron Spectroscopy (XPS)	49
6.2 Electrochemical properties for ORR	55
6.2.1 Cyclic voltammetry	55
6.2.2 Rotating disk electrode	56
6.2.3 Rotating ring disk electrode	59
6.2.4 Electrochemical impedance spectroscopy	63
6.2.5 Chronoamperometry	68
6.2.6 Discussion of results	69
6.3 CO ₂ RR characterization	70
6.3.1 NG2	70
6.3.2 NG2_S	72
6.3.3 NG2_SMn	73
6.3.4 NG2_SFe	75
6.3.5 NG2_Mn	76
6.3.6 NG2_Cu	77
6.3.7 NG2_Co	79
6.3.8 Comparison of results	82
7. Conclusion	85
Bibliography	87
Acknowledgements	93

List of abbreviation and symbols

AC	Alternating Current
CA	Chronoamperometry
CNTs	Carbon Nanotubes
C_{O_2}	Oxygen Concentration (mol/cm ³)
CO ₂ RR	CO ₂ Reduction Reaction
CV	Cyclic Voltammetry
CVD	Chemical Vapor Deposition
D_{O_2}	Diffusion coefficient of oxygen (cm ² /s)
E^0	Standard Electrode Potential (V)
E	Applied Potential (V)
E_{ads}	Adsorption Energy
EIS	Electrochemical impedance spectrometry
F	Faraday constant (A s /mol)
GCE	Glassy carbon electrode
GDL	Gas Diffusion Layer
GN	Graphene Nanosheet
GO	Graphene Oxide
h	Planck constant (kJ s)
HER	Hydrogen Evolution Reaction
I	Current (A)
I_D	Disk Current (A)
I_K	Kinetic Current (A)
I_R	Ring Current (A)
J	Specific Current (mA/cm ²)

LSV	Linear sweep voltammetry
N	Collection efficiency of RRDE
n	Number of transferred electrons
NHE	Normal Hydrogen Electrode
ORR	Oxygen Reduction Reaction
R	Universal gas constant
RDE	Rotating Disk Electrode
RRDE	Rotating Ring Disk Electrode
RHE	Reversible Hydrogen Electrode
rGO	reduced Graphene Oxide
R_{sh}	Sheet Resistance (Ωsq^{-1})
T	Temperature
t_1	Thickness (m)
T_c	Critical Dissociation Temperature ($^{\circ}C$)
XPS	X-ray Photoelectron Spectroscopy
σ	Bulk Conductivity ($S m^{-1}$)
δ'	Dielectric constant
δ''	Dielectric loss
μ	Kinetic viscosity (cm^2/s)
ν	Frequency (Hz)
ω	Rotating speed (rad/s)

Riassunto in italiano

I. Introduzione

Negli ultimi decenni la domanda di energia è cresciuta esponenzialmente e, probabilmente, continuerà a crescere anche nei prossimi anni, portando a due conseguenze: un eccessivo sfruttamento dei combustibili fossili e un massiccio rilascio di CO₂ nell'atmosfera. Per contrastare il problema sono state prese due direzioni: da una parte, è stata avviata la ricerca di nuovi fonti energetiche a basso impatto ambientale e, possibilmente, rinnovabili, dall'altra parte, si è cercato di sviluppare delle tecniche in grado di ridurre la CO₂ presente nell'atmosfera. Nel primo caso, sono state sviluppate delle celle a combustibile, che forniscono energia pulita e sostenibile, e delle batterie metallo-aria. Tuttavia, attualmente il loro sviluppo è limitato dalla reazione di riduzione dell'ossigeno (ORR) che avviene al catodo. Nel secondo caso, lo sviluppo di un'efficiente reazione di riduzione della CO₂ (CO₂RR) è alla base della diminuzione dei livelli dello stesso gas presenti nell'atmosfera. Per farlo, è necessario lo sviluppo di un materiale che non sia solo in grado di catturare e immagazzinare la molecola, ma anche di convertirla in un prodotto economicamente valido. Inoltre, i due approcci possono essere considerati complementari perché i prodotti ottenuti dalla CO₂RR possono essere usati come reagenti nelle celle a combustibile. Il grosso limite, comune ad entrambe le reazioni, è che possono essere lente e poco efficienti, per esempio, a causa della presenza di reazioni secondarie. Risulta, quindi, essere indispensabile l'utilizzo di catalizzatori appropriati, tali da permettere l'utilizzo di queste tecnologie efficientemente.

Lo scopo principale della tesi è quello di produrre un catalizzatore efficace per le reazioni di riduzione dell'O₂ e della CO₂. A tale scopo, sono stati sintetizzati dei campioni di ossido di grafene ridotto (rGO) dopati in alcuni casi tramite il solo utilizzo di eteroatomi, in altri aggiungendo anche ioni metallici. A ciò è seguita una caratterizzazione fisica, morfologica e chimica, volta a capire se gli elementi dopanti sono stati incorporati nella matrice e quali strutture hanno, eventualmente, formato, e, poi, una caratterizzazione elettrochimica. Nel caso dell'ORR, le prove elettrochimiche hanno permesso di quantificare l'attività elettrochimica di ogni campione e il cammino di reazione seguito (a 4 o a 2 elettroni). Inoltre, è stata valutata la potenziale a cui la reazione di riduzione inizia, in quanto la sua minimizzazione permette di consumare minore energia. Nel caso della CO₂RR, sono stati testati solo i campioni che avevano mostrato prestazioni migliori nelle precedenti prove. Oltre a valutare l'attività elettrochimica, sono stati caratterizzati i prodotti gassosi e liquidi del processo di riduzione in modo da capire se l'azione del catalizzatore ha permesso la formazione di prodotti di valore.

II. Carbocatalizzatori

I catalizzatori sono delle molecole in grado di abbassare l'energia di attivazione di una specifica reazione senza essere consumati o prenderne parte. Possono essere classificati in omogenei o eterogenei, a seconda se siano nella stessa fase o in una fase diversa rispetto ai reagenti.

I catalizzatori, sia omogenei che eterogenei, più comuni ed efficienti sono i metalli di transizione (Ni, Cu, ecc.) e i metalli nobili (Pt, Pd, ecc.). Tuttavia, sono caratterizzati anche da forti limitazioni come il costo, la disponibilità e la tossicità.

Un'alternativa, che recentemente ha suscitato molto interesse, sono i catalizzatori a base di carbonio, i quali possono essere ottenuti dalle biomasse, avendo quindi un bassissimo impatto ambientale. Possono essere utilizzati come supporto per i catalizzatori metallici o come catalizzatori essi stessi, per via della loro elevata superficie specifica, stabilità termica e buone proprietà meccaniche. Nel primo caso, permettono di mantenere lo stesso livello di efficienza, ma utilizzando una quantità minore di particelle metalliche, mentre nel secondo caso, la frazione metallica viene eliminata completamente.

In particolare, il grafene e i suoi derivati, come l'ossido di grafene ridotto (rGO), permettono di abbassare l'energia di attivazione di molte reazioni di ossidazione e riduzione, grazie alla loro particolare struttura, che rende possibile la formazione di legami π , consentendo, quindi, di accettare temporaneamente elettroni. L'attività catalitica è, inoltre, promossa dall'elevato rapporto area-volume e l'alta stabilità chimica, termica, ottica ed elettrochimica, che assicura un maggior tempo di vita per i catalizzatori. Allo stesso tempo, il grafene è un materiale inerte e quindi necessita di essere attivato attraverso l'utilizzo di dopanti. La difficoltà, perciò, risiede proprio nel controllare i metodi di attivazione e nella produzione su larga scala.

Il grafene puro, ottenuto tramite chemical vapour deposition (CVD), solitamente non viene utilizzato perchè costoso e più inerte dei suoi derivati. L'rGO, invece, caratterizzato da una minor purezza, sembra essere il candidato ideale, in quanto i difetti possono comportarsi come centri attivi.

Il processo di sintesi dell'rGO prevede l'ottenimento dell'ossido di grafene (GO) e la sua successiva riduzione. Il GO è ottenuto principalmente attraverso un processo chimico. Si parte da scaglie di grafite, le quali subiscono un trattamento di ossidazione ed esfoliazione. Durante il processo di ossidazione, gruppi contenenti ossigeno vengono introdotti all'interno della struttura grafitica, abbassando le forze di interazione tra i vari strati e, quindi, agevolando la successiva esfoliazione, che è eseguita tramite trattamenti ultrasonici o termici. Nel corso degli anni sono stati sviluppati vari metodi, ma oggi quello più utilizzato è il metodo di Hummer, che viene condotto utilizzando NaNO_3 e KMnO_4 in acido solforico. Il successo di questo metodo risiede nell'elevata efficienza di ossidazione e nella facilità di rimozione di metalli pesanti e ammoniaca. Tuttavia, detriti di carbonio amorfo potrebbero bloccare i siti attivi, ma, dato che questi hanno carattere acido, possono essere agevolmente eliminati tramite trattamento con NaOH e successiva neutralizzazione con HCl .

Alternativo al processo chimico, è il processo elettrolitico, che è caratterizzato da un minore impatto ambientale, maggiore efficienza e minor costo. Prevede l'utilizzo di elettrodi di grafite immersi in una soluzione acquosa contenente acido nitrico. Applicando un potenziale, il GO è ottenuto per ossidazione anodica degli elettrodi. I limiti di questa tecnica sono dovuti al fatto che l'ossidazione non avviene in maniera omogenea, rendendo anche più difficile l'esfoliazione.

Un modello che descriva in maniera definitiva la struttura del GO non esiste ancora a causa dell'elevata complessità e variabilità da campione a campione. Nel corso degli anni si sono avvicinate varie ipotesi: dai primi modelli, che erano improntati sulla ricerca di una regolarità nel reticolo, fino agli ultimi modelli, che accettano l'idea di una struttura non stechiometrica e amorfa. Ciò che si può dire con certezza, è che la struttura può essere divisa in tre regioni: una

regione grafitica (~16% del volume totale), le cavità (~2%) e le regioni ad alto grado di ossidazione (~82%). I gruppi funzionali maggiormente presenti sono gruppi epossidici e idrossilici sul piano basale e gruppi carbonilici sui bordi, mentre le cavità si formano a causa dello sviluppo di CO e CO₂ durante il processo di sintesi.

Il GO è idrofilo, infatti l'acqua e altri solventi polari possono facilmente inserirsi tra i suoi strati ed espandere ulteriormente la struttura. Ciò è agevolato anche dal fatto che presenta un coefficiente di compressibilità negativo, aumentando il volume della cella quando viene applicata una pressione. Il processo di espansione è reversibile, per questo motivo si dice che la struttura "respira". La presenza di domini sp³ rende il materiale isolante. In ogni caso, le proprietà fisico-chimiche possono essere modificate, variando il livello di ossidazione.

La riduzione del GO permette di abbassare il livello di ossigeno e ottenere l'rGO. Tuttavia, la riduzione non avviene mai in maniera completa e un certo numero di gruppi funzionali contenenti ossigeno rimane, creando quei difetti tipici che lo rendono attivo. L'rGO è conduttivo e idrofobo. Infatti, i fogli di rGO sono dei precipitati aggregati tra di loro e di forma irregolare a causa delle interazioni aromatiche e idrofobe. Il processo di riduzione può avvenire attraverso un metodo chimico, termico o elettrochimico. Le proprietà e la morfologia della superficie che si ottiene varia in base al metodo utilizzato.

La riduzione chimica del GO avviene solitamente a temperatura ambiente o leggermente superiore, ma comunque inferiore alla temperatura che si raggiunge per la riduzione termica, il che si traduce in un vantaggio economico. Allo stesso tempo, l'utilizzo di agenti chimici pone il problema della tossicità e pericolosità degli stessi. Tra quelli più utilizzati, c'è l'idrazina monoidrata, che, rispetto ad altre sostanze, non è reattiva con l'acqua e, inoltre, lascia delle impurezze di eteroatomi (tra cui l'azoto), che possono essere sfruttate per l'eventuale drogaggio del materiale. Una valida alternativa è data dal boridruro di sodio (NaBH₄), che è più efficiente dell'idrazina nella riduzione delle specie C=O, ma meno nella riduzione di gruppi epossidici e acidi carbossilici. Può anche essere usato l'idrogeno, che permette di ottenere elevati rapporti C/O e, infine, l'acido solforico, che facilita il processo di disidratazione della superficie e, per questo, utilizzato come secondo stadio di riduzione nel caso in cui sia presente un'elevata quantità di gruppi alcolici.

La riduzione termica è il processo più utilizzato per via della sua semplicità. Infatti, consiste in un rapido aumento della temperatura che, a causa della presenza di gruppi contenenti ossigeno, porta alla produzione di CO e CO₂, espandendo la struttura e favorendo il distacco tra i vari strati. Tuttavia, con questa tecnica si ottengono fogli di grafene di piccola taglia e distorti, data la rimozione di alcuni atomi di carbonio ad opera dei gas che si formano. La presenza di difetti nel reticolo influenza le proprietà elettriche, risultando in una conducibilità inferiore rispetto a rGO prodotti con altre tecniche. In ogni caso, le proprietà finali dipendono da alcuni parametri come la temperatura di riscaldamento (aumentandola, aumenta la conducibilità) e l'atmosfera, che deve essere inerte, riducente o può anche essere utilizzato il vuoto.

La riduzione termica può essere condotta anche per mezzo delle microonde. Rispetto al metodo convenzionale, il loro uso permette di accorciare i tempi di processo, diminuire i costi e ottenere un riscaldamento uniforme su tutto il materiale, aumentando così l'efficienza di riduzione. Le microonde agiscono attraverso due meccanismi: polarizzazione dipolare e conduzione ionica.

Infatti, interagiscono con le cariche elettriche mobili come le molecole polari o gli ioni, che sono presenti nel mezzo liquido in cui il materiale è immerso. Molecole polari e ioni si orientano e si muovono collidendo tra di loro e creando attriti, che generano calore. Inoltre, mentre nella riduzione termica convenzionale, prima si riscaldano le pareti del reattore e poi queste trasferiscono il calore ai reagenti per convezione o conduzione, portando all'ottenimento di un gradiente di temperatura tra la zona più interna e più esterna, nella tecnica a microonde, viene riscaldato direttamente il materiale, senza l'intermediazione del reattore. Infine, l'energia associata alle microonde non è così elevata da causare reazioni chimiche, ma è sufficiente a provocare la rotazione delle molecole.

L'ultima alternativa è data dalla riduzione elettrochimica. Il meccanismo si basa semplicemente sullo scambio di elettroni tra il GO e gli elettrodi, non vengono usati agenti chimici e non si formano sottoprodotti. Tuttavia, la produzione di rGO è limitata dall'area dell'elettrodo e la riduzione avviene solo nella zona in cui l'elettrodo è in contatto con la soluzione tampone della cella elettrochimica.

Tutte le tecniche descritte per ridurre il GO hanno come obiettivo l'eliminazione dei gruppi funzionali e dei difetti strutturali in modo tale da restaurare la conducibilità. In particolare, l'eliminazione dei gruppi funzionali si concentra sul piano della struttura del materiale, piuttosto che sui bordi, in quanto lì avviene il trasporto di elettroni, che determina la conducibilità. Di conseguenza, le tecniche di riduzione mirano ad eliminare gruppi idrossili e epossidici, cioè i gruppi che più facilmente si trovano in quell'area. Il GO è caratterizzato da isole di atomi ibridizzati sp^2 ; durante la riduzione, tali isole si avvicinano fino a toccarsi tra loro, raggiungendo il limite di percolazione e restaurando, quindi, la conducibilità.

Per esempio, nel caso di riduzione termica si deve considerare l'energia di legame (specifica di ogni gruppo) risultante nella temperatura critica di dissociazione, la posizione e il grado di ricoprimento. Generalmente, la riduzione avviene abbastanza agevolmente nelle prime fasi, per poi diventare più difficile a causa dell'interazione tra gruppi epossidici e idrossilici vicini che formano composti stabili termicamente. Inoltre, la concentrazione di difetti strutturali dipende dal livello di ossigeno perché, durante la riduzione, vengono liberati gas che creano vacanze e costringono gli atomi di carbonio a riarrangiarsi, formando strutture disordinate. Eseguire il trattamento termico in presenza di H_2 aiuta a preservare l'uniformità della struttura.

III. Reazione di riduzione dell'ossigeno (ORR) e sue applicazioni

La ricerca di catalizzatori per ORR è principalmente focalizzata allo sviluppo di celle a combustibile e batterie metallo-aria.

Una cella a combustibile è un dispositivo in grado di convertire l'energia chimica di un combustibile in energia elettrica e calore. La reazione che avviene all'interno della cella è la reazione opposta a quella di elettrolisi, in particolare al catodo l'ossigeno è ridotto, mentre all'anodo l'idrogeno è ossidato. Le celle a combustibile sono caratterizzate da una buona efficienza elettrica (dal 40% al 60%), capacità di modulare la potenza in funzione della domanda di energia elettrica, possibilità di unire più celle in serie formando le cosiddette stacks e basso impatto ambientale. Tra i combustibili che possono essere usati: metano, metanolo, gas naturale e gas di sintesi.

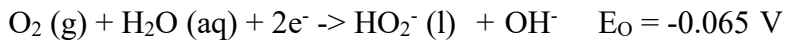
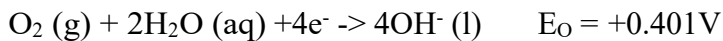
Le batterie metallo-aria rappresentano una tecnologia emergente, che può essere usata per i veicoli elettrici e che mira a soppiantare le tradizionali batterie al litio, costose e facilmente infiammabili. I materiali che costituiscono queste innovative batterie sono economici e sicuri. In particolare, per l'anodo il metallo più usato è lo zinco, che è economico, abbondante in natura, ha un potenziale di equilibrio basso, basso impatto ambientale, un potenziale di scarica piatto e lunga durata. L'altro elettrodo è costituito da carbonio poroso, il quale permette la riduzione dell'ossigeno.

Solitamente, la sovratensione è maggiore in quest'ultimo elettrodo, richiedendo quindi l'utilizzo di catalizzatori adatti per abbassarla.

Quando la ORR è condotta in soluzioni acquose, può seguire due strade: un percorso di riduzione a quattro elettroni, partendo dall'O₂ e ottenendo H₂O, o a due elettroni, in cui si ottiene H₂O₂. In ogni caso le semireazioni e i valori di potenziale, a cui queste avvengono, dipendono dal livello di pH e, quindi, dal mezzo in cui gli elettrodi sono immersi. Nel caso di mezzo acido:



Mentre, nel caso di mezzo alcalino:



dove E₀ rappresenta il potenziale standard dell'elettrodo. Nella maggior parte dei casi, il percorso a quattro elettroni è preferito perché più efficiente. Infatti, nel percorso a due elettroni, la formazione del perossido può essere pericolosa perché diventa altamente aggressivo quando la molecola si spezza, rilasciando radicali liberi.

La maggiore problematica legata all'ORR è la cinetica lenta, dovuta all'elevata energia di legame, che caratterizza la molecola d'ossigeno. Di conseguenza, l'utilizzo di un appropriato catalizzatore è fondamentale. Il catalizzatore ideale deve garantire:

- elevata attività catalitica
- conducibilità elettrica
- elevata stabilità chimica, elettrochimica e catalitica
- morfologia adatta, elevata area superficiale specifica, taglia ridotta delle particelle, elevata porosità e distribuzione uniforme delle particelle del catalizzatore sul supporto
- buona interazione tra particelle del catalizzatore e superficie del supporto.

Nella maggior parte dei casi, i catalizzatori candidati non presentano tutte queste proprietà, per questo motivo, per ogni applicazione e condizione, deve essere scelto quello che si adatta meglio al sistema.

Il Pt è il catalizzatore più usato, ma presenta forti limitazioni come il costo e l'elevata sovratensione. Per questo, sono state sviluppate delle alternative come l'utilizzo di altri metalli nobili (Au, Pd, Ag, Ru, Rh), metalli di transizione (Cu, Co, Fe, Ni, W, Mo), ossidi di metalli (IrO_2 , NiO , CeO_2 , ZrO_2 , TiO_2 , SnO_2) e, soprattutto, strutture carboniose (grafene, rGO, nanotubi), che possono fare da supporto alle particelle metalliche o essere essi stessi dei catalizzatori. Queste, inoltre, possono essere drogate con eteroatomi in modo da aumentare il numero di siti attivi o creare dei siti di ancoraggio per i metalli.

L'azoto, in particolare, è il dopante più utilizzato dato che ha dimensioni molto simili a quelle dell'atomo di carbonio ma presenta una configurazione elettronica diversa. La sua introduzione all'interno di una struttura carboniosa avviene tramite l'utilizzo di precursori, come l'urea. Infatti, la decomposizione dell'urea genera CO_2 , che rende la struttura porosa, e NH_3 , che è un agente riducente e dopante. Le strutture che l'azoto può formare all'interno della matrice sono diverse, tra queste le specie piridiniche e i gruppi amminici agiscono come siti di ancoraggio per le particelle metalliche e sono in grado di accettare elettroni, mentre le strutture grafitiche presentano la più alta attività elettrochimica. L'attività catalitica del grafene dopato con azoto può essere spiegata tramite un riarrangiamento delle cariche sulla superficie. Infatti, gli atomi di carbonio vicini agli atomi di azoto presentano una densità di carica positiva più alta, che permette di controbilanciare la forte affinità elettronica con l'azoto e migliorare le capacità di adsorbimento dell'ossigeno, dato che la reazione di riduzione avviene seguendo la via a 4 elettroni, solo se il legame tra i due atomi di ossigeno, che formano la relativa molecola, si rompe. Ne consegue che l'attività ORR del materiale dipende dalla microstruttura e, in particolare, dalla dimensione dei cluster di azoto e la presenza di imperfezioni nella struttura, come i difetti di Stone-Wales. La massima efficienza si raggiunge quando si formano cluster di dimensione ridotta (costituiti da 3 o 4 atomi di azoto) in combinazione con la presenza di difetti strutturali.

Un altro eteroatomo efficace per il drogaggio è lo zolfo, che presenta una struttura simile all'azoto, ma una diversa elettronegatività. Come l'azoto, all'interno del grafene, può formare varie specie: può adsorbirsi in superficie, sostituire un atomo di carbonio come singolo atomo o come ossido, o può connettere due strati, formando un anello. Il meccanismo, che permette la riduzione dell'ossigeno, è simile a quello precedente, ma in questo caso, se gli atomi di carbonio adiacenti allo zolfo promuovono la via a 4 elettroni, gli atomi di zolfo stessi promuovono la via a 2 elettroni. Ciò vuol dire che è in grado di attivare gli atomi di carbonio, ma riduce l'efficienza. Il problema può essere superato nel caso in cui la specie che si forma è data dall'ossido di zolfo, anziché dal singolo atomo, anche se tra tutte le strutture, che possono formarsi, l'adsorbimento del singolo atomo sulla superficie è quella energeticamente favorita. Per questo motivo, anche in questo caso la presenza di difetti di Stone-Wales è vitale, in quanto permette di abbassare l'energia di formazione dei cluster di dopante.

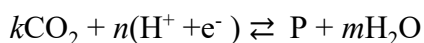
Nonostante i risultati promettenti riportati in letteratura sui catalizzatori costituiti da rGO dopato con azoto o zolfo, i valori di attività catalitica sono ancora lontani dai tradizionali catalizzatori di Pt. Allora il passo successivo è stato quello di incorporare all'interno della struttura eteroatomi diversi in modo da creare un effetto sinergico. Questo è quello che è successo con azoto e zolfo. Infatti, S e N vanno a sostituire un legame C-C, pur essendo la distanza di legame diversa e non formando un legame covalente. L'azoto rompe l'inerzia chimica del grafene, interrompendo la struttura aromatica, mentre lo zolfo attiva gli atomi di carbonio. Il risultato è

che l'attività catalitica è aumentata, anche se la concentrazione di zolfo deve essere controllata, in modo da non avere un effetto controproducente.

IV. Reazione di riduzione della CO₂ (CO₂RR)

La reazione di riduzione della CO₂ è alla base di un processo, noto anche come fotosintesi artificiale, che permette il riciclo di questo gas inquinante come in un circuito chiuso. Avviene all'interno di un reattore elettrochimico, dove all'anodo avviene l'ossidazione dell'acqua ad ossigeno molecolare e al catodo la riduzione della CO₂. Affinché questa avvenga, è necessario stabilire un potenziale tra gli elettrodi, fornendo energia elettrica. L'energia elettrica può essere ottenuta da fonti rinnovabili e il risultato del processo è la formazione di combustibili "puliti" come CO, HCOOH, CH₄, ecc., i quali possono essere sfruttati dalle attività industriali, che a loro volta genereranno nuova CO₂.

In generale, la reazione può essere vista come uno scambio multiplo di protoni e elettroni. Quando si verifica in un mezzo acquoso, è la seguente:



dove P rappresenta il prodotto che si è formato, n il numero di elettroni coinvolti nella reazione, mentre k e m sono dei coefficienti stechiometrici.

A questo punto, è lecito chiedersi qual è il prodotto più conveniente o che abbia una maggiore applicazione. L'aspetto economico si concentra principalmente sul costo dell'energia elettrica necessaria a produrre un determinato prodotto. Il risultato è che le specie più convenienti e, che allo stesso tempo garantiscono un buon mercato, sono CO, acido formico e formaldeide. Tuttavia, nel caso di prodotto liquido, si devono considerare costi aggiuntivi legati alla separazione. Allora si può concludere affermando che il CO risulta essere il prodotto migliore essendo gassoso anche a temperatura ambiente e facile da separare dall'elettrolita, senza contare la sua centralità nell'industria chimica come feedstock o componente dei gas di sintesi.

Nonostante le promettenti premesse, varie limitazioni sono legate a questo processo, come l'alto sovratensione, scarsa selettività del prodotto e bassa efficienza faradica. In particolare, il maggior problema è dovuto alla reazione di evoluzione d'idrogeno (HER), che avviene a potenziali simili e quindi compete con la riduzione della CO₂. Per superare tali limitazioni è necessaria una corretta scelta del catalizzatore e altri parametri, che saranno discussi in seguito.

Come nel caso della riduzione dell'ossigeno, il catalizzatore gioca un ruolo fondamentale. Esso deve essere attivo, altamente selettivo, economico e stabile. Fino ad oggi, il rame e le sue leghe sono stati gli unici catalizzatori in grado di produrre idrocarburi dalla riduzione della CO₂ in quantità significativa. Tuttavia, tali reazioni richiedono un'alta sovratensione, rappresentando una barriera di energia abbastanza elevata. Allora sono state proposte due soluzioni: diminuire le dimensioni delle particelle metalliche a nanoparticelle e distribuirle su un substrato, formando così un catalizzatore eterogeneo con un'area attiva maggiore.

Il supporto utilizzato è stato l'rGO. L'adsorbimento della CO₂ su questo materiale è favorito dal fatto che entrambi posseggono legami π in grado di interagire tra loro. Inoltre, anche in questo caso l'rGO può essere opportunamente drogato per aumentare il numero di siti dove le particelle metalliche possono ancorarsi. Oltre a tutte le considerazioni fatte nel capitolo precedente, un caso particolare è dato dalla struttura formata da un anello porfirinico integrato nella matrice

grafitica (in Figura I). I 4 atomi di azoto sono in grado di coordinare un atomo metallico di opportune dimensioni e far avvenire la conversione della CO_2 in CO con un'alta efficienza faradica e ad un basso sovratensione.

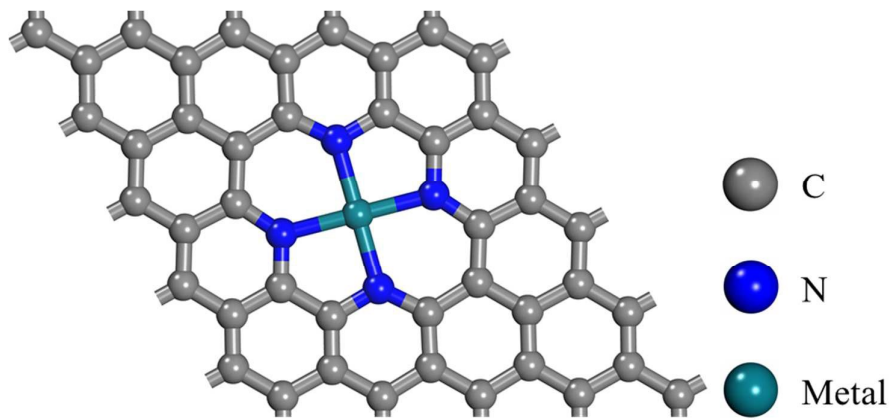


Figura I: Struttura di un anello porfirinico integrato nella struttura del grafene.

Per aumentare la selettività e l'efficienza faradica è possibile anche ottimizzare alcuni parametri come la scelta dell'elettrolita, il pH, la pressione parziale del gas e la temperatura. Solitamente si sceglie un'elettrolita acquoso, tra cui NaHCO_3 , KHCO_3 o KOH . Ultimamente sono anche stati proposti elettroliti a base di liquidi ionici, che si sono distinti per l'abilità di abbassare il sovratensione. Per quanto riguarda il pH, è meglio utilizzare soluzioni alcaline per massimizzare l'efficienza faradica, anche se si potrebbe formare carbonato e bicarbonato. Ciò può essere prevenuto utilizzando una soluzione che presenti anche proprietà tampone. Inoltre, si è notato che diminuendo la temperatura, la produzione di idrogeno diminuisce, mentre variando la pressione parziale di CO_2 la reazione può essere accelerata e la bassa solubilità del gas contrastata.

V. *Materiali e metodi*

La sintesi dei campioni è stata condotta nei laboratori del DISAT del Politecnico di Torino, mentre le prove elettrochimiche al "Center for Sustainable Future Technologies" dell'"Istituto Italiano di Tecnologia" di Torino.

La preparazione dei campioni è iniziata con la pesatura di tutti i prodotti chimici (polveri di GO e precursori dei dopanti), i quali sono stati versati all'interno di un reattore con acqua deionizzata e sonicati per circa 30 minuti in modo da creare uno slurry omogeneo. In Tabella I è presente la lista e la quantità di ogni prodotto chimico: si noti che come precursore per l'azoto è stato usata l'urea, per lo zolfo la tiourea, mentre per i metalli i rispettivi solfati. Tre dei campioni presenti in tabella (evidenziati con l'asterisco) erano già stati sintetizzati dal gruppo di ricerca IIT/Polito. Il reattore è stato, poi, riscaldato all'interno di un forno a microonde (Milestone FlexiWAVE) per ridurre il GO e incorporare gli elementi dopanti nella struttura. È stata impostata una rampa di temperatura, consistente in un riscaldamento per 2 minuti fino a 180°C , un mantenimento per 15 minuti a 180°C e infine raffreddamento in aria fino a temperatura ambiente. La potenza massima è stata impostata a 800 W e la pressione massima a

25 bar. Infine, i campioni sono stati messi in un freeze dryer (Lio 5P, 5 Pascal) per rimuovere l'acqua.

Tabella I: Tipo e quantità di precursori utilizzati per la preparazione dei campioni (* già sintetizzati).

Sample	GO (mg)	Urea (mg)	Thiourea (mg)	M-SO ₄ (mg)	H ₂ O (mg)
NG2	50	20	-	-	30
NG2_Ni	23	10	-	12	15
NG2_S	50	-	20	-	30
NG2_SNi	27	-	10	12	15
NG2_SMn	25	-	10	11	15
NG2_SFe	25	-	10	12	30
NG2_Mn*	50	20	-	25	30
NG2_Cu*	50	20	-	25	30
NG2_Co*	50	20	-	25	30

La caratterizzazione fisica, morfologica e chimica ha previsto l'utilizzo dell'XPS (PHI 500 Versa Probe System) per determinare gli elementi presenti sulla superficie del materiale e il tipo di legame tra questi, il FESEM (SUPRA 40, ZEISS) per ottenere informazioni morfologiche, anche a livello nanometrico, e il TEM (G2 F20 S-TWIN, FEI) per ottenere informazioni ancora più dettagliate sulla superficie dei campioni grazie all'elevata risoluzione.

La caratterizzazione relativa all'ORR ha previsto, per prima cosa, la preparazione dell'elettrodo. 2 mg di campione sono stati immersi in una fase liquida, costituita da 175 µl di resina di Nafion (5% in peso), 24 µl di acqua distillata e 100 µl di isopropanolo; l'intera miscela è stata sonicata per circa 30 minuti per creare una dispersione omogenea, simile ad un inchiostro. A ciò, è seguita la deposizione di 10 µl di inchiostro sulla zona in carbonio vetroso dell'elettrodo in GC/Pt in modo da avere una quantità di catalizzatore pari a 0,5 mg/cm² (Figura II) e, infine, l'elettrodo è stato lasciato ad asciugare per tutta la notte. Nel caso dei campioni contenenti sia lo zolfo che un metallo, la dispersione precedentemente descritta ha portato alla formazione di uno strato disomogeneo sulla superficie dell'elettrodo (Figura II), così la ricetta è stata cambiata, eliminando l'acqua e ricalcolando le proporzioni dei restanti prodotti chimici per avere lo stesso carico di catalizzatore.



Figura II: Corretta (a sinistra) ed errata (a destra) deposizione dell'inchiostro sull'elettrodo in GC/Pt.

Le misure elettrochimiche sono state condotte in un apparato RRDE (RRDE-3A) con un bipotenziostrato CHI760D e i relativi grafici elaborati con il software CH Instruments, Inc. È stata scelta una configurazione a 3 elettrodi, costituita dall'elettrodo precedentemente descritto come elettrodo di lavoro, un elettrodo in Ag/AgCl come elettrodo di riferimento e un filo di Pt come contro elettrodo. L'elettrolita era KOH 0,1 M saturato in N₂ o in O₂ in soluzione acquosa. Per avere un confronto diretto con la letteratura, tutti i potenziali sono stati convertiti e riferiti all'elettrodo reversibile d'idrogeno (RHE), secondo l'equazione di Nernst (eq. I):

$$E_{RHE} = E_{Ag/AgCl} + E_{Ag/AgCl}^0 + 0,059pH \quad (\text{eq. I})$$

dove E_{RHE} è il potenziale misurato secondo l'elettrodo di riferimento, $E_{Ag/AgCl}$ è il potenziale misurato rispetto l'elettrodo in Ag/AgCl, $E_{Ag/AgCl}^0$ è il potenziale standard dell'elettrodo in Ag/AgCl, che è uguale a 0,197 V a 25° C, 0,059 è il numero di Nernst e il pH è uguale a 13 per la soluzione 0,1 M di KOH.

Le prove elettrochimiche condotte sono state:

- voltammetria ciclica (CV) con una velocità di scansione di 10 mV/sec e in un range di potenziale compreso tra 0,16 e 1,16 V vs. RHE sia in soluzione saturata con azoto che con ossigeno
- elettrodo a disco rotante (RDE), utilizzando la voltammetria a scansione lineare (LSV) con una velocità di scansione di 5 mV/sec e a differenti velocità di rotazione dell'elettrodo rotante (400, 625, 900, 1225, 1600, 2025 e 2500 rpm) in soluzione saturata con ossigeno. A partire dai risultati di questa prova, è stato possibile elaborare il diagramma di Koutecky- Levich, tramite l'eq. II:

$$\frac{1}{I} = \frac{1}{I_K} + \frac{1}{\beta\omega^{1/2}} \quad (\text{eq. II})$$

dove I (A) è la corrente risultante, I_K (A) è la corrente cinetica della reazione elettrochimica, ω è la velocità di rotazione (rad/s) e β è un parametro che contiene il numero di elettroni (n), eq. III:

$$\beta = 0.62nFC_{O_2}D_{O_2}^{2/3}\mu^{-1/6} \quad (\text{eq. III})$$

dove F è la costante di Faraday, C_{O_2} è la concentrazione di ossigeno (mol/cm³), D_{O_2} è il coefficiente di diffusione dell'ossigeno (cm²/s) e μ è la viscosità cinematica (cm²/s).

- elettrodo ad anello-disco rotante (RRDE), utilizzando la LSV con una velocità di scansione di 5 mV/sec, un range di potenziale per il disco compreso tra 0,16 e 1,16 V vs. RHE, una velocità di rotazione dell'elettrodo di lavoro di 2500 rpm e un potenziale per l'anello di 1,16 V vs. RHE in soluzione saturata con ossigeno. Conoscendo i valori di corrente del disco (I_D) e di corrente dell'anello (I_R), è stato possibile calcolare il numero di elettroni (n) e la percentuale di perossido tramite l'eq. IV e l'eq. V, rispettivamente:

$$n = \frac{4I_D}{I_D + \frac{I_R}{N}} \quad (\text{eq. IV})$$

$$\% H_2O_2 = 200 \frac{I_R/N}{I_D + \frac{I_R}{N}} \quad (\text{eq. V})$$

dove N è l'efficienza di RRDE

- spettroscopia d'impedenza elettrochimica (EIS) con un segnale a tensione alternata con un'ampiezza di 10 mV in un range di frequenze compreso tra 100 kHz e 10 mHz, una velocità di rotazione dell'elettrodo di lavoro di 2500 rpm e un potenziale del disco di 0,66 V vs. RHE in soluzione saturata in ossigeno. I risultati sono stati comparati con un circuito equivalente (Figura III), costituito da R_s (resistenza interna), R_t e C_t (resistenza e capacità relative al trasporto elettronico, rispettivamente) in parallelo e R_{ct} (resistenza relativa al trasferimento di elettroni) e C_{dl} (capacità relativa al doppio strato) in parallelo.

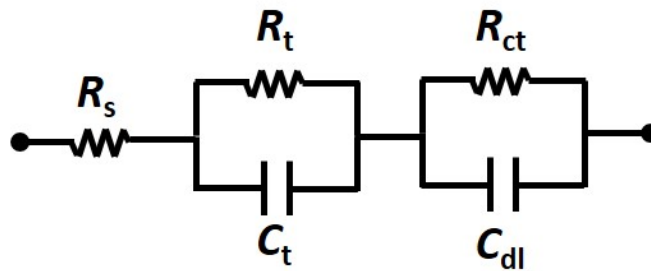


Figura III: circuito elettrico equivalente.

- cronoamperometria (CA) con un potenziale al disco di 0,66 V vs. RHE, una velocità di rotazione dell'elettrodo di lavoro di 2500 rpm in soluzione saturata in ossigeno per 15.000 secondi.

La caratterizzazione relativa alla CO₂RR è stata condotta solo sui campioni che avevano mostrato soddisfacenti risultati nelle precedenti prove (NG2, NG2_S, NG2_SMn e NG2_SF)

e sui campioni non testati precedentemente (NG2_Mn, NG2_Cu e NG2_Co). Anche in questo caso per avere un rapido confronto con la letteratura, tutti i potenziali, misurati con l'elettrodo di riferimento, sono stati convertiti ad RHE, usando l'equazione di Nernst (eq. I). A differenza dell'ORR, l'elettrolita usato è stato il KHCO_3 e quindi il valore di pH relativo alla soluzione 0,1 M saturata in ossigeno è pari a 6,8.

Similmente al caso precedente, è stata preparata una pasta, contenente le polveri di materiale (2 mg), resina di Nafion 5% in peso (180 μl) e isopropanolo (420 μl). La dispersione è stata sonicata per circa 30 minuti e poi l'inchiostro depositato sulla superficie di un carbon paper (GDL 28 BC, Sigracet) di dimensioni 1x1,5 cm^2 in modo da avere una quantità di catalizzatore pari a 0,66 mg/cm^2 (Figura IV).

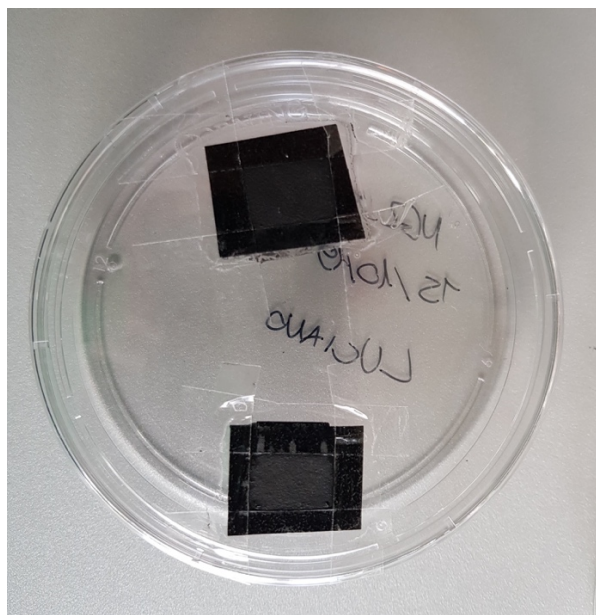


Figura IV: elettrodi con inchiostro deposto.

A questo punto, è stata montata la cella elettrochimica, costituita da due camere, quella relativa al catodo dove è presente l'elettrodo di lavoro e quella relativa all'anodo costituita da un foglio di Pt, separate da una membrana in grado di lasciar passare solo i protoni (Nafion membrane N117, Sigma-Aldrich). Entrambe le camere sono state riempite con una soluzione acquosa 0,1 M di KHCO_3 saturata in CO_2 . In particolare, 7 ml sono stati inseriti nel catodo e 10 ml all'anodo. A questo punto, è stata condotta una CA a -0,79 e a -0,89 V vs. RHE per un'ora.

La caratterizzazione dei gas prodotti durante la reazione di riduzione è avvenuta tramite un gas cromatografo (GC Fusion, Inficon) equipaggiato con dei microrilevatori di conducibilità termica (micro-TCD) e un filtro Genie per rimuovere l'umidità prima dell'ingresso nel GC. Durante la CA, la cella elettrochimica era collegata a due mass flow controller, che lasciavano passare un certo flusso di CO_2 , 15 ml/min per il catodo e 3 ml/min per l'anodo. I risultati sono stati comparati tra di loro tramite l'efficienza faradica, eq. VI:

$$FE_X = \frac{\dot{V}_{\text{CO}_2} C_x n F}{10^6 V_m I 60} \quad (\text{eq. VI})$$

dove FE_x è l'efficienza faradica per una determinata specie (H o CO in questo caso), \dot{V}_{CO_2} è il flusso di gas che attraversa la cella (ml/min), C_x è la concentrazione della specie formata in ppm, n è il numero di elettroni trasferiti (uguale a 2 per H e CO), F è la costante di Faraday (C/mol), V_m è il volume molare (22.4 ml/mmol) e I è la corrente risultante dalla CA.

La caratterizzazione dei prodotti liquidi è stata condotta tramite cromatografia liquida ad alta prestazione (HPLC), usando a Shimadzu Prominence HPLC. La colonna era una ThermoScientific Dionex e il software per elaborare i dati era Chromeleon Chromatography Data System. Il test è stato condotto per ogni campione con una lunghezza d'onda del rivelatore UV-VIS di 210 nm per 15 minuti. Anche in questo caso è stata calcolata l'efficienza faradica relativa all'acido formico (unico prodotto misurato), eq. VII:

$$FE_{HCOOH} = \frac{C_{HCOOH} \cdot V \cdot d_{HCOOH} \cdot n \cdot F}{PM_{HCOOH} \cdot I \cdot t} \quad (\text{eq. VII})$$

dove C_{HCOOH} è la concentrazione di acido formico (in ppm), V è il volume del catolita (in l), d_{HCOOH} è la densità dell'acido formico (1,22 g/ml), n il numero di elettroni (anche in questo caso uguale a 2), PM_{HCOOH} è la massa molare dell'acido formico (46,03 g/mol).

VI. Risultati e discussioni

Il FESEM non ha permesso di indagare accuratamente l'effetto dei dopanti su rGO, ma ha permesso di capire che il processo di riduzione condotto tramite microonde è stato efficace, in quanto il materiale non ha riportato danni. In Figura V la micrografia di NG2.

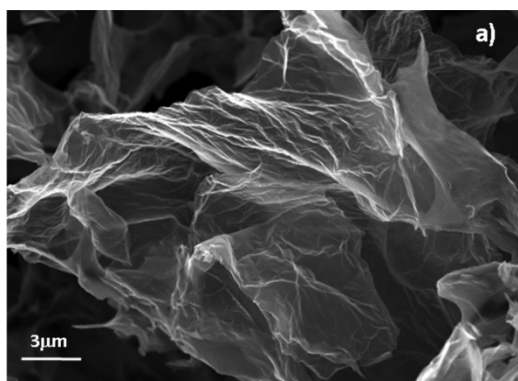


Figura V: Micrografia FESEM di NG2.

I campioni osservati al TEM appaiono con una struttura uniforme senza nanostrutture evidenti, segno del fatto che i dopanti sono effettivamente entrati in struttura, in Figura VI a-b sono riportate le immagini TEM di NG2_S a titolo di esempio. Unica eccezione NG2_SFe, per il quale i fogli di grafene sono decorati da nanocristalli (Figura VI c-d), identificati come ematite (α -Fe₂O₃) dalla Trasformata di Fourier veloce (FFT). Gli spettri EDX (Figura VI e) hanno confermato la presenza di tutti gli elementi dopanti più C, Cu, Fe e Co relativi a contaminazione dello strumento.

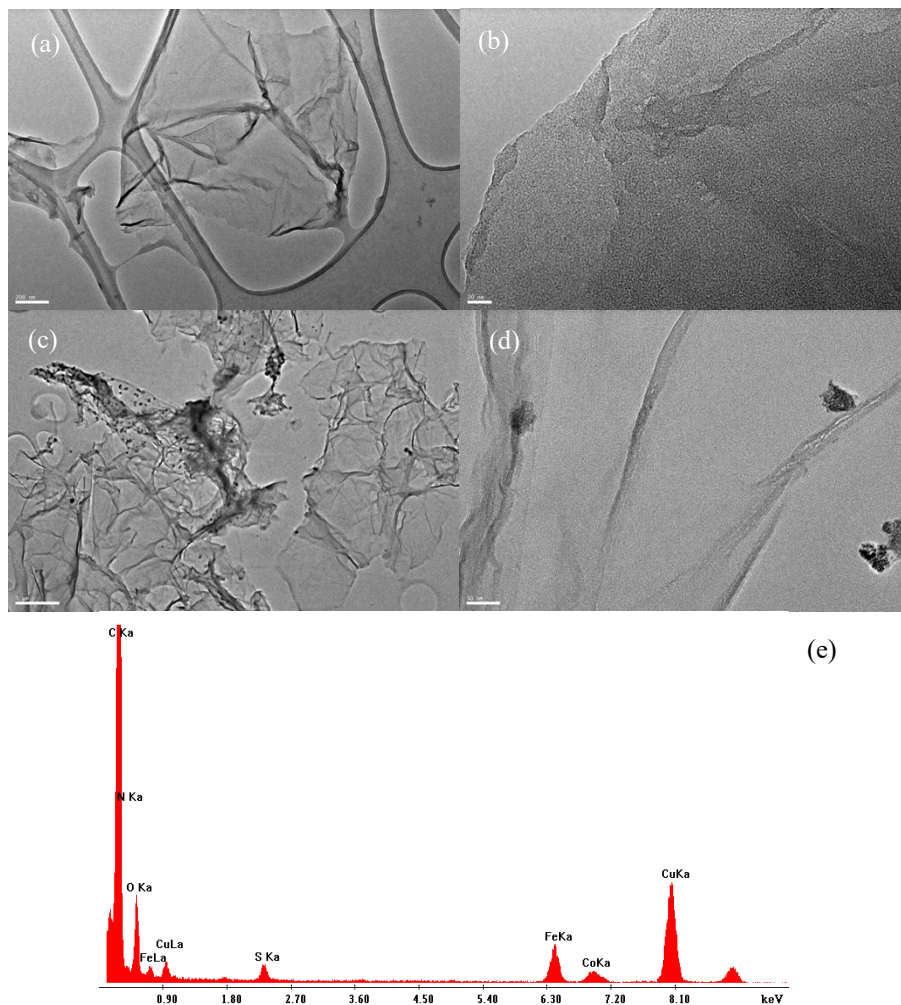


Figura VI: Immagine TEM di NG2_S (a-scala: 200 nm, b-scala: 20 nm) e di NG2_SFe (c-scala: 1 μm, d-scala: 50 nm) e spettro EDX di NG2_SFe (e).

L'XPS ha confermato i risultati del TEM, infatti come si può vedere dalla Figura VII, tutti gli elementi dopanti sono presenti. Unica eccezione è NG2_Ni, dove è stata registrata una contaminazione di zolfo. Inoltre, è stato calcolato il rapporto C/O, che è risultato essere circa o poco superiore a 4 per tutti i campioni, confermando ancora una volta l'efficacia del processo di riduzione. I risultati di NG2 non sono stati riportati, perché possono essere trovati in [72].

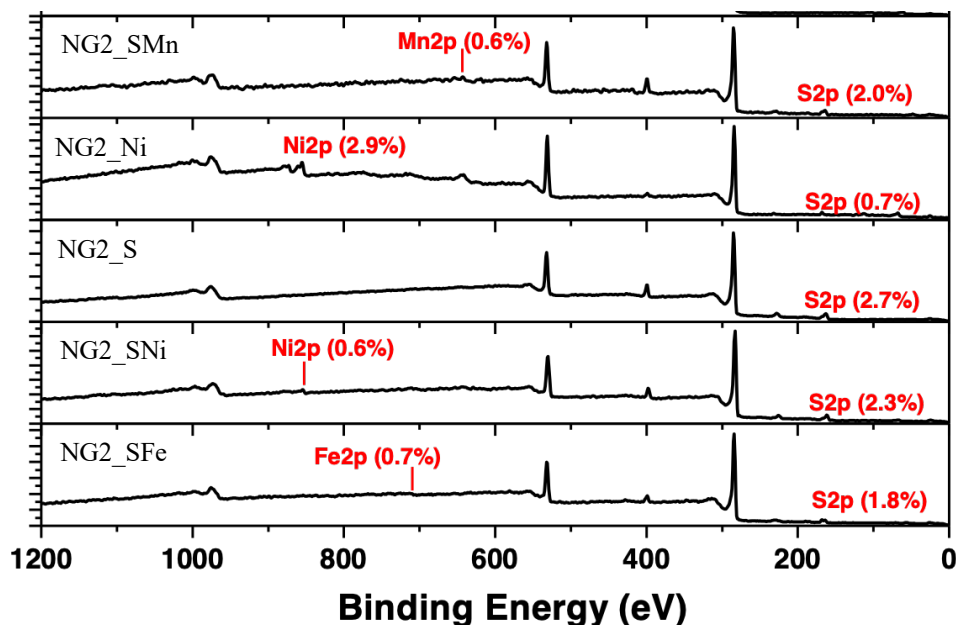


Figura VII: Spettri XPS di tutti i campioni.

Per capire lo stato di ossidazione e quali specie ogni elemento ha formato all'interno della matrice devono essere analizzati gli spettri di deconvoluzione. Tutti i campioni hanno mostrato per C1s lo stesso andamento (Figura VIIIa), infatti sono stati registrati i tipici chemical shift di C-(C, H), con la percentuale più alta, e poi di C-(O, N, S), C=O, O=C-O e O-C-O e della transizione $\pi - \pi^*$ (Figura VIIIb).

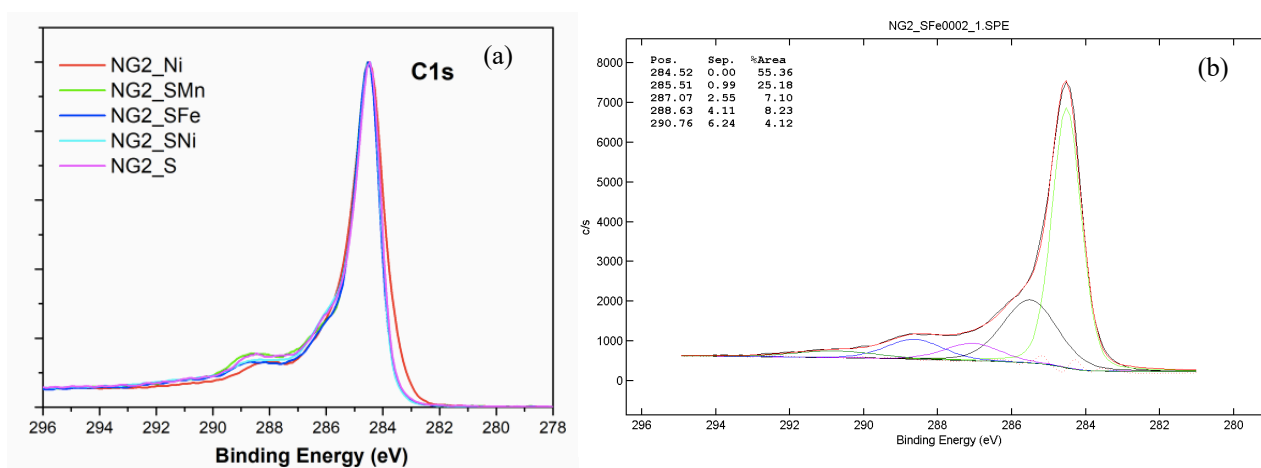


Figura VIII: Spettro di deconvoluzione di C1s per tutti i campioni (a) e spettro di deconvoluzione di C1s per NG2_SFe (b).

Lo spettro di deconvoluzione di N1s mostra per tutti i campioni due picchi, tipici dell'azoto pirrolico e dell'azoto grafatico. Inoltre, NG2_SNi presenta anche un terzo picco relativo all'azoto piridinico. Analizzando la percentuale di ogni specie (Tabella II), l'azoto pirrolico è quello più presente, in particolare in NG2_SMn. La bassa percentuale di azoto grafatico in questo campione potrebbe essere alla base di una sua limitata attività elettrochimica.

Gli spettri di deconvoluzione di S2p mostrano un numero variabile di picchi per i vari campioni. In particolare, NG2_S e NG2_SNi mostrano dei picchi che possono essere assegnati a solfuro,

R-SH e solfato, mentre NG2_SMn e NG2_SFe dei picchi che possono essere assegnati solo al solfuro e al solfato. Dato che solamente i solfati catalizzano la reazione a 4 elettroni per ORR, i campioni che presentano una concentrazione limitata di questa specie, probabilmente presenteranno un'efficienza minore (Tabella II).

Tabella II: Riassunto delle percentuali delle specie di azoto e zolfo presenti.

Campione	N pirrolico (%)	N grafítico (%)	N piridinico (%)	Solfuro (%)	R-SH (%)	Solfato (%)
NG2_Ni	69,95	30,05	-	-	-	-
NG2_S	88,08	11,92	-	33,3	46,18	19,92
NG2_SNi	66,00	16,67	17,34	36,3	45,77	17,90
NG2_SMn	96,97	3,03	-	63,39	-	36,61
NG2_SFe	77,38	22,62	-	50,58	-	49,42

Lo spettro di deconvoluzione del Ni2p per NG2_Ni (Figura IXa) mette in evidenza picchi e satelliti tipici del Ni²⁺ e quello relativo al Ni LMM (Figura IXb) può essere comparato allo spettro tipico di NiSO₄•6H₂O. Le stesse considerazioni possono essere fatte per NG2_SNi. Per NG2_SMn, sono mostrati gli spettri di deconvoluzione di Mn2p e Mn3s (Figura IXc-d), applicando il metodo dello stato di ossidazione medio, risulta che il Mn è presente con uno stato di ossidazione pari a 2. Infine, lo spettro di deconvoluzione di Fe2p per NG2_SFe (Figura IXe) mostra chiaramente un picco relativo alla presenza dell'ossido, che era già stato osservato dalle misure TEM.

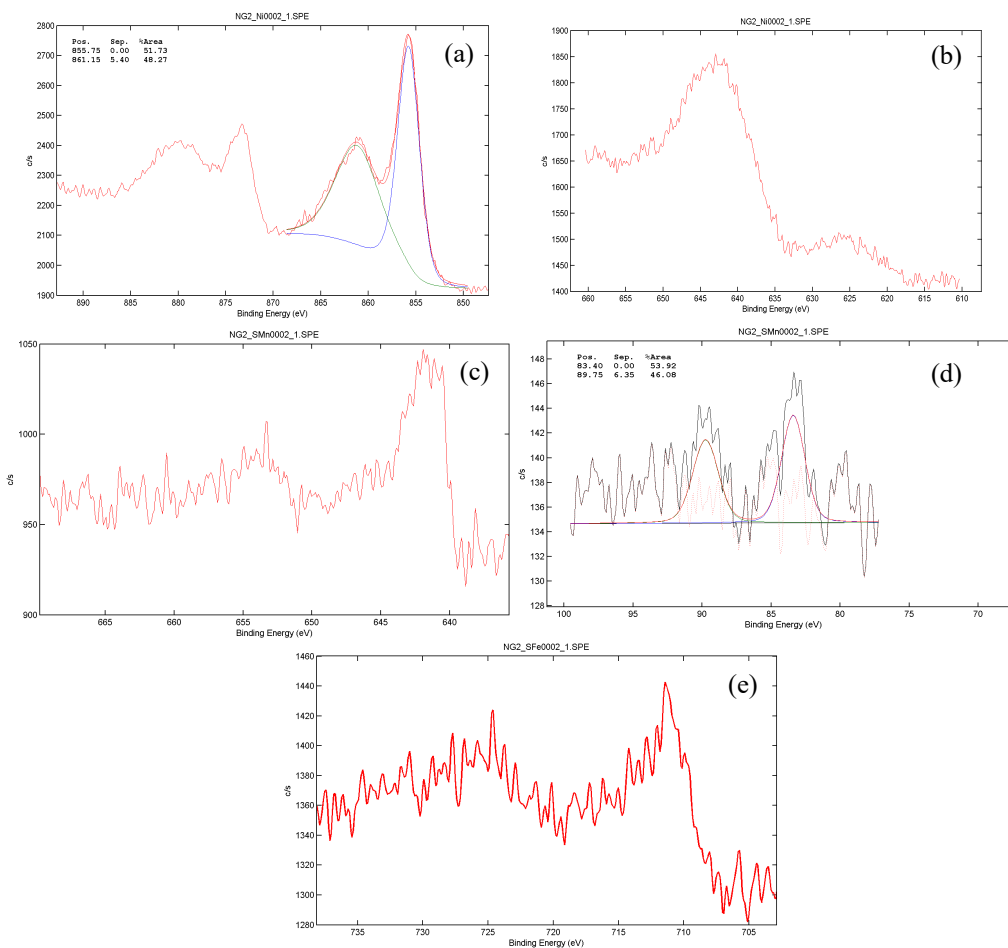


Figura IX: Spettri di deconvoluzione di Ni_{2p} (a) e Ni LMM (b) per NG2_Ni, Mn_{2p} (c) e Mn_{3s} (d) per NG2_SMn e Fe_{2p} (e) per NG2_SFe.

La caratterizzazione elettrochimica dei campioni relativa all'ORR è iniziata con le misure di voltammetria ciclica, che hanno permesso di scoprire il potenziale da cui parte il processo di riduzione e le proprietà capacitive di ognuno di loro (Figura V). Partendo da rGO dopato solo con azoto (NG2), l'aggiunta di altri elementi dopanti ha raramente portato a variazioni del potenziale relativo al picco di riduzione (nel peggiore dei casi ha anche richiesto una sovratensione maggiore), mentre la capacità è diminuita in tutti i casi. NG2_SFe è stato il campione che ha mostrato il comportamento più simile a NG2.

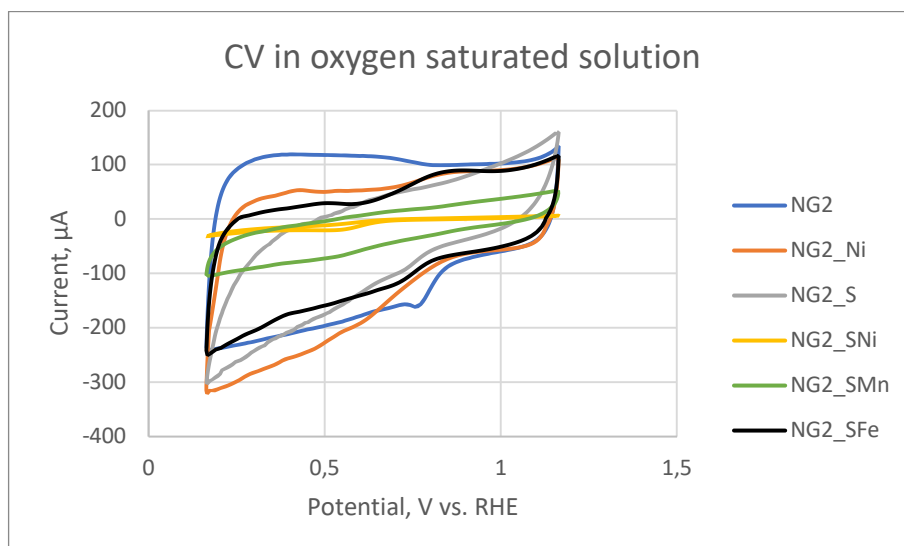


Figura V: Voltammetria ciclica in soluzione 0,1 M di KOH saturata in ossigeno.

L'analisi RDE ha permesso di ottenere i dati per costruire il grafico di Koutecky-Levich e ottenere il numero di elettroni trasferiti durante il processo di riduzione. Tuttavia, a causa di un errore relativo troppo elevato alla finestra di potenziale considerata, i valori sono risultati essere sottostimati.

L'analisi RRDE ha permesso di capire la frazione di corrente che passa attraverso il disco, che quindi viene effettivamente utilizzata per la riduzione dell'ossigeno seguendo il percorso a 4 elettroni, e la frazione che passa attraverso l'anello e viene dissipata per la reazione a 2 elettroni. Da queste, è stato poi possibile calcolare il numero di elettroni trasferiti e la percentuale di perossido prodotta. I dati ottenuti sono stati confrontati con un campione commerciale in Pt-C. Come evidenziato dalla Tabella II, il riferimento commerciale è il campione che globalmente presenta il comportamento migliore, nonostante ciò le correnti al disco dei campioni studiati sono confrontabili soprattutto ad alti potenziali. Unica eccezione è NG2_SMn, che presenta valori di corrente significativamente inferiori. La corrente all'anello, il numero di elettroni trasferiti del riferimento e la percentuale di perossido prodotto è confrontabile solo con NG2_S, NG2_SMn e, soprattutto, con NG2_SFe.

Tabella II: Corrente al disco e all'anello, numero di elettroni trasferiti e perossido prodotto misurati tramite RRDE.

Sample	I_D (μA)	I_R (μA)	n	H ₂ O ₂ (%)
Pt-C	-381	1.5	3.96	2.0
NG2	-250	7.5	3.72	13.9
NG2_Ni	-345	20.5	3.48	25.8
NG2_S	-266	2.1	3.92	3.8
NG2_SNi	-326	18.0	3.52	24.2
NG2_SMn	-114	1.9	3.84	8.0
NG2_SFe	-308	1.1	3.97	1.7

L'EIS è stato condotto come una sorta di approfondimento in modo da confermare i precedenti risultati. In particolare, facendo riferimento al circuito equivalente mostrato in Figura III, la resistenza al trasferimento di elettroni (R_t) è molto alta per NG2_SMn, mentre i valori più bassi sono stati registrati per NG2, NG2_S e NG2_SFe. Inoltre, moltiplicando R_{ct} e C_{dl} è stato possibile calcolare il tempo impiegato dalla carica per trasferirsi, mettendo in luce che l'aggiunta di elementi dopanti ha avuto un effetto benevolo in questo senso (Figura VI).

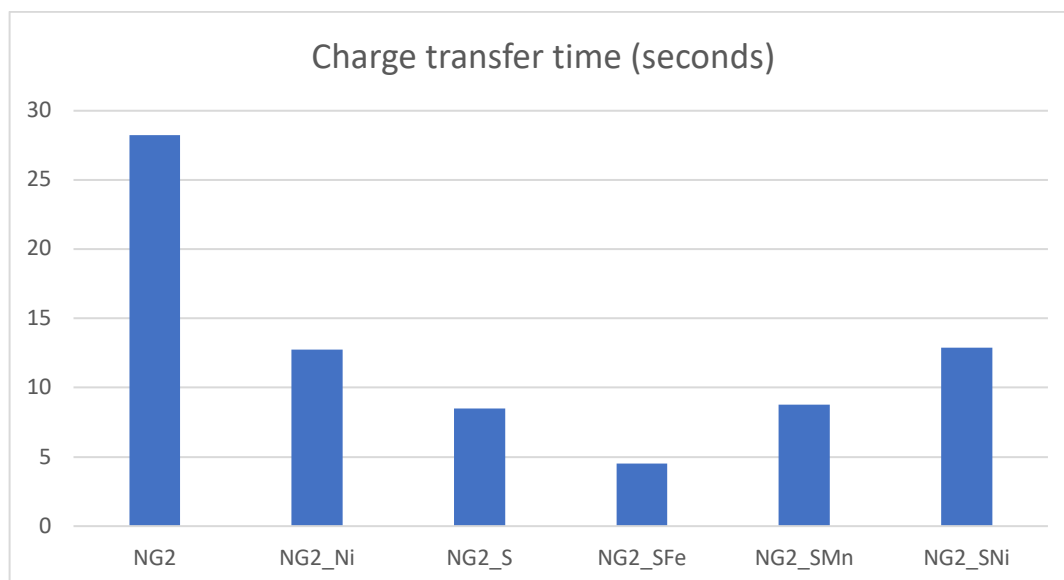


Figura VI: Tempo di trasferimento della carica.

La cronoamperometria è stata condotta solo su NG2_Ni, NG2_S e NG2_SFe a causa di problemi con il flusso di ossigeno. In tutti i casi, i campioni sono risultati essere stabili, mostrando delle perdite di corrente limitate (tra il 15 e il 30%) in un intervallo di 15.000 secondi.

In conclusione, partendo dalle buone potenzialità di NG2, si è cercato di migliorare le prestazioni del catalizzatore aggiungendo Ni, in un caso, e S, nell'altro. Il primo tentativo si è distinto per l'ottima attività elettrochimica, ma non per l'efficienza, mentre il secondo, pur avendo un'attività minore, ha mostrato un'efficienza paragonabile al campione commerciale in Pt-C. Sperando in un effetto sinergico, è stato aggiunto al campione contenente azoto e zolfo anche il nichel, ma il risultato si è rivelato controproducente. Allora, sono stati studiati altri metalli in sostituzione al Ni, cioè Mn e Fe. NG2_SMn ha rivelato un'efficienza interessante (poco inferiore a NG2_S), ma al contempo un'attività elettrochimica troppo bassa. NG2_SFe, invece, può essere considerato il campione migliore sotto tutti i punti di vista. Nel confronto con Pt-C, ha fatto vedere un'efficienza lievemente superiore e una buona attività elettrochimica, anche se più bassa rispetto al riferimento.

Le analisi condotte sui catalizzatori per testare il loro comportamento nella reazione di riduzione della CO₂ non hanno portato all'ottenimento di un campione, che mostrasse una prestazione notevole come era stato nel caso di NG2_SFe per l'ORR. In particolare, analizzando i valori di corrente ottenuti dalla cronoamperometria (Figura VII), si nota che solo pochi campioni (NG2_SFe, NG2_Cu e NG2_Co) presentano un'attività elettrochimica sufficientemente alta da

far presupporre una produzione di specie chimiche considerevole. In ogni caso per tutti i campioni, il livello di corrente misurata è rimasto stabile durante l'intervallo della prova (1 ora).

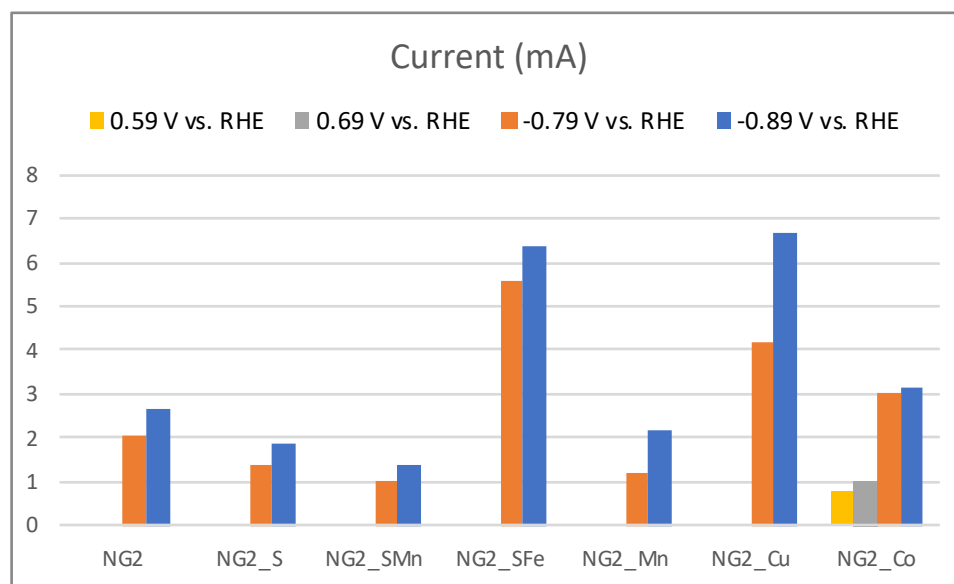


Figure VII: Corrente misurata durante la cronoamperometria per tutti i campioni a vari potenziali.

Dalla caratterizzazione dei prodotti della reazione di riduzione è emersa una tendenza comune a tutti i campioni nel privilegiare la reazione di evoluzione d'idrogeno rispetto la produzione di prodotti come CO e HCOOH (Tabella III). Considerando nel dettaglio i campioni che avevano mostrato una buona attività elettrochimica, NG2_SFe si è distinto per la produzione totale d'idrogeno, NG2_Cu ha registrato un'efficienza faradica per l'acido formico pari a 6,8 % a 0,89 V vs. RHE, che è la più alta tra tutti i campioni per questo prodotto, e infine NG2_Co è stato il campione più interessante perché ha mostrato un'efficienza faradica per il CO pari a 19,1% e 9,2% rispettivamente a 0,79 V vs RHE e 0.89 V vs. RHE. Ipotizzando che diminuendo ulteriormente il potenziale tale efficienza faradica potesse essere incrementata, è stata condotta la prova su questo campione anche a 0.69 V vs. RHE e 0,59 V vs. RHE, tuttavia nel primo caso è diminuita (14,1 %) e nel secondo caso non è stato registrato CO.

Tabella III: Riassunto dei risultati dei campioni migliori per CO₂RR.

Sample	Potential (V vs. RHE)	Current (mA)	H ₂ (ppm)	CO (ppm)	HCOOH (ppm)	FE _{H₂} (%)	FE _{CO} (%)	FE _{HCOOH} (%)
NG2_SFe	-0.79	5.59	2628	-	-	100	-	-
	-0.89	6.37	2913	-	-	100	-	-
NG2_Cu	-0.79	4.18	1825	-	7	98.8	-	1.2
	-0.89	6.67	2779	-	48	93.2	-	6.8
NG2_Co	-0.59	0.76	210	-	-	100	-	-
	-0.69	1.02	280	46	-	85.9	14.1	-
	-0.79	3.03	1030	243	-	80.9	19.1	-
	-0.89	3.17	1268	129	-	90.8	9.2	-

VII. Conclusioni

In questo lavoro di tesi, è stato studiato l'rGO dopato come possibile catalizzatore per la riduzione dell'ossigeno e dell'anidride carbonica in sostituzione ai tradizionali catalizzatori metallici (Pt, Cu, ecc.). Infatti, la sua particolare struttura contiene numerosi siti attivi sulla superficie, che permettono di ancorare le particelle metalliche o di promuovere delle reazioni.

La sintesi dei campioni è iniziata dalle polveri di GO, le quali sono state ridotte e dopate attraverso l'utilizzo di microonde, per via dell'elevata efficienza, il consumo limitato di energia e il breve tempo necessario, che sono tipici di questo metodo. Infatti, FESEM e XPS hanno confermato che il processo non ha comportato danni ai fogli di rGO e ha permesso di raggiungere un sufficiente rapporto C/O. Come dopanti sono stati utilizzati eteroatomi (N e S), introdotti tramite urea e tiourea, con, in alcuni casi, ioni metallici (come Ni, Mn e Fe), introdotti attraverso i rispettivi solfati. TEM e XPS hanno mostrato che i dopanti sono stati effettivamente incorporati nella struttura dei campioni perché non sono state viste strutture cristalline, ad eccezione di NG2_SFe, che ha presentato una struttura decorata da parecchi nanocristalli, che sono stati identificati come ematite (α -Fe₂O₃).

Le prove elettrochimiche per indagare il comportamento dei catalizzatori per ORR hanno rivelato che NG2_SFe è stato il campione migliore perché ha messo in evidenza una buona attività elettrochimica e un'alta efficienza, come confermato dalle analisi RRDE e dall'EIS, e una buona stabilità nel tempo, come riportato dalla CA. In realtà, anche NG2_SMn e NG2_S hanno mostrato alte efficienze, ma il primo si è contraddistinto per un'attività elettrochimica molto bassa e un'alta resistività e il secondo ha presentato un comportamento medio inferiore a NG2_SFe. La prestazione anomala di NG2_SMn può essere spiegata tramite XPS, infatti mostra una percentuale abbastanza bassa di azoto grafítico, che è responsabile dell'attività elettrochimica per ORR. L'XPS ha permesso anche di capire perché NG2_S e, soprattutto, NG2_SNi, nonostante la sua buona attività elettrochimica, hanno fallito: infatti, la percentuale di solfati, che è la sola specie dello zolfo che catalizza la reazione a 4 elettroni, è molto bassa per questi campioni. In ogni caso, per tutti i campioni l'aggiunta di dopanti non è stata sufficiente a diminuire la sovratensione rispetto a quella del materiale di partenza (NG2), come riportato dai grafici CV.

Le prove per indagare il comportamento dei catalizzatori per CO₂RR hanno rivelato che la reazione principale è HER per tutti i campioni. Infatti, nonostante la CA ha riportato alti livelli di attività elettrochimica per NG2_SFe, NG2_Cu e NG2_Co, il GC e l'HPLC hanno registrato una concentrazione molto scarsa di prodotti commercialmente validi. In particolare, il calcolo dell'efficienza faradica ha mostrato che solo NG2_Cu ha una percentuale non trascurabile di HCOOH, mentre NG2_Co ha un'interessante percentuale di CO.

In conclusione, NG2_SFe può rappresentare una valida alternativa al catalizzatore commerciale Pt-C per ORR perché ha mostrato un comportamento simile ma in più permetterebbe di superare le tipiche limitazioni che sono associate al riferimento. Tuttavia, lo stesso catalizzatore non può essere usato per CO₂RR a causa dell'assenza di formazione di prodotti validi commercialmente. Mentre NG2_Cu e NG2_Co possono essere soggetto di ulteriori studi, data la loro abilità di formare HCOOH e CO dalla riduzione della CO₂, rispettivamente.

Abstract

In the last years the demand of energy grew exponentially, leading to two consequences: a greater exploitation of the fossil fuels and a massive release of CO₂ in the atmosphere. In order to contrast these problems two routes are followed. The first is the research on new fuels with low environmental impact and, possibly, from renewable sources, that resulted in the development of fuel cells. Oxygen reduction reaction (ORR) is one of the fundamental as well as a limiting reaction for their diffusion. The second is the development of methods to reduce efficiently CO₂ (CO₂RR). In particular, ORR can follow two different pathways: the 4-electron reaction, that is direct and leads to the formation of water, and the 2-electron one, that pass through the formation of hydrogen peroxide. Whereas CO₂RR is a proton-electron exchange reaction, that can lead to the formation of gaseous and liquid products. Its limit is that it occurs at the same potentials of hydrogen evolution reaction (HER). So, in both cases the use of catalyst, that is able to select the useful reaction, is needed.

Until today, Pt and its alloys (for ORR) and Cu and its alloys (for CO₂RR) are used as catalysts. Despite of their good efficiency, they present some serious restrictions such as the cost, limited availability and high overpotential. However, it was proved that carbonaceous structures and, in particular, reduced graphene oxide (rGO) can be used as support for metal particles, lowering their concentration, or as catalysts themselves, completely removing them. To reach a good level of efficiency is necessary to dope properly the material in order to create some structure into the matrix able to coordinate metal particles or to increase the number of active sites.

Thus, the aim of this work is to find the doping agent, or mix of doping agents, for rGO that allows to reach the best efficiency for ORR and CO₂RR. For this scope, it resulted necessary to verify the interaction between dopants and matrix, electrochemical activity and efficiency of catalysts.

The starting point was GO powders, that were reduced and doped through microwave irradiation because of its efficiency, velocity and low cost. As dopant heteroatoms (N and S) and metal ions (Ni, Mn, Fe) were used. The list of samples and precursors was presented on the Table 1. For chemical, physical and morphological characterization FESEM, TEM and XPS were used. The ORR characterization consisted on the preparation of electrodes with the deposition of an ink, containing the sample powders, on their surfaces in order to carry out electrochemical tests like cyclic voltammetry, RDE and RRDE analysis, EIS and chronoamperometry. Whereas for CO₂RR characterization the inks were deposited on a carbon papers and this incorporated in an electrochemical cell. Chronoamperometry and gas chromatography were run simultaneously and after tests also high-performance liquid chromatography (HPLC), in order to characterize the reaction products.

Table 1: List of samples and precursors.

Sample	GO (mg)	Urea (mg)	Thiourea (mg)	M-SO ₄ (mg)	H ₂ O (mg)
NG2	50	20	-	-	30
NG2_Ni	23	10	-	12	15
NG2_S	50	-	20	-	30
NG2_SNi	27	-	10	12	15
NG2_SMn	25	-	10	11	15
NG2_SFe	25	-	10	12	30
NG2_Mn*	50	20	-	25	30
NG2_Cu*	50	20	-	25	30
NG2_Co*	50	20	-	25	30

Chemical, physical and morphological analysis showed that the samples did not undergo any damage during the reduction process and C/O ratio is sufficiently high, confirming the goodness of MW-assisted process. In addition, all dopant elements were incorporated into the matrix with an oxidation state equal to two for Ni and Mn, whereas Fe formed several hematite nanocrystals, that decorated rGO flakes. Also, N and S were incorporated into the structure, forming various species.

Electrochemical tests revealed that NG2_SFe was competitive with the commercial Pt-C for ORR because of its electrochemical activity, efficiency and stability. Also, NG2_S and NG2_SMn showed a good efficiency, but inferior to NG2_SFe and, in the case of NG2_SMn with a poor electrochemical activity. NG2_Ni and NG2_SNi, despite of their interesting electrochemical activities, reported poor efficiencies, even lower than base material, NG2. All samples were not able to lower the overpotential than NG2.

Only the most efficient catalysts were chosen to be investigated for CO₂RR. However, HER was the prominent reaction for all samples, this means that the formation of valuable products was limited. In this context, the best catalysts were NG2_Cu for the production of HCOOH and NG2_Co for CO.

1. Introduction

In the last decades the demand of energy grew exponentially [1], especially in the developing countries due to the strong demographic growth and the improvement of life condition. Likely this trend will be valid also in the future, leading to two main consequences: a greater exploitation of the fossil fuels, that are ending, and the serious issues of the global warming and the climate change due to the massive release of greenhouse gases like CO₂.

The fossil fuels (oil, coal and natural gas like methane) [2] represent the main source of greenhouse gases because, when they burn, they produce a large amount of CO₂ and other polluting substances, that impact strongly on the environment. Nevertheless, they are currently employed in a massive way because their cost is lower than renewable energy sources and they are able to give off more energy. In addition, they are easy to transport, encouraging the interest of multinationals and, also, political interests should not to be underestimated.

Hence, several researches are carried out in order to counteract these problems. The approaches mainly followed are two: researching on new fuels with low environmental impact, and possibly from renewable sources, and reducing CO₂ in the atmosphere, as nowadays it is at critical level. For the first approach, fuel cells [3], due to the fact that supply green power, and metal-air batteries are promising alternatives. In this type of system, the critical step, that limits their exploitation, is the oxygen reduction reaction (ORR), which occurs at the cathode. The second approach is based on CO₂ reduction reaction (CO₂RR) [4]. In this case, the challenge is to find materials able not only to capture and store the molecule but also convert it into added value chemicals, as it is a very stable. This approach can be considered complementary to first one because the products obtained by CO₂RR can be used in fuel cells. However, the efficiency of these reduction reactions can be very low because they are slow or secondary competing reactions are promoted. So, the use of catalysts is necessary in order to turn these laboratory technologies into marketable ones.

The aim of this work is to find a suitable catalyst for electrochemical reduction of O₂ and CO₂. As base material, it was used reduced graphene oxide (rGO) because it presents a chemical behavior similar to graphene but is cheaper. It was doped in order to improve the efficiency of reduction processes. Different doping strategies were used: in some cases, “free-metal” catalysts were produced, using nitrogen and/or sulfur, whereas in other cases, also a metal like Mn, Fe, Ni, etc. was incorporated.

The synthesis of samples was carried out by thermal reduction through the use of a microwave oven because it is a simple and fast method. In addition, it is not necessary the use of toxic solvents, but it is possible to run the process in water.

The physical, morphological and chemical characterization (like XPS, TEM and FESEM) of each sample demonstrate that how doping elements were bonded to matrix and help to understand which structures were formed into it.

Electrochemical measurements were performed in order to demonstrate the activity of the proposed catalysts towards the reduction reactions and if they are able to select the useful reaction. In particular, the tests for ORR were carried out also to find a material able to low the potential at which the desired reaction takes place. Considering the electroactivity of the samples tested for ORR, the best performing ones were chosen to be tested for CO₂RR. In addition, gaseous and liquid products of reduction process were analyzed in order to understand if the reaction leads to the formation of valuable substances (like CO and HCOOH). The Faradaic efficiency will be used as parameter to rank and compare the behavior of samples.

The presentation of this thesis work is divided in the following way: in the chapter 2 carbocatalysts are presented, focusing on rGO properties and synthesis; in the chapter 3 the mechanism, the application and the catalysts of ORR are treated; chapter 4 presents the mechanism, the application and the catalysts of CO₂RR; chapter 5 starts the experimental part with materials and methods used; in the chapter 6 results and discussion are shown; finally, in the chapter 7 the conclusions of this work are presented.

2. Carbocatalysis

Catalysts [5] are molecules able to lower the activation energy of a specific reaction without being modified during the reaction. They can be classified in homogeneous and heterogeneous catalysts. The former are in the same phase of the reactants, whereas the latter are in a different phase than reactants; they can be solid or liquid substances and often they are constituted by particles dispersed in a matrix, which acts as a support. Their properties are function of their surface properties, electronic or crystal structures, especially for solid catalysts. Catalysts are at the base of many industrial processes, in fact typical reactions that involve catalysts and reactants are oxidation-reduction reactions, acid-base reactions, formation of coordination complexes and formation of free radicals.

The most important materials used as both homogeneous and heterogeneous catalysts are transition metals like nickel and copper and noble metals like palladium, platinum, ruthenium and rhodium [6]. However, they have significant limitations due to their costs, availability and environmental impact.

Hence arises the need for innovative materials, which acts like transition and noble metals, but at the same time allowing for reduction of cost and toxicity. A solution that satisfies these requirements is the use of carbon-based catalysts [7], which can be derived from biomass, through daily recycle of agricultural waste, for instance. In the past, carbon materials have been regarded only as support to deposit transition metals, so main requirements were wide surface area, thermal stability and good mechanical properties. Later, for some application they have been also used as effective catalysts. In summary, it is possible to define carbocatalysis [8] as a branch of catalysis, which deals with various forms of carbon structure, eventually modified with heteroatoms, and it is different from organocatalysis, where organic molecules are the active center. Carbocatalysts are usually used as heterogeneous catalysis and the main advantage is that they tend to eliminate metal atoms.

2.1 Graphene

For carbocatalysis, graphene plays a central role because of its chemical-physical properties, that can be also seen into their derivatives like graphite, carbon nanotubes (CNTs) and, especially reduced graphene oxide (rGO) (Figure 2.1).

Graphene [3] is characterized by a honeycomb structure, where a carbon, belonging to the structure, is linked to three close ones, resulting in a hexagonal and aromatic geometry. In plane C-C bonds are covalent and are due to sp^2 hybridized orbitals. The $2p_z$ orbital is not involved in the hybridization, it is placed perpendicular to graphitic plane and it forms delocalized π bonds, which are responsible for high electrical in plane conductivity. The reason because these materials are suitable for catalysis is due to the presence of π bonds, that are able to give and to accept temporarily electrons, allowing for high electron density transfer reactions (like oxidation and reduction reactions) [8]. This results in a lowering of activation energy for those reactions.

When graphene or its derivatives are used as a support, the type of interaction between carbon material and the external atom is function of external atom species and site, which the interaction occurs in [9]. In the typical honeycomb structure of graphene, there are three different sites where external atom can be adsorbed (Figure 2.2):

- Hollow site (H), at the center of hexagon;
- Bridge site (B), at the center of bond between two carbon atoms;
- Top site (T), on the top of carbon atom.

The choice of adsorption site depends on filling level of d orbital. Usually H sites are preferred by metal atoms with almost empty d orbital like Sc, Ti, V, Fe, whereas B and T sites are preferred by transition metals with almost full d orbital like Pd, Pt and Cu. Moreover, atoms like Au, Ag and Cu interact only physically, while atoms like Co, Ni, Pt and Pa interact chemically, forming covalent bonds.

Catalytic activity [10, 11] is promoted by high surface-volume ratio and good stability, especially in chemical, electrochemical and thermal terms, because it can improve the lifetime of catalysts. Unfortunately, at the same time graphene is inert because the gap between the bands is almost zero, so it must be activated by means of dopants, mechanical strains or chemical alterations. The difficulty is to control activation methods and then large-scale production is limited.

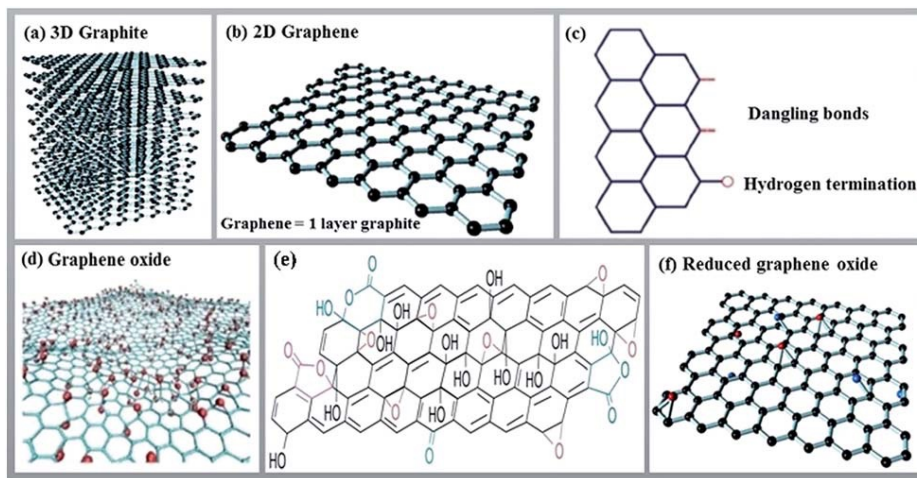


Figure 2.1: Representation of structure of a) graphite, b) graphene, c) graphene edge, d) and e) graphene oxide (GO), f) reduced graphene oxide (rGO) [12].

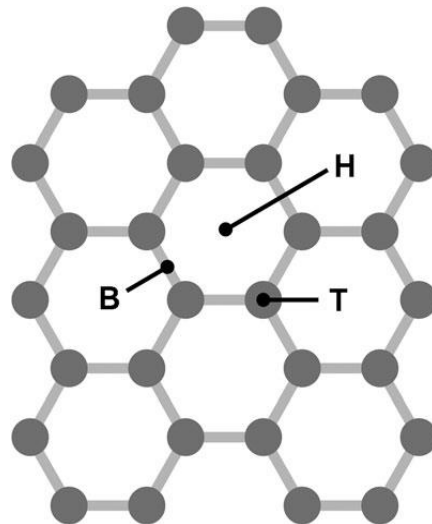


Figure 2.2: Representation of adsorption sites: H) hollow site, at the center of hexagon, B) bridge site, at the center of bond between two carbon atoms, T) top site, on the top of carbon atom.

2.1.1 Synthesis

Graphene was first obtained by mechanical exfoliation of graphite in 2004 [13]. From there, the interest on this material is increased exponentially and today it can be produced by several different ways, approaching through top down or bottom up techniques (Figure 2.3).

Top down approach consists on easy techniques as mechanical or chemical exfoliation (for instance using an adhesive tape), or more complex techniques as chemical synthesis. In particular, reduced graphene oxide will be deeply treated later because of its advantages as carbocatalysts.

Bottom up approach involves several techniques as pyrolysis, epitaxial growth and the most important method, that is chemical vapor deposition (CVD) [14, 15].

CVD is the most diffused method for graphene production because it allows for the formation of very pure material. It consists on decomposition of a precursor on a hot metallic surface. Copper and Nickel are metals that are usually used, they have a double effect because they act as templating agents as well as dehydrogenating centers. The precursors are usually hydrocarbons like methane, that at high temperature (about 1000°C) decompose, leaving a carbon layer on metal surface. Despite of high quality of CVD graphene, it is not characterized by several active centers, so it is not the best solution as carbocatalysts [8].

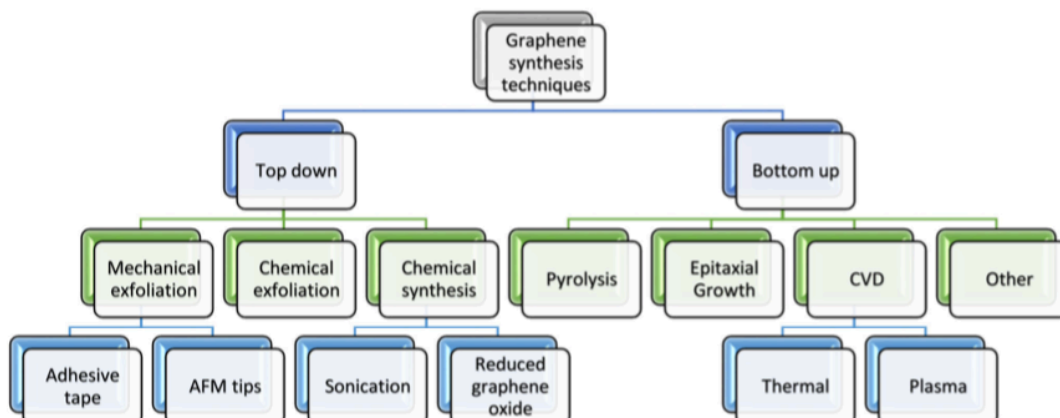


Figure 2.3: Scheme of graphene synthesis techniques [14].

2.2 Graphene Oxide (GO)

The discovery of graphene oxide (GO) occurs in 1859 by means of British chemist B. C. Brodie [16] and his study on structure and properties of graphite. Starting from flake graphite and using potassium chlorate and fuming nitric acid, he obtained a material characterized by an elevated concentration of oxygen and good water dispersion, but only in basic medium. He named it *Graphon*.

The success of GO is due to the fact it can be used as a cost-effective precursor of graphene-based material, such as reduced graphene oxide (rGO), but also it can be used as a catalyst itself because of its affordability and sustainability; at the same time reusability and stability limit its use [8, 17].

Today GO can be produced mainly by means of three different processes: the Staudenmaier process, the Hummers process and the anodic oxidation of graphite electrodes in nitric acid. At the same time, characterization of GO structure is complex and for this reason there are four main structural models: Hofman's model, Ruess's model, Sholtz and Bohem's model and Lerf and Klinowski's model [18].

2.2.1 Synthesis

All methods used to prepare GO start from graphite flakes. The mineral is purified in order to remove heteroatomic contaminations. Their removal causes the formation of several punctual defects in the graphite plane. This is positive because they are higher energy areas, therefore more reactive for the following steps of the process [17, 18].

GO synthesis consists of two main steps: oxidation and exfoliation. During oxidation, oxygen groups are introduced in graphite system and they also allow for the decrease of Van der Waals forces between the graphite sheets and for introduction of negative Coulombic charges. Then, exfoliation step can be easily carried out through ultrasonic or heat treatments. Exfoliation allows to turn graphite oxide in graphene oxide. The result of these process is hardly replicated because it is function as several parameters like the type of oxidant, the starting condition of graphite and external conditions. One of the most used oxidizing agents is nitric acid because it interacts strongly with aromatic carbon surfaces and leads to formation of various oxide-containing species as carboxyls, ketones and lactones [17, 18].

After the Brodie process, GO synthesis was improved by the Staudenmaier process [19], which involves concentrated sulfuric acid and, like Brodie process, potassium chlorate and fuming nitric acid. However, only with the Hummer process [20] it was possible to produce GO for industrial purpose.

Hummer's method uses NaNO_3 and KMnO_4 in concentrated sulfuric acid during oxidative exfoliation. Recently, it was proposed an improvement of this method that involves a higher use of potassium permanganate in acid medium of $\text{H}_2\text{SO}_4/\text{H}_3\text{PO}_4$. The advantages are due to elimination of potassium nitrate (because its presence results in formation of toxic gases), better control of temperature and better efficiency. In comparison with the other methods, Hummers' method involves shorter reaction times and a less risk of self-ignition or explosion. In addition, it shows several advantages, like larger oxidation fixation, higher yield of oxidation, better adsorption capability for the removal of heavy metals (as Pb and Cd) and ammonia. Finally, owing to a higher concentration of carboxylic groups, the oxygen moieties are easier to remove

through thermal annealing, that is important for following reduction process of GO, allowing for a better electrochemical performance [17]. At the same time, GO obtained by Hummers' method can contain some amorphous carbon debris that can block the active sites of GO that are mostly located on holes and defects. They have acid character and so, they can be removed by base treatment with NaOH, followed by neutralization with acid agents like HCl. Finally, ba-GO (basic-acid treated GO) is obtained with activated sites [8] (Figure 2.3).

The synthesis through electrolytic methods would represent a good alternative because it is environmentally friendly, highly efficient and relatively low cost. Graphite electrodes are used in a water solution with nitric acid and GO is formed by anodic oxidation of the electrodes. The products are characterized by low C/O ratio (about 2.2), but there are several drawbacks like the fact that the products are mainly oxidized at edges, they suffer from low oxidation and exfoliation degree, making difficult expansion and delamination of graphite. So, for these reasons chemical via is usually preferred [21].

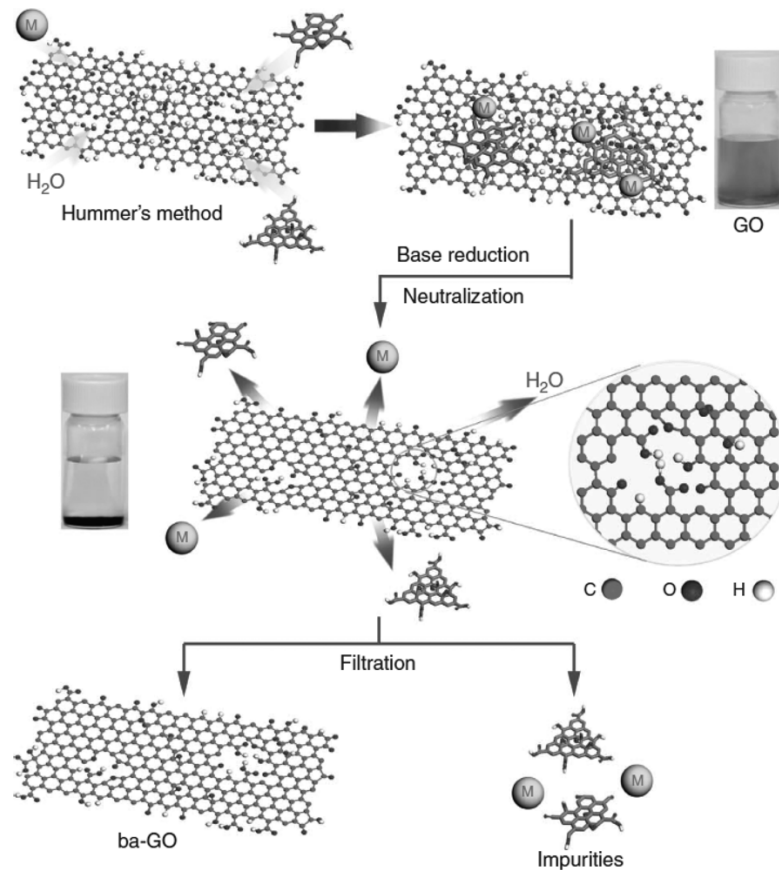


Figure 2.3: Scheme of activation process for GO obtained through Hummers' method [8].

2.2.2 Structure

A definitive model for the GO structure does not exist until today because of the complexity of the material as amorphous and non-stoichiometric character, sample-to-sample variability and the absence of suitable method for its characterization. Despite these impediments, many researchers tried to find a solution in the course of history.

The first structural model is due to Hofmann and Holst [22] in 1939. It resulted in a net of epoxy groups dispersed along graphite basal plane with C/O ratio of 2.

In 1945 Ruess [23] added to the Hofmann and Holst model hydroxyl group, considering the presence of hydrogen atoms. In addition, he changed basal plane structure from the sp^3 hybridized model of Hofmann and Holst to the sp^2 hybridized structure with an arm-chair conformation. Repeat units of this model were constituted by $\frac{1}{4}$ th of cyclohexanes with epoxides and hydroxyl groups in determined positions, resulting in a lattice structure. This come from Mermoux model [24] of poly-carbon monofluoride $(CF)_n$ because of some similitude with GO structure.

In 1969 Scholz-Boehm model [25] replaced epoxide and other groups with a regular quinoidal species in a corrugated backbone¹⁹.

Finally, the last of earlier models is due to Nakajima-Matsuo [26, 27], that considered GO structure similar to poli-dicarbon monofluoride $(C_2F)_n$ (Figure 2.4) [28].

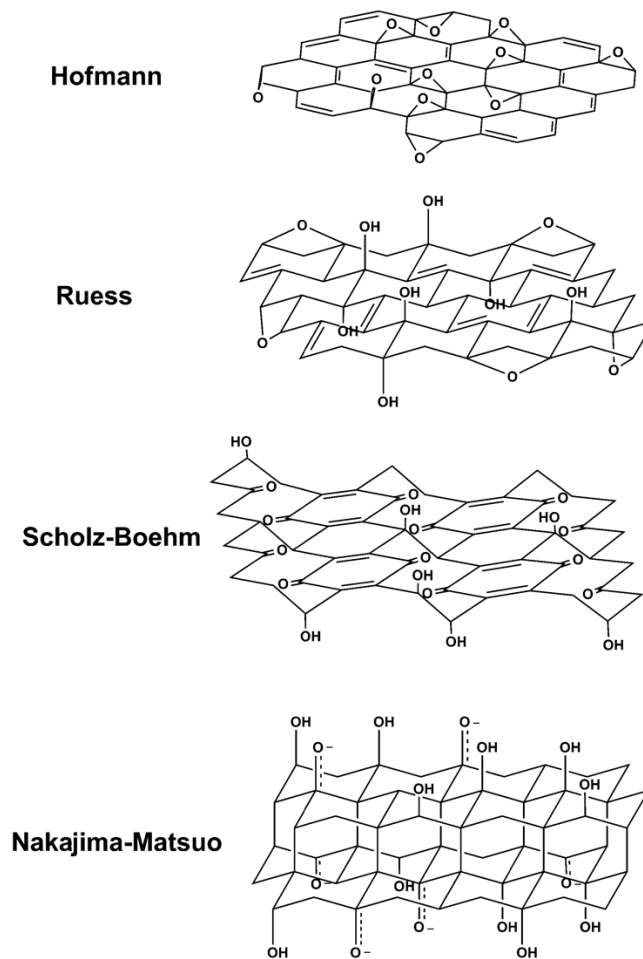


Figure 2.4: Scheme of Hofmann and Holst, Ruess, Scholtz-Boehm and Nakajima-Matsuo for GO structure [28].

All earlier models are characterized by the research of regular lattices with repeat units, whereas the most recent models start from the concept of non-stoichiometric and amorphous structure. Among these Lerf and Klinowski model [29, 30] is the most important. According to them, GO structure is constituted by 1-2 epoxy groups, tertiary alcohols and widely distributed double bonds^{22,23}. Afterwards, also this model was modified, considering the presence of carboxylic groups along the perimeter of the plane (Figure 2.5). They also explain stacking structure with the presence of hydrogen bonds between tertiary groups and epoxy groups, so water is able to bind strongly to basal plane and reinforce interaction between near GO plane. The strong

interaction between basal plane and water is at the base of a distinctive feature of GO: the affinity with many kinds of solvent, due to number of functional groups on the GO surface [31] (Figure 2.6).

Some points are still unexplained like functional groups disposition, in fact double bonds difficulty can survive to strong oxidation condition and for this reason it thinks double bonds are in aromatic or conjugate structures [28].

There is another model by Dekany [32], which is linked to the earlier model of Ruess and Scholz-Boehm and it is characterized by a quinoidal structure with a corrugated form and composed by some cyclohexyls, where alcohols and 1,3 ethers are present (Figure 2.7).

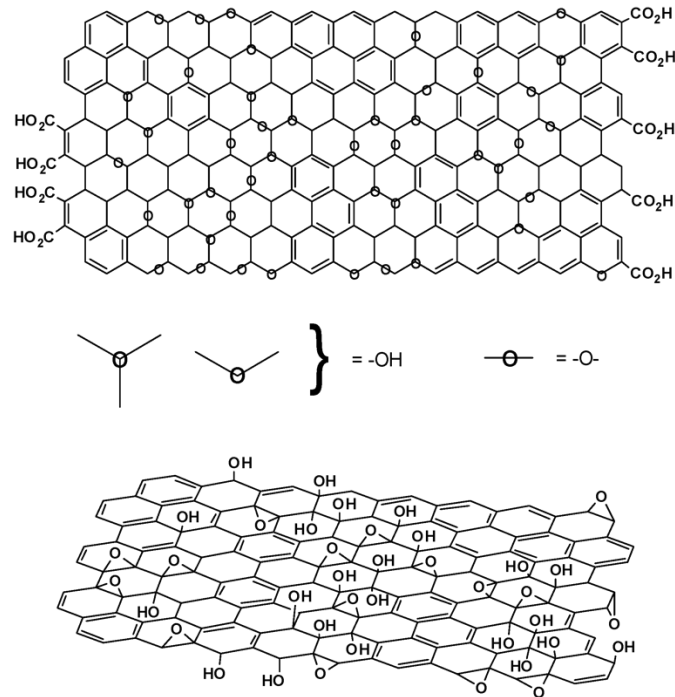


Figure 2.5: Scheme of Lerf and Klinowski model [28].

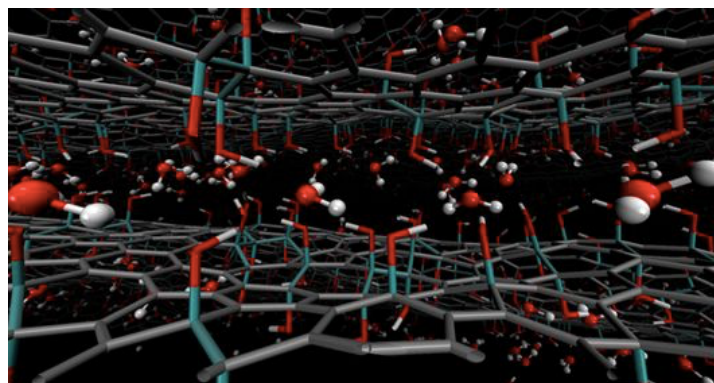


Figure 2.6: Representation of stacking GO structure [33].

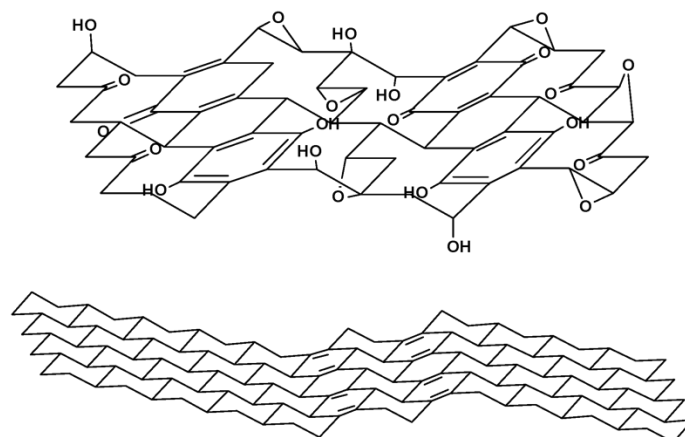


Figure 2.7: Scheme of Dekeny model [32].

Finally, GO structure can be mainly divided in three regions:

- graphitic regions, where there are hybridized sp^2 carbon, fill about 16% of total volume and with variable thickness between 1-6 nm^2 ;
- cavity, that fill about 2% and have thickness of about 5 nm^2 ;
- high degree oxidation regions, that fill about 82%.

The most important functional groups present are hydroxyl and epoxy ones on the basal face and carbonyl on the fracture edges. Cavities are formed because of the development of CO and CO₂ during oxidation and exfoliation processes. GO planes interact themselves through Van der Waals forces, dipole-dipole interactions and oxygen bridge.

2.2.3 Properties

For GO, the presence of water molecules, adsorbed on the surface, is a key factor for its chemical-physical properties. GO is hydrophilic and water and other polar solvents can be easily inserted between GO layers, leading to formation of an expanded structure. In fact, the interlayer distance moves from about 6 Å to 12 Å when water molecules interact with GO. The particularity is that GO shows a negative compressibility coefficient, so cell volume increases increasing the pressure, promoting the insertion of molecules between GO layers. The expansion can be high, reaching 25-30% of the initial dimension. In addition, the process is reversible, so cell size can be return to the initial dimension. For this reason, this phenomenon is called “breathing” of the structure [34] as a function of the pressure and of pH and it is possible thanks to weak Van der Waals interaction occurring between GO layers.

The oxidation process leads to the loss of conductivity, due to the presence of sp^3 domains. So, GO has to be regarded as an insulating material. But controlling the level of oxidation is possible to tune chemical and physical properties [28].

2.3 Reduced Graphene Oxide (rGO)

Graphene is one of the most important materials that can be used as catalysts, but at the same time its synthesis process through chemical vapor deposition (CVD) is expensive and it is not

easy to produce enough catalyst for industrial purpose. Reduced graphene oxide (rGO) represents an alternative and economical material that shows similar properties to graphene. rGO is obtained by reduction of GO, that allows for a decrease of oxygen content. However, GO reduction is hardly complete and so, rGO usually contains a variable concentration of oxygen containing functional groups as well as holes and other defects, contrarily to graphene obtained by CVD, that does not contain any oxygen and it is highly pure. Purity can be a disadvantage because material is less reactive due to lesser number of active sites [8].

rGO is conductive because of the presence of several conjugated domains, also it has a poor affinity with water. Therefore, the hydrophobic forces and π bonds form irregular aggregated, that are rGO. In addition, it can be doped with heteroatoms, that modify geometrically the structure, changing the behavior of the active sites in a similar way to other defects like vacancies, holes and surface defects. Then, rGO can be used as catalysts as well as a material for hydrogen storage [12].

GO reduction can be carried out through different approaches like chemical, thermal or electrochemical methods. The obtained rGO may have different properties and surface morphologies as function of the used method, that can be characterized through [28, 35]:

- optical absorption measurement, because GO and rGO have a markable different visual aspect; in fact, the reduction process increases the electron movement and their concentration, changing the optical properties, so the material will be lucent likewise a metal, while GO is brown color and semi-transparent (Figure 2.8);
- B.E.T. measurement of the surface area, that consists on the measurement of the amount of gas (usually nitrogen) physisorbed on the surface;
- Raman spectroscopy, that gives information about vibrational modes of the dominant bands of graphitic structure and about stacking behavior;
- electronic properties of the material, as the aim of the reduction process is restoring the electrical conductivity. The electrical conductivity can be measured by different ways as measuring an individual rGO sheet or an assembly of rGO sheets, powder conductivity or bulk conductivity. But the most used parameter is the sheet resistance (R_{sh}), that is independent of the thickness of the sheet. R_{sh} is described by Eq. 2.1, where σ intended as the bulk conductivity and t as the thickness:

$$R_{sh} = \frac{1}{\sigma t} \quad (2.1)$$

- C/O ratio, that can be measured through X-ray photo-electron spectroscopy (XPS) analysis. In addition, XPS can give more information on the chemical structure of GO and rGO.

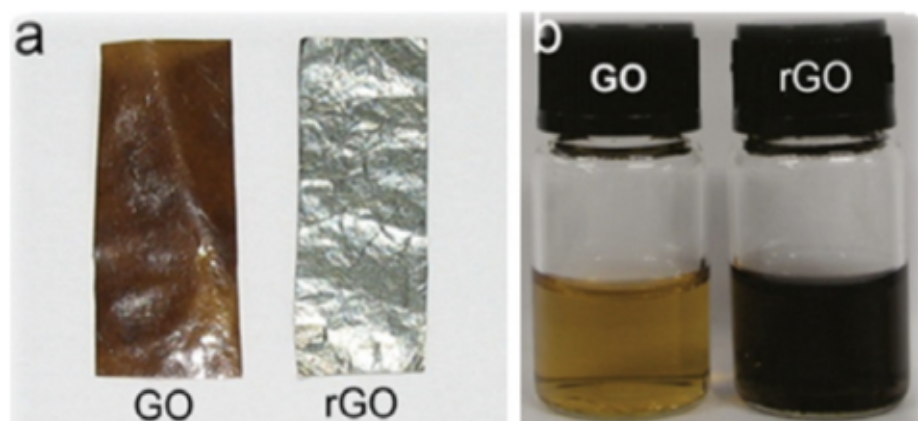


Figure 2.8: Aspect of GO and rGO deposited on a solid substrate (a) and in a solution (b) [35].

2.3.1 Chemical reduction

For chemical reduction of GO, different chemical agents can be used like hydrazine monohydrate, sodium borohydride (NaBH_4), gaseous hydrogen, sulfuric acid or other strong acids. Chemical reduction is carried out at room temperature or few grades above, in any case the annealing temperatures, that characterize thermal reduction, are not reached, resulting in a lower cost and easy way for mass production. The main disadvantage is the environmental impact of these solutions, that are toxic and harmful.

Hydrazine monohydrate is certainly the most used reductant agents for GO reduction. The process through which hydrazine reacts is still unclear, but the addition of this reductant to a graphene oxide dispersion (around 100°C) allows for the precipitation of a black solid from suspension. This can be explained because of the increase of hydrophobicity on the surface of the material after reduction. The surface area, calculated by BET, is significantly less than pristine graphene because the sonication process was not enough to achieve a good level of GO exfoliation and due to formation of inaccessible region on the material surface because of agglomeration during precipitation. C/O ratio is about 10.3, that is higher than GO (about 2.7), as expected. From Raman spectra observation, a reduction of sp^2 domain size occurs but at the same time their overall presence in graphene structure increases, also resulting in an increment of conductivity. One of the advantages linked to the use of hydrazine is the absence of reactivity with water, leading to easier reduction of GO in aqueous dispersion, at variance with other strong reductants. At the same time, hydrazine usually leaves heteroatomic impurities in rGO, in particular nitrogen because it tends to create covalent bonds on the surface, making several species. This results in changes of electronic structure because C-N groups are n-type dopants. An effective alternative is given by sodium borohydride (NaBH_4). NaBH_4 is more effective than hydrazine for what concerns C=O species reducing, but less effective for reduction of epoxides and carboxylic acids. rGO obtained by the use of NaBH_4 shows a lower sheet resistance in comparison to hydrazine. In addition, the C/O ratio is usually higher than the one obtained with hydrazine. Main impurities are alcohols, that are generated during the reducing process because of the hydrolysis of boronic ester.

For what concerns the other reductants, hydrogen can be mentioned because it allows to reach high enough C/O ratio. The strong acid, especially sulfuric acid, are used as a second step for the materials, that have a high level of contamination, because they make a dehydration of the

surface. An example of application is on the materials treated with NaBH_4 , that show several alcohols groups on the surface [28, 35].

2.3.2 Thermal reduction

Thermal reduction is the most diffused method for GO reduction and it is also called “thermal annealing”. Unlike chemical reduction, in this method chemical reductants are not used, but the only effect of temperature is enough to exfoliate and reduce GO.

The basic principle on this method consists on a rapid heating that leads to the formation of gases, like CO and CO_2 , in the space comprised between GO sheets, allowing for an easy detachment of them. The formation of CO and CO_2 gases is due to the species, that also have oxygen atoms, on the surface, that decompose because of the rapid temperature increases, forming gases and increasing the pressure between the stacked layers. If state equation is considered, a few amount of pressure (like 2.50 MPa) has to be applied in order to split two GO sheets, also if during the process the pressure theoretically moves in a range between 40 and 130 MPa, calculated at the decomposition temperature (200°C) and just below furnace temperature (1000°C) [14]. So, rapid heating has a double effect: it exfoliates sheets of GO and decomposes oxygen-containing groups.

The drawback of this method is that it leads to the formation of small and wrinkled pieces because the formation of CO and CO_2 gases takes away carbon atoms from graphene plane, resulting in a distortion of final planes. This causes a significant loss of weight of GO and the formation of structural defects. Structural defects affect the electronic properties because they promote electronic scattering. So, the conductivity decreases, reaching surely lower values than pure graphene. However, typical conductivity values are not too low, indicating effective overall GO reduction.

Among principal parameters, heating temperature is one of the more important. Heating temperature affects C/O ratio: higher temperature, higher C/O ratio. But also, it affects conductivity, that is higher at higher temperature, as possible to see in figure 2.9. In order to reach rapidly heating temperature, arc-discharge can be used.

The control of atmosphere is fundamental for a good reduction process because increasing the temperature increases the etching effect of the oxygen. For this reason, the content of oxygen must be minimized through the use of vacuum, inert or reducing atmosphere. An example is the use of H_2 , that is a reducing gas able to consume oxygen present in the atmosphere and also allows to carry out the process at lower temperatures. An alternative can be using a mixture of argon and ammonia in order to have not only GO reduction, but also doping effect because of the presence of nitrogen. The presence of nitrogen doping into the structure leads to enhance the conductivity.

The most important limitations linked to thermal reduction are the energy consumption, due to the reaching of elevated temperatures, and the reaction conditions, that can be dangerous. If heating is carried out too quickly, the structure may explode, especially in the case of GO films, but, at the same time, if heating is carried out too slowly, reduction process becomes a time-consuming process [28, 35].

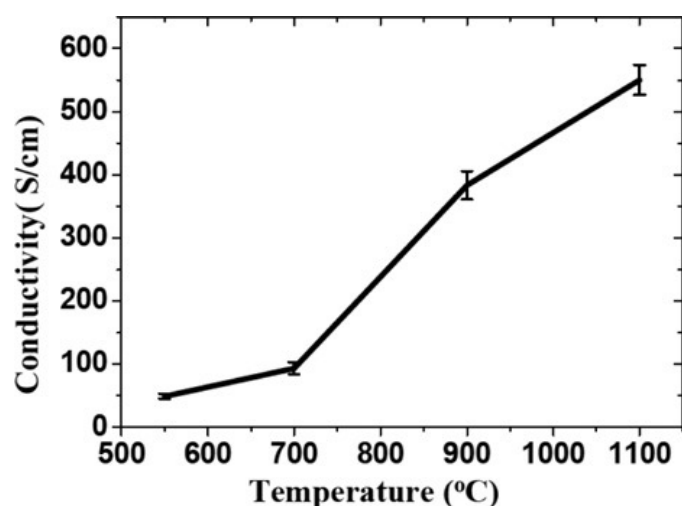


Figure 2.9: Conductivity as a function of temperature in thermal reduction [35].

2.3.3 Microwave reduction

When reduction is run thermally, thermal irradiation is operated, but other sources can be used like microwave irradiation. The advantages of the use of microwaves consist on saving time, cost and for high efficiency due to uniform heating.

The usually used frequency in laboratory for this scope is 2.45 GHz, which corresponds a wavelength of 12.24 cm.

The material is firstly prepared in a solution with a solvent like nitric acid and potassium permanganate or through suspensions in aqueous or organic media and then puts in microwave oven. Microwaves use dipolar polarization and ionic conduction in order to reach the aim. In fact, they interact with electric charges and ions, that are present in liquid media. Molecules like water ones orientate in the direction of the electric field, but, being alternating, they are forced to change their orientation quickly. Then, the probability, that they collide, is high and this causes the generation of heat. The same discussion can be made in the case of ions, leading to the same result. In the case of semiconducting or conducting samples, ions and electrons form an electric current and energy lost due to the electrical resistance of the material generates heat. In the conventional thermal reduction, the reactor walls are the first to be heated and only after the heat is transferred to the materials through conduction and convection. So, the intermediation of the reactor increases the process time. Core zone employs more time to reach the target temperature, so a thermal gradient is usually formed. The consequences concern inefficient and nonuniform reactions. On the contrary, in the microwave heating only the target materials are heated, so the vessel does not act as intermediary and temperatures that can be reached are higher in the materials because heat dispersion is less, saving cost and time (Figure 2.10).

Microwave energy is not enough high to break chemical bonds and often is also lower than the Brownian motion, but is able to affect molecular rotations. For this reason, microwave processes are used to improve the efficiency of heating without producing undesired reactions [15, 35, 36].

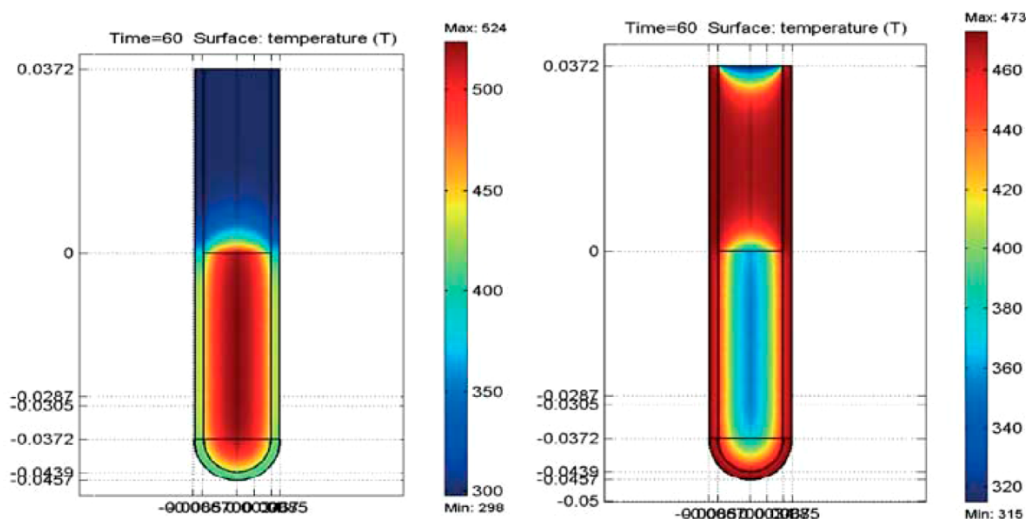


Figure 2.10: Temperature profile for microwave heating (left) and heating in oil bath (right) [15].

2.3.4 Electrochemical reduction

Reduction of GO can be also carried out through electrochemical way. The main advantage of this method is that special chemical agents are not necessary because the mechanism founds only on the motion of electrons between the material and the electrodes. So, the use of hazardous reducing agents is not needed, avoiding also the formation of byproduct. At the same time, the production of GO with electrochemical tends to low-yield because it is strongly dependent on the limited area of electrodes, and the underplayed parts that are not in touch with the solution could not easily reduced.

The process consists on first depositing of a thin film of GO on the surface of substrate, that can be made of glass, plastic, indium tin oxide, etc. and electrodes are placed at the opposite end of the film inside electrochemical cell. At this point, electrode with GO is reduced during a cyclic voltammetry, that is run in a buffer solution. One scan can be enough to the reduction of GO and, in any case, it is irreversible. The exact process is unclear, but an important role is played by pH level of the solution, in particular low pH values promote the right development of the process. The crucial role of hydrogen ions is described in Figure 2.11 [28, 35, 37].



Figure 2.11: Scheme of electrochemical reduction process [28].

2.3.5 Reduction mechanism

All GO reduction strategies that are mentioned above have two aims: the removal of functional groups and the restoration of lattice defects in order to restore electrical conductivity.

The last can be solved through one step of graphitization at elevated temperature, followed by an epitaxial growth or CVD in the affected region by requiring a provision of carbon, for the removal of oxygen-containing groups, it is important to remove them and to restore a long-range conjugated structure. In particular, for conductivity of monolayer graphene oxygen-containing groups, that are on the plane, are the most impacting, whereas the ones, that are on the edges are less influential. This is due to the fact that carrier mobility on the plane determines

the conductivity and results in the need for reduction of epoxy and hydroxyl groups, while carboxyl, carbonyl and ester groups are less important because they are mainly placed on the edges.

When thermal energy is used to deoxygenation, parameters like binding energy between graphene and a specific oxygen-containing functional group, location and coverage of functional groups on the graphene plane have to be considered. Binding energy affects the critical dissociation temperature (T_c). For epoxy groups, the binding energy with graphene is 62 kcal/mol, while for hydroxyl groups is 15,4 kcal/mol, so the former results being enough more stable than the latter. This causes that hydroxyl groups have a lower T_c (above 650° C) and the dissociation produces two radical moieties, which does not lead to the creation of structural defects on the plane. For epoxy groups the T_c cannot be calculated, but below 1200° C epoxy groups are certainly retained. At the same time, carboxyl groups are much easier to remove because their T_c is around 130° C, whereas carbonyl ones are eliminated only above 1730°C. Finally, in the case of high coverage of functional groups on the plane the interaction between close groups and the structural defects, can make removal easier. So, GO reduction from 75% to 6.25% coverage is relatively easy, but further reduction becomes more difficult because interaction between two close hydroxyl and epoxy groups generate thermally stable groups.

Also, when chemical reactions are used to deoxygenation, functional groups are not completely removed, but the advantages are that the process can be carried out with low or moderate temperatures and the reducing agent can able to eliminate only specific species. In the case of the use of hydrazine, the reduction mechanism is based on epoxide ring opening, thanks to hydrogen shift, and on the generation of by-products with hydroxyl groups. Hydroxyl groups, that are in the plane of aromatic areas, are unstable also when the temperature is not too high and, for this reason, their elimination is easy, allowing to restore the conductivity.

Whatever reduction method is used, the final aim is to reach a level of conductivity similar to graphene, restoring the long-range structure, that was destroyed by oxidation. With thermal annealing, initially the sp^2 cluster are isolated, but by reducing the material interactions among the clusters increase (Figure 2.12 a-d). If the amount of sp^2 cluster reaches 60 %, threshold of percolation is obtained and conductivity restored. Indeed, only 25 % can be enough, but C/O ratio has to be above 4. As possible to see in Figure 2.12 e, f, h and i, the initial concentration of oxygen affects the final structure. In particular, GO with higher oxygen concentration becomes further from ideal one with a thermal treatment above 1000 K. The increase of number of vacancies can be explained by the elimination of epoxides, that form CO and CO₂, while the structural disorder is due to rearrangement of carbon atoms to release stresses. An alternative is showed in Figure 2.12 g and j, that consists on thermal annealing in presence of hydrogen. This pathway is more effective because the deoxygenation process is given by several reaction, that are characterized by limited energy barriers as opposed to one step breaking of carbon-oxygen bonds.

Finally, chemical reduction allows to preserve the morphology of the plane, while thermal reduction, thanks to use of elevated temperatures, facilitates the elimination of some oxygen-containing groups. So, the best option is to use both in a sort of mixture [35].

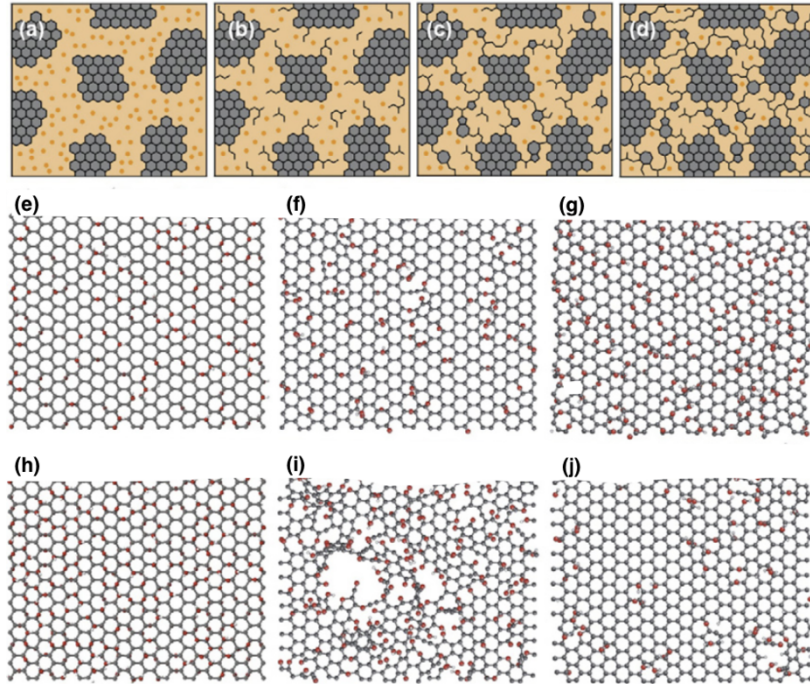


Figure 2.12: The development of GO structure during reduction through thermal annealing (a-d), structure of GO with different content of oxygen (e and h) after thermal annealing at 1500 K in vacuum (f and i) and in hydrogen atmosphere (g and j) [35].

3. Oxygen Reduction Reaction (ORR) and applications

The research for the oxygen reduction reaction (ORR) catalysts is mainly focused on the development of fuel cells. A fuel cell is a device able to convert chemical energy of a fuel into electrical energy and heat, avoiding the use of thermal cycle. In particular, when the fuel cell is powered by hydrogen, electrical energy and hot water are produced by starting from only hydrogen and oxygen. Hydrogen can be ionized easily because its molecule is constituted by two atoms that are weakly bonded. Oxygen is used as fuel because it is abundant and free in the atmosphere and reacts with the hydrogen, forming a harmless product like water. The process that occurs into fuel cell is exactly the opposite reaction of electrolysis: in fact, for water splitting it is necessary to supply energy, whereas inverting the process electrical current and water is formed. At the cathode of cell, oxygen is reduced, while at the anode hydrogen is oxidized. The two electrochemically active electrodes are immersed in an electrolyte, usually KOH.

Fuel cells are characterized by high electrical efficiency (from 40 to 60%), power tunability as function of the demand of electrical energy, possibility to be arranged in series to form *stacks*, low environmental impact. Moreover, several fuels can be used (like methanol, methane, natural gas, syngas) [38].

Another emerging technology that employs ORR at cathode are metal-air batteries, that were recently used in electric vehicles. In this field, lithium ion batteries are the most used, however they have a high cost because lithium is a rare material and can easily developed a fire in the case of a crash. Metal-air batteries allow to overcome these issues thanks to economical and safe materials that constitute the cell. They are composed by an anode, a cathode, that is composed by a gas diffusion layer and a catalytic layer, and a separator, as it can be seen in the figure 4.1. Metals that can be used for anode are Ca, Al, Fe, Cd and Zn. In particular, Zn-air batteries are the most used because Zn has moderate price, high availability, low equilibrium potential, a smooth discharge voltage, a long durability and eco-friendly. The process starts with the entrance of the oxygen from the air, passing through the gas diffusion layer. Then, the catalyst allows for the oxygen reduction to OH^- , while at the anode side the zinc is oxidized, generating electrons in a basic electrolyte. At this point, hydroxyl ion moves to the other side and meets zinc ion in order to finish the reaction cycle. Usually, the overpotential of the anode is lower than that the cathode, so the use of an efficient catalyst is necessary in order to lower it [39, 40].

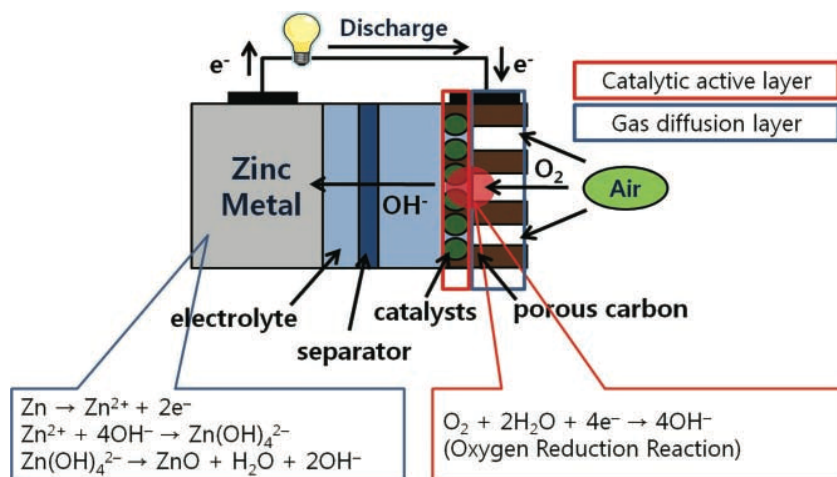


Figure 4.1: Structure and reaction of a Zn-air batteries [40].

3.1 Oxygen reduction reaction (ORR)

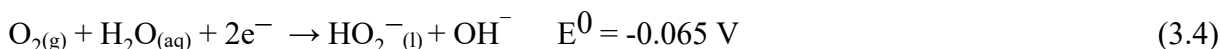
As anticipated above, the ORR is a fundamental reaction for several electrochemical devices like fuel cells, metal-air batteries and oxygen sensors. However, ORR continues to be a challenge because of its complex kinetics and the need for electrocatalysts. Generally, the most used materials are platinum and its alloys because they have superior performance than many other electrocatalysts, but scarce availability, high costs and the slow oxygen reduction kinetics, limit their applications. Therefore, other alternative catalysts are needed for the development of systems of fuel cells on a large scale like derivative-graphene materials.

When oxygen reduction occurs in aqueous solution, mainly two pathways are possible: a four-electron reduction path from oxygen to water and a two-electron reduction path from oxygen to peroxide, that can further evolve to water. The reaction steps that occurs during reduction process have been unclear for many years because currently available experimental techniques were not capable of detecting all possible reaction intermediates, but recently the model suggested by *Damjanovic et al.* [41], and then fixed by *Wroblowa et al.* [42], was considered as the most accepted mechanism of ORR. Reactions and potentials are different as function of pH values and therefore of medium [43, 44, 45, 46, 47].

In acidic media,



In alkaline media,



where E^0 is the standard electrode potential.

In most cases, the four-electron pathway is preferred as in fuel-cells because it is more efficient than the two-electron pathway. In fact, in the second pathway the formation of peroxide can be

dangerous because it becomes highly aggressive when breaks down into free radicals like OH• and OOH• [48].

3.2 Catalysts

The peculiarity of ORR is the slow kinetic, mainly due to the high bond energy of the oxygen molecule. For this reason, in order to proceed with the reaction, a catalyst has to be used.

An ideal catalyst has to be some features to guarantee good performance like:

- high catalytic activity towards ORR,
- high electrical conductivity,
- high chemical, electrochemical and catalytic stability, because it should not be oxidized by proton, oxygen or at high electrode potentials,
- should not dissolve in electrolyte,
- suitable structural composition, suitable morphology, high specific surface area, small particle size, high porosity and uniform distribution of catalyst particles on the support,
- high interaction among the support surface and the catalyst

In particular, the interaction force between the catalysts and substrate plays an important role because if interaction is too weak, bonds fail and reactions do not take place, whereas if it is too strong, dissociation will be very slow [46].

In the most cases, materials used as catalysts do not show all requirements mentioned above, for this reason for each application and condition the catalyst that fits better to the system has to be chosen.

As anticipated earlier, Pt catalysts are certainly the most used up to now, but because of several limitation linked to their use like limited availability, high cost and high overpotential, so new catalysts for the ORR are needed. These studies lead to the development of materials alternative to Pt-based catalysts like as metal oxides and carbonaceous materials [46, 49].

As alternative, other noble metals beyond Pt are also studied like Pd, Ag, Ir and Ru. In particular, Pd was the most studied because of the electron properties, that are similar to Pt: it showed a better ORR activity in a basic medium, whereas it is inert in an acid one. The noble metals in terms of ORR activity follows the trend: Pt > Pd > Ir > Rh (Figure 3.1). Ag shows less electrocatalytic activity but is more stable³⁶.

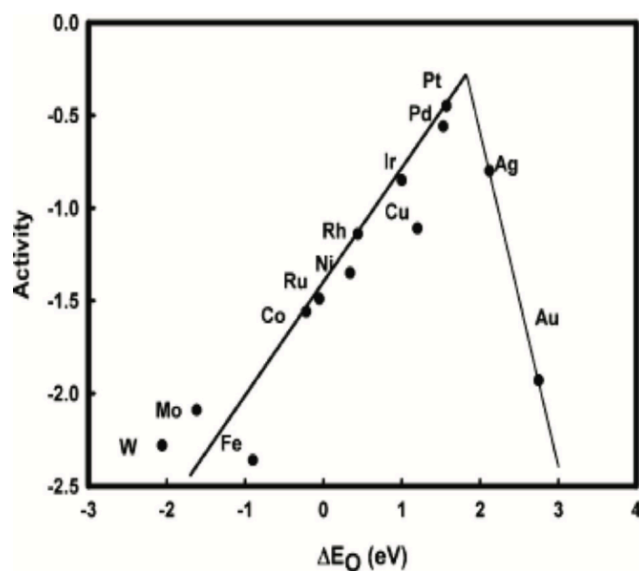


Figure 3.1: ORR activity of noble metals [45].

The aim of use Pt-alloy is that of reducing the use of Pt and while maintaining high electrocatalytic activity. Alloying element can be other noble metals like Pd, Au, Ag, etc. or transition metals like Ni, Fe, Cu, Co, etc. Pt-alloys with noble metals present superior electrocatalytic activity in comparison with Pt catalysts and this can be explained by fully occupied d-orbital of noble metals. In fact, the effect given by the d-orbitals of these metals is able to decrease the Gibbs free energy, resulting in enhanced ORR kinetics. Transition metals have showed similar effect but due to modifications on electron configuration and changes of surface species and composition. At the same time, there are not preparations methods to control large synthesis and transition metals are not electrochemically stable in the typical range potentials in acid medium, limiting strongly the application [45, 49].

Another possibility is the use of metal oxides like IrO_2 , NiO , CeO_2 , ZrO_2 , TiO_2 and SnO_2 as ORR catalysts in basic media. They are not able to enhance electrocatalytic activity, but they have an excellent corrosion resistance because of their limited conductivity [45, 49].

Recently, the use of carbon materials has rapidly grown as support for metal particles and metal oxides as well as catalysts themselves because of their mechanical properties, significant surface area, good conductivity and electrochemical stability. *Majidi M. R. and Ghaderi S.* [50] studied the effect of palladium particles on a carbon support such as graphene nanosheets (GN), graphene oxide (GO) or directly glassy carbon electrode (GCE) for ORR. They reported from cyclic voltammograms that the use of GN or GO leads to higher catalytic peak current of O_2 than GCE, proving the increase of the specific surface area and the electrocatalytic activity of GN and GO. In addition, the RDE measurements allow to know the number of transferred electrons in oxygen reduction, that it was estimated to be 3.7, indicating the four-electron ORR. Often carbon materials like graphene, rGO or nanotubes can be doped in order to provide more chemically active sites for reactions and anchoring sites for metal particles. For this purpose, generally heteroatom (like N, S, B, P or mixtures of them) are used. They can substitute some carbon atoms on the typical honeycomb lattice, partially destroying it and creating defect points. As matter of fact, dopant atoms are characterized by different radius, orbitals, electron density and electronegativity and they change unavoidably electronic properties and the charge distribution. The functionalization of graphene-based materials with dopants can be carried out

after the synthesis process through thermal treatment, for instance, or also during the synthesis, during the reduction step of GO or in-situ with CVD, that allows to incorporate the heteroatoms more homogeneously [3, 11, 51]. The introduction of dopant particles in their structure makes possible to limit the use of precious metals, maintaining similar levels of catalytic activity. *Ganesan et al.* [52] proposed a nitrogen/sulfur dual doped graphene oxide with cobalt sulfide nanoparticles. The experimental tests show that ORR performance are a bit lower than typical Pt/C catalysts, however if the cost and availability of platinum is considered, then CoS₂/N,S-GO has several advantages such as cost and earth abundance. The transferred electron number is 3.87, that is higher than previous example.

Among dopant atoms, nitrogen is certainly the most used. In the periodic table of elements, nitrogen occupies a position close to carbon: this means that atomic sizes are similar, but electron configuration is different, coupling the minimization of lattice mismatch and the possibility of multifunctional electronic properties. Besides, nitrogen atoms provide both active sites, where the reduction can take place, and sites, where metal particles can attach [3, 11]. In particular, GO shows a huge amount of oxygen moieties on the surface and therefore, it can represent a wide base for the entrance of nitrogen atoms in the structure. In fact, oxygen atoms can bond directly with N precursors or oxygen-containing species can undergo thermal decomposition and, then, react with them. In any case the presence of N precursors is necessary, it can be used organic salts (like urea, cyanamide and melamine) or inorganic (like NH₄Cl or NH₄NO₃) species. In particular, urea is a good candidate as N precursor because its decomposition generates CO₂ (that can modify structure) and NH₃ (that is a reductant and a dopant), can form a porous structure and a good reduction degree, furthermore, gives the possibility to tune the doping level [51]. The introduction of N atoms in the lattice can generate different configurations like graphitic, pyrrolic and pyridinic nitrogen, and nitrogen-containing species like amino groups and oxynitride. Pyridinic species as well as the amino groups act as anchoring sites for Pt particles and are able to accept electron, therefore in this way they adsorb the oxygen, and capture easier electrons from cathode, graphitic N shows the highest ORR activity because it is able to move electrons quite effectively and the adsorption energy is enough low, whereas oxynitride groups are ineffective for catalytic reaction [11, 53]. In each case, by tuning the synthesis conditions like annealing temperature is possible to select the type of configuration of N atom because the different groups show different doping ability and thermal stability [51]. Also, the charge reorganization on the graphene plane affects the catalytic activity when nitrogen doping is present. In fact, carbon atoms and nitrogen atoms have a certain, but for the first one it is positive and higher, allowing to balance the intense electronic affinity with nitrogen, the result is that the adsorption of O₂ or other intermediates improves (Figure 3.2A). Then, ORR activity is related to the microstructure, therefore reduction reaction could naturally occurs following the four-electron pathway. The process is composed by the follow steps:

- O₂ or OOH⁺ is adsorbed on the surface plane of N-doped graphene (Figure 3.2B-a);
- the graphene plane is warped into a shape similar a saddle with the carbon and oxygen atoms, that create a tetrahedral structure, rising out of the plane (Figure 3.2B-b);
- in the case of O₂ adsorption, O₂ interacts with hydrogen ions, forming OOH;
- the interaction between a hydrogen and oxygen atom, that is attached onto the surface, creates a new bond and the rupture of oxygen molecule, forming an hydroxyl groups;

the dissociated OH gets away from the graphene plane, while the other OH remains bonded on the graphene surface (Figure 3.2B-c);

- adding other two H atoms in the reaction system, two water molecules are formed, moving away from the graphene, so the structure returns to starting flat shape and can undergo a new cycle of reaction (Figure 3.2B-d, e) [46].

All this represents the description of four-electron reaction path because of the rupture of oxygen molecule, that is not involved in two-electron path because of the formation of peroxide. In addition, this mechanism clarifies what are the parameters that can be tuned to optimize the catalytic properties: doping cluster size and the presence of defects like Stone-Wales defects, that consist on 90° rotation of a C=C bond and formation of two pentagon and two heptagon rings in place of typical hexagonal rings [54]. A large nitrogen clusters have fewer active sites as well as nitrogen isolated atoms have not a good catalytic behavior for reduction reaction. So, the optimal is small N clusters (constituted of three or four N atoms) in combination with material defects [46].

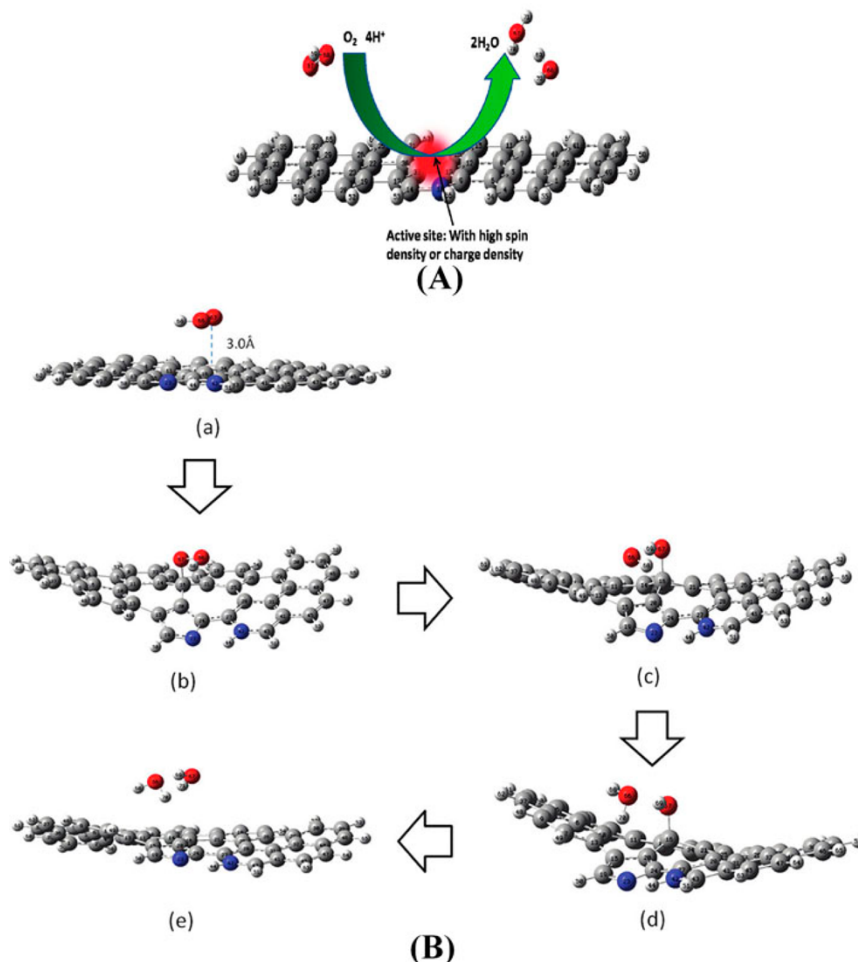


Figure 3.2: A) Structure of N-doped graphene, B) the process steps of four-electron ORR: a) O_2 or OOH^+ is adsorbed, b) the graphene plane is distorted, c) the O-O rupture and formation of OH, d, e) the formation of water molecules. Red, grey, blue and white balls represent respectively oxygen, carbon, nitrogen and hydrogen atoms [46].

Another interesting element that can be used in order to dope graphene-based materials is sulfur. Sulfur is an element characterized by p orbitals, so it shows a similar electronic structure than nitrogen, but different electronegativity. Similar to N-doped graphene, S-doped graphene shows optimal catalytic activity and good durability. The functionalization with sulfur on GO can lead to four types of structure in a graphene cluster: the adsorption of a sulfur atom on the surface of cluster (Figure 3.3-a), a sulfur atom, that replace a carbon atom at the zig-zag or armchair border of the cluster (Figure 3.3-b, c), the substitution of the carbons at the border (zig-zag or armchair) with SO₂ groups (Figure 3.3-d, e) and connection of two graphene layers through a sulfur ring (Figure 3.3-f). Looking at the formation energy, it is negative for sulfur adsorbed on the graphene surface, whereas for all other cases is positive. As a consequence, the adsorbed sulfur is advantageous, if it is seen in comparison with the other structure, that sulfur can form. Moreover, as in the nitrogen case, Stone-Wales defects play an important role because the formation energy of clusters with or without them is significantly different. In particular, Stone-Wales defects lowered it, promoting the effect of sulfur dopants. An explanation of that is the defects change the local charge distributions and crystal lattice [11, 55].

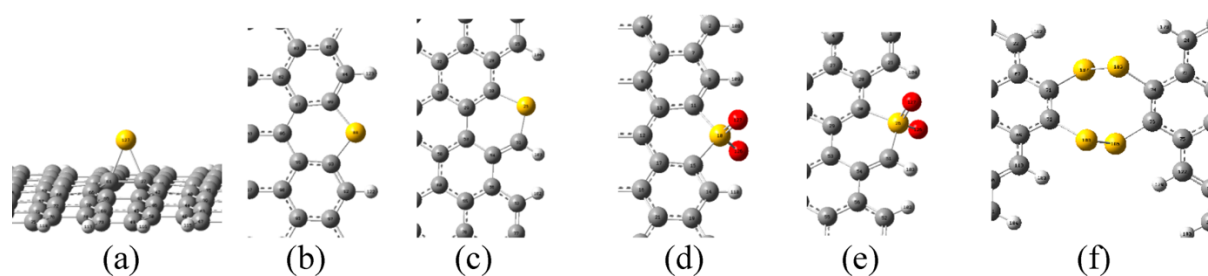


Figure 3.3: Sulfur doped graphene structure: the adsorption of a sulfur atom on the surface of cluster (a), the sulfur atom substitution at the zig-zag or armchair edge of the graphene cluster (b, c), the SiO₂ groups substitute the carbon atoms at the graphene border (zig-zag or armchair)(d, e), connection of two graphene layers through a sulfur ring (f). Grey, yellow, white and red balls represent respectively carbon, sulfur, hydrogen and oxygen atoms [55].

The mechanism for ORR is similar to that described for nitrogen doping, but in this case, the sulfur atom has not an additional electron, this means that the material does not show an extra spin density, but the charge densities redistributes on S-doped graphene cluster. Here, the critical point is that the carbon atoms near sulfur atom with elevated spin density or charge promote four-electron pathway, but the sulfur atoms would promote two-electron pathway. So, on one side sulfur doping activates carbon atoms, but in the other hand it reduces the efficiency of ORR. However, this issue can overcome selecting the desired sulfur doping structure. In fact, it was demonstrated that sulfur oxide is the only structure that does not catalyze the two-electron transfer reaction but activating alike the carbon atoms. So, it can be used to optimize the efficiency of ORR [55].

Nevertheless, the graphene, doped with an only heteroatom, showed encouraging conclusions, the electrocatalytic activity is much lower than typical Pt catalysts, then several authors tried to incorporate various dopants together into material.

Sulfur and nitrogen can be also used together, creating a dual-doped graphene with a synergic effect. As regard the structure, S and N replace a C-C bond, also if the distance between two atoms is large and they do not form a covalent bond. The synergic effect relies on the fact that

nitrogen acts on the graphene structure because it destroys the aromatic domains in some areas, making the material more reactive, while sulfur acts on the carbons near to N, that, as it is said before, have a more elevated spin and charge, activating them. As consequence, the energy barrier of reaction is lowered, positively charged regions are enlarged, which is advantageous for providing large catalytic areas. At the same time, the concentration of sulfur has to be controlled because an excess can lead to the loss of synergic effect because of the redistribution of electrons and spins [51, 56]. This type of doping allows to create catalysts without metals. For example, *Zhang et al.* [57] treated the behavior of nitrogen/sulfur co-doped graphene as catalyst for ORR. Cyclic voltammetry shows that no-doped rGO has a weak catalytic activity due to modest current density, in the nitrogen doped graphene catalytic activity is more important, but in the nitrogen/sulfur doped graphene the peak current is much higher, suggesting significantly improved catalytic activity. However, the number of transferred electrons, calculated by Koutechy-Levich plot, moves in a range of values between 2.98 and 3.36 as function of applied potential (from -0.30 to -0,60), suggesting there is still space to further improve the catalytic performances. At the same time, nitrogen/sulfur doped graphene as well as nitrogen doped graphene show excellent stability as function of the time as reported by chronoamperometric measurements, in fact they display only a loss of 5,40% and 5,80%, respectively in 15 hours, whereas on a typical catalyst, composed by Pt on a carbonaceous support, the current density drop is around 30% in only 7 hours, indicating a higher durability of nitrogen/sulfur doped graphene than traditional catalyst, in a basic medium.

Molina-Garcia et al. [58] tried to use four different atoms, that is N, S, B and P to dope the structure of graphene. Each different heteroatom plays a specific role inside the carbon structure, resulting in an improving of catalytic activity. In fact, the result is the current density of co-doped graphene is much more elevated in comparison with no-doped graphene from CV (cyclic voltammetry) tests, the number of electron is considerably higher with a value of 3.7 and the chronoamperometric tests proved their higher stability than Pt-catalysts in an aggressive basic medium.

4. CO₂ Reduction Reaction (CO₂RR)

Nowadays, CO₂ is the most important waste produced by industrial activities. Each year millions and millions of CO₂ tons are poured into atmosphere, making global warming a serious issue. As total replacement of fossil fuels with renewable energy is still a far achievement, a way to reuse CO₂ is needed, in order to rebalance the amount between CO₂ generated and consumed [59].

The reduction of CO₂ should be a way to recycle it. This process is also known as artificial photosynthesis because it follows a scheme similar to normal photosynthesis, that consists on capturing and storing energy in the chemical bonds of a fuel. It occurs in an electrochemical reactor, constituted by an anode where water is oxidized to molecular oxygen and a cathode where CO₂ is reduced. Electrical energy is necessary to establish a potential between two electrodes of cell in order to convert CO₂. This energy can be obtained from a renewable source like sun or wind and the process leads to generation of carbon-neutral fuels and industrial chemicals that otherwise are derived from petroleum. Organic molecules like formic acid (HCOOH), methanol (CH₃OH), methane (CH₄), etc. can be obtained from CO₂ reduction, and used by human activities, generating new H₂O and CO₂. Like in a close loop, these byproducts can be then captured and transformed again inside the cell (Figure 4.1) [4, 49].

An example is methanol: it is a green fuel and an important medium for several chemical products used in everyday life such as silicone, paints and plastics. It can be used directly in combustion engines or in fuel cells or indirectly after conversion into hydrogen by reforming. The most diffused way to produce methanol is from methane through syngas by steam reforming with a not negligible environmental impact. On the contrary, it can be obtained from the electrochemical transformation of CO₂, that is can be carried out under ambient conditions, using renewable sources [49].

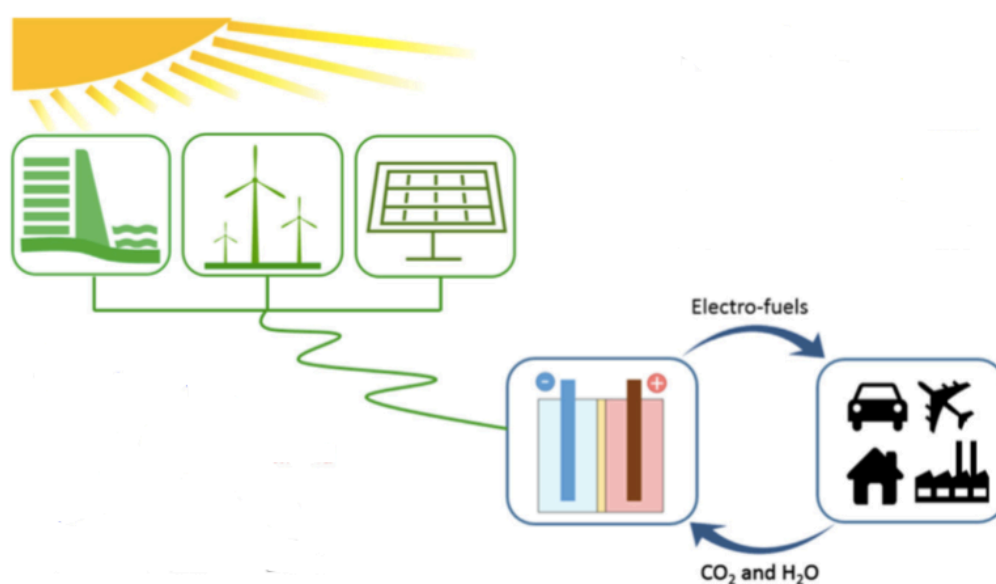


Figure 4.1: Scheme of closed loop of CO₂RR process [4].

In most cases, reaction pathway is not clear, but in general CO₂RR can be seen as a multiple proton-electron reaction. When it occurs in aqueous media, the general reaction is:



where P is one of the typical products of this reaction, n represents the number of electrons involved, while k and m are stoichiometric coefficients. Various reduction possibilities with the equilibrium potentials are shown in Table 4.1 [60].

Table 4.1: Typical products, coefficients and equilibrium potential values of CO₂RR [60].

product name and formula	k	n	m	E^0 (V versus RHE)
carbon monoxide, CO	1	2	1	-0.10
formic acid, HCOOH	1	2	0	-0.20 (for pH < 4); -0.20 + 0.059[pH-4] (for pH > 4)
formaldehyde, HCHO	1	4	1	-0.07
methanol, CH ₃ OH	1	6	1	0.02
methane, CH ₄	1	8	2	0.17
ethanol, CH ₃ CH ₂ OH	2	12	3	0.09
ethylene, C ₂ H ₄	2	12	4	0.08

At this point, it is clear that CO₂ reduction process can follow different pathways and accordingly it is necessary understanding what product is more convenient or has more application. The discussion about economical aspect relies mainly on the cost of electricity, assumed as the only significant cost. A comparison of price between various products is summarized in Table 4.2 and shows as methanol, methane, ethanol and ethylene are very expensive, while carbon monoxide, formic acid, formaldehyde and propanol are characterized by good market values. However, this table does not consider the cost for post-electrolysis separation, that can be very high. In fact, in the case the product is liquid (and diluted), like propanol, formaldehyde and formic acid, separation consumes much energy, turning the process uneconomic. In theory, the problem may be overcome producing a very concentrated substance, but simultaneously side reactions and other problems may arise, resulting in a more complex process. Regarding all this, CO results the best CO₂RR product since it is gaseous at room temperature and the separation from the rest of electrolyte is not difficult. In addition, it plays a central role in the chemical industry as a chemical feedstock or a component of syngas to convert it in a synthetic fuel [33].

Table 4.2: Cost comparison of the main CO₂RR products [33].

Product	# of electrons per product molecule	Market price	Estimated cost
Syngas	2	25–90	376
Carbon monoxide	2	600	271
Formic acid	2	1200–1600 (90%)	163
Formaldehyde	4	3500	501
Methanol	6	350	705
Methane	8	150–250	1880
Ethanol	12	700–1000	981
Ethylene	12	950–1200	1611
Propanol	18	1800	1128

As regard electrolyzer design, it depends on what kind of product is desired. In the case of CO, electrolyzer system design is used (Figure 4.2 a,b). There are two chambers (anode and cathode) separated by an ion-conducting membrane. The process starts when carbon dioxide is injected into the cathode by a contactor in order to have a CO₂-saturated electrolyte. After that, CO₂-saturated electrolyte moves towards the electrolyzer and carbon dioxide is transformed in carbon monoxide, through the help of a pump. Finally, product separation process is carried out at separator and electrolyte is compressed by a pump in order to return to the contactor. On the anode side, the overall process is similar, but the contactor is not necessary [33].

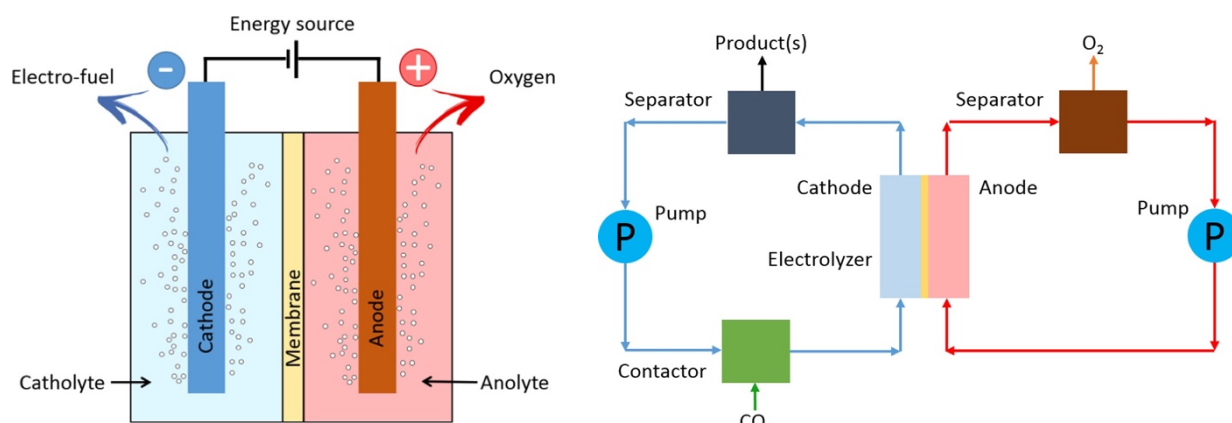


Figure 4.2: a, b) Scheme of typical CO₂ electrolyzer for CO [33].

Despite of promising aims of CO₂RR process, some limitations have to be regarded like the high overpotential, poor product selectivity and low faradaic efficiency. Overpotential, that is the difference between the applied potential and the equilibrium potential, has to be minimized because its value is linked to reaction rate and represents a sort of barrier for reaction starting. As for poor product selectivity, it is due to an inadequate adsorption strength of some reaction

intermediates, which causes the contemporary production of different species during CO₂RR. In this regard, Faradaic efficiency indicates the affinity toward a desired product. Another issue is represented by the competition between CO₂RR and hydrogen evolution reaction (HER), an unwanted reaction that occurs in similar potential values of CO₂RR in aqueous electrolytes. These limitations can be overcome through the use of electrocatalysts, a correct choice of the electrolyte and other parameters, discussed in detail in the following paragraph [61, 62].

4.1 Catalysts

As it was explained above, electrocatalysts play a role of big importance and their choice has undergone constant developments during the years. They must have some requirements: they have to be active, highly selective, inexpensive and stable. Today it is possible to divide electrocatalysts for CO₂RR in three big families: metallic, non-metallic and molecular catalysts. The first electrocatalysts that were studied are polycrystalline monometallic catalysts because of their several advantages like their simple structure, their handling and their strength. They can be also divided as function of the main reduction product, so there are: carbon monoxide forming metals as Zn, Ag and Au, HCOO⁻ forming metals as Pb, Sn and In and H₂ forming metals as Pt, Fe and Ni. However, copper and its alloys are the only catalysts capable of producing significant amounts of hydrocarbons from CO₂ like CO, formate, ethylene and ethanol. However, the reactions on copper require high overpotential in excess of 1 V, that is a high kinetic reaction barrier. To overcome this problem, two solutions were found: decreasing the dimension of metal particles to nanoparticles and dispersing them on a substrate, forming heterogeneous catalysts in order to enhance the amount of active catalysts area per unit of electrode and maximize the efficiency [33, 61].

Graphene or rGO are the supports commonly used. The coupling between the graphene-base materials and metal particles shows important advantages due to large surface area, good conductivity and high flexibility. In addition, graphene allows to improve CO₂ adsorption because both graphene and CO₂ structures have π -conjugated structures and a π - π conjugation interaction can be established between them, improving catalytic activity. Residual functional groups and/or their introduction on the surface of graphene-based materials can act as anchoring sites for nanoparticles or as active groups. In this way, catalysts are uniformly deposited and their aggregation is limited [63].

A particular case can be represented by a porphyrin ring embedded in graphene that is able to coordinate a metal atom. This N₄ macrocyclic complexes are capable to convert CO₂ in CO with high Faradaic efficiency at low overpotentials.

According to *Wang et al.* [61], a way to establish how a catalyst works for CO₂RR is measuring CO adsorption strength on transition metal-porphyrin-functionalized graphene (TMN₄/graphene) and the free energies of formation of COOH*, that is usually the first step of CO₂RR process. CO is used as reference because is a key intermediate and the value that is obtained determines whether CO act as the main product or undergo further reductions. CO molecules prefer to adsorb on the central transition metal site and three groups of materials can be distinguished as function of the adsorption energy (E_{ads}) (Figure 4.3):

- for Fe, Ru and Os, the adsorption energies are very high because the bond between carbon and metal atom is short, while the bond between carbon and oxygen atom is

elongated than the bond in the isolated CO molecule. This is due to the influence of the σ -bonding and π -backbonding between CO and TMN₄/graphene. The too strong adsorption blocks active sites, so these catalysts have to be avoided;

- for Co, Rh and Ir, the adsorption strength is weaker, this means that the adsorbed CO molecule could be protagonists of other reductions;
- for Ni, Cu, Pd, Ag, Au and Pt, the adsorption energies of CO molecules are weak, so CO can be easily released.

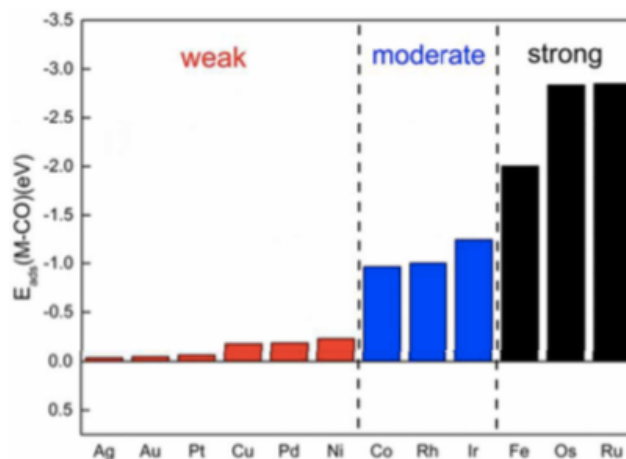


Figure 4.3: The adsorption energies of CO molecule on TMN₄/graphene [61].

As regard free energy of formation of COOH*, it is enough high for the catalysts of last group. This means that there is a high free energy barrier and therefore they have a weak chemical activity toward COOH*. So, they have to be excluded because they are not able to activate easily CO₂ molecule. On the contrary, Co, Rh and Ir show low free barrier energies for COOH* generation, so they are good candidates to be used on TMN₄/graphene for CO₂RR because of their good interaction with CO and COOH.

Co, Rh and Ir are bonded to four unsaturated N atoms through dangling bonds. They can be fully incorporated into graphene structure because the voids between carbon atoms are enough spacious to accommodate transition metal atoms (Figure 4.4). In their side, transition metal atoms use their d orbitals to overlap with N-2p orbitals of porphyrin-like graphene and to facilitate the bonding with CO₂ to promote formation and desorption of the reduction products [49, 61].

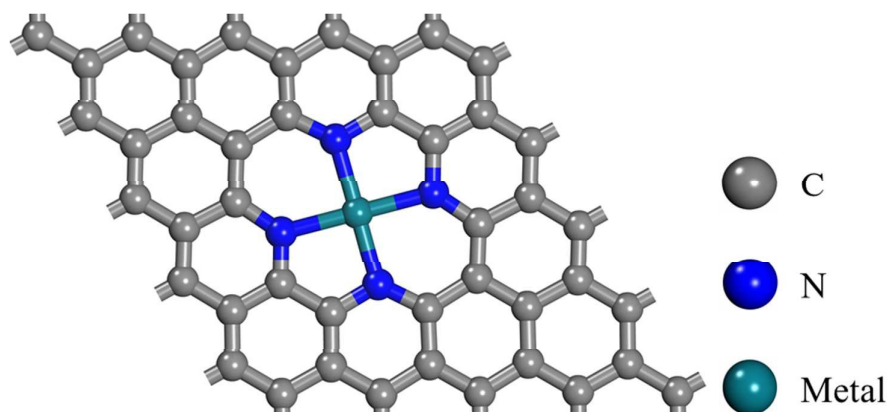


Figure 4.4: Structure of TMN₄/graphene [61].

4.2 Other parameters

Despite of many efforts are focused on the selection of catalyst, it was demonstrated that changes of electrolyte, pH and temperature can affect remarkably the Faradaic efficiency and selectivity of final products.

In particular, the concentrations of reactants, CO_2 , H^+ and H_2 , the settling of reaction intermediates or their inhibition depend on solvent, pH and the presence of some ions. It is important the use of suitable electrolytes at the right value of pH, since pH allows to control proton availability. Neutral or basic solutions allow to obtain a higher Faradaic efficiency. However, when CO_2 is in contact with alkaline solutions, it tends to form bicarbonate and carbonate. In fact, both CO_2RR and HER act on the protons at the electrode surface and, as a consequence, the local pH near the electrode is higher than that in the bulk. Then, CO_2 can react easily with OH^- in that zone, forming carbonate and bicarbonate and electrolytes with buffering properties have to be used. Finally, the variation of pH values can affect the selectivity of reaction [49, 60].

For CO_2RR , aqueous and non-aqueous electrolytes can be used. The first are more common, although several drawbacks are present like:

- low selectivity for CO_2 reduction, due to the concurrent HER;
- slow reaction kinetics, whose consequence is an increase of overpotentials and costs;
- several byproducts of reaction in the reaction medium, increasing separation costs;
- low solubility of CO_2 in water and surface contamination because of the impurities in the electrolyte, which results in a lower productivity [49].

The most commonly used are NaHCO_3 and KHCO_3 , while KOH is showing excellent properties like optimal anion absorption and limited anion overpotential. But the limitation of KOH is that it is too reactive with carbon dioxide, forming carbonate. In fact, the reduction of carbonate is quite complex at the cathode. Recently, electrolytes, composed by ionic liquids, are suggested because their high carbon dioxide solubility and low overpotential for carbon dioxide reduction, even if they are characterized by low current density, low endurance with water and high cost [33].

As regard the methods to suppress HER, non-aqueous solutions (like propylene carbonate, acetonitrile, DMF and DMSO) can be used, but also it is noted that decreasing the temperature, the hydrogen formation is significantly depressed and CO_2 solubility improves. In addition, tuning the partial pressure of CO_2 can help to speed up the reaction process and to contrast low solubility of CO_2 in aqueous solutions [61, 64].

5. Materials and methods

In this chapter, employed materials and methods used to synthesize and characterize the catalysts are reported. Synthesis of samples were carried out in the DISAT laboratories of Politecnico di Torino, while electrochemical tests for ORR and CO₂RR at the “Center for Sustainable Future Technologies” of the “Istituto Italiano di Tecnologia”.

5.1 Samples preparation

The preparation of the samples started with weighing all the chemicals needed: graphene oxide (GO) powder and dopant precursors. Then, they were put in a reactor with deionized water and stirred for about 30 minutes in order to create a homogeneous slurry. The list and the amount of precursor that were used are reported in the Table 5.1. Urea (CO(NH₂)₂) was used as precursors for N doping, while thiourea (SC(NH₂)₂) was selected as precursor for N and S codoping. Metal ions like Ni, Mn and Fe were inserted through respective sulphates (M-SO₄). The samples prepared with urea were named as “NG2_M”, while those prepared with thiourea were named as “NG2_SM”. In both cases, “M” stands for the chosen metal ion. Three samples (namely NG2_Cu, NG2_Co and NG2_Mn) that have already been synthesized by the research group of Polito/IIT were tested for CO₂RR.

The slurry, inside the reactor, was heated with the use of a microwave oven (Milestone flexiWAVE) (Figure 5.1). The reactor vessel consists in a Teflon cylinder, covered by a rigid mantle for security reasons. In this step, GO was reduced to rGO and dopant elements were incorporated into the rGO structure (Figure 5.2). In the microwave oven, a temperature ramp was set: the heating is carried out in 2 minutes from room temperature to 180° C, the maintenance for 15 minutes at 180° C, and cooling to room temperature. Max power was set to 800 W and max pressure to 25 bar. Finally, the samples were put into a freeze dryer (Lio 5P, 5 Pascal) for the removal of water (Figure 5.2).

Table 5.1: Type and quantity of precursors used for the production of samples.

*Already synthesized.

Sample	GO (mg)	Urea (mg)	Thiourea (mg)	M-SO ₄ (mg)	H ₂ O (mg)
NG2	50	20	-	-	30
NG2_Ni	23	10	-	12	15
NG2_S	50	-	20	-	30
NG2_SNi	27	-	10	12	15
NG2_SMn	25	-	10	11	15

NG2_SFe	25	-	10	12	30
NG2_Mn*	50	20	-	25	30
NG2_Cu*	50	20	-	25	30
NG2_Co*	50	20	-	25	30

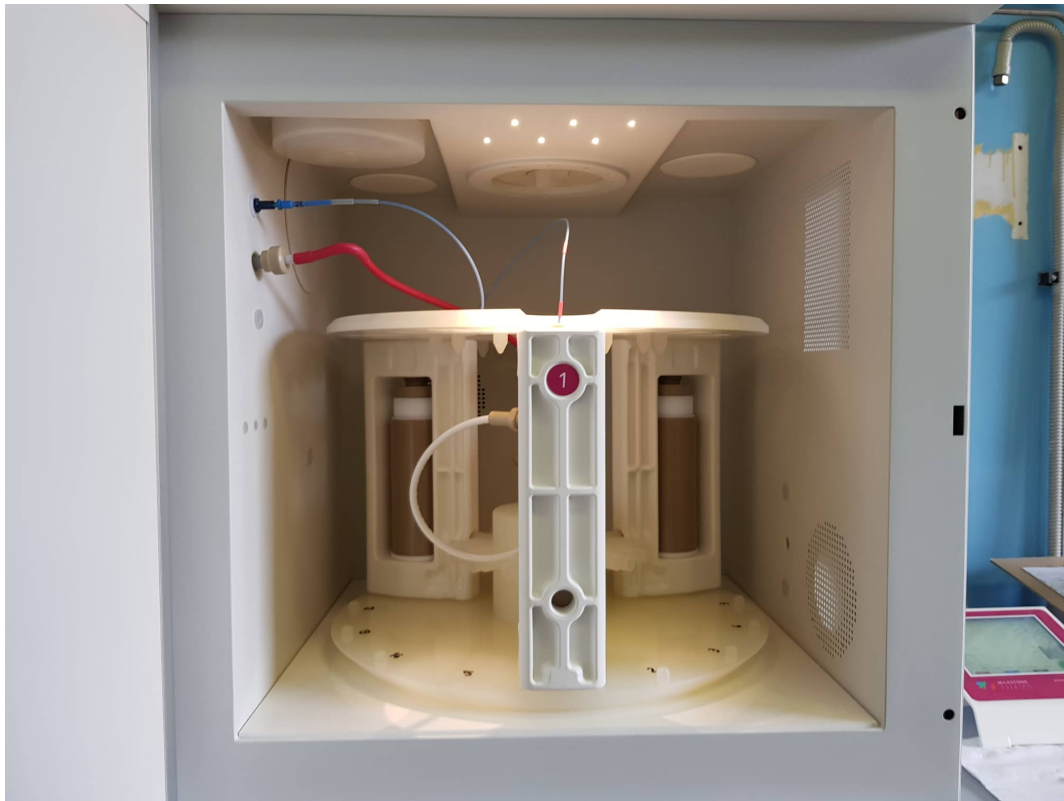


Figure 5.1: Microwave oven used for the sample preparation.



Figure 5.2: The material after the reduction into the microwave oven (left) and after freeze dryer (right).

5.2 Physical, morphological and chemical characterization

Material characterization was carried out through the use of X-ray Photo-electron Spectroscopy (XPS), Transmission Electron Microscopy (TEM) and Field Emission Scanning Electron Microscope (FESEM) because they provide complementary information about chemistry and morphology of samples.

XPS allowed to analyze the surface of samples, determining the chemical elements, the type of bonds between them, functional groups and the state of oxidation. It was used a *PHI 5000 Versa Probe* system. The X-ray source was a monochromatic Al K_{α} radiation ($h\nu = 1486.60$ eV). The compositional analysis has been performed with an EDAX energy dispersive X-ray (EDX) detector.

TEM allowed to obtain more precise information about sample surfaces due to higher resolution. It was used Tecnai G2 F20 S-TWIN, made of FEI Company, operating at 200 kV. FESEM allowed to reveal information about the morphology and the composition of samples, even in a nanometric scale. It was used the *SUPRA 40 (ZEISS)* system.

5.3 ORR characterization

5.3.1 Electrode preparation

The testing electrode consists on a paste, where sample powders are dispersed in a liquid phase, and its deposition in the form of ink on the surface of a GC/Pt rotating ring disk electrode (RRDE) measurement. This particular GC/Pt electrode is constituted by a concentric electrode, where the innermost, called disk, is made of glassy carbon (GC) and it has a diameter of 4 mm diameter, this is separated by an insulating layer in PTFE from a platinum ring, with internal and external diameters of 5 mm and 7 mm, respectively, then the outermost layer consists in a ceramic mantle, that has a diameter of 12 mm [65] (Figure 5.3). The ink has to be able to create a good adhesion with both the glassy carbon electrode, to avoid the detachment during the test,

and sample powders between them in order to have a compact and uniform layer on the electrode surface. For the main part of synthesized materials, 2 mg of sample were immersed in a solution constituted by Nafion perfluorinated ion-exchange resin (5% wt.) (175 μ l), distilled water (24 μ l) and isopropanol (100 μ l). Then, the mixture was stirred for about 30 minutes in order to create a homogeneous dispersion. Before proceeding with the deposition, the electrode surface was polished, by using ethanol and a suspension of alumina particles, in order to remove residues of other inks. Finally, 10 μ l of the ink were deposited on the glassy carbon area of GC/Pt electrode in order to have a final catalyst loading of 0.5 mg/cm², then it was left to dry overnight in air. As for samples containing sulfur and a metal (NG2_SFe and NG2_SMn) this solution led to a discontinuous and unbonded layer (Figure 5.4), alternative ways were tried. So, the first attempt concerned the use of polyacrylic acid (40 mg) with water (about 138 mg) and 1,5 mg sample, but it failed because polyacrylic acid, that acts as binder, is insulating and measured currents were too low. The successful attempt consisted on the use of a solution similar to original one, but without water (Figure 5.4). In particular, it was constituted by 180 μ l Nafion perfluorinated ion-exchange resin (5% wt.) and 420 μ l isopropanol with 2 mg sample. In addition, as the liquid part is doubled, 20 μ l ink were deposited on the electrode surface for maintaining the same catalyst loading.

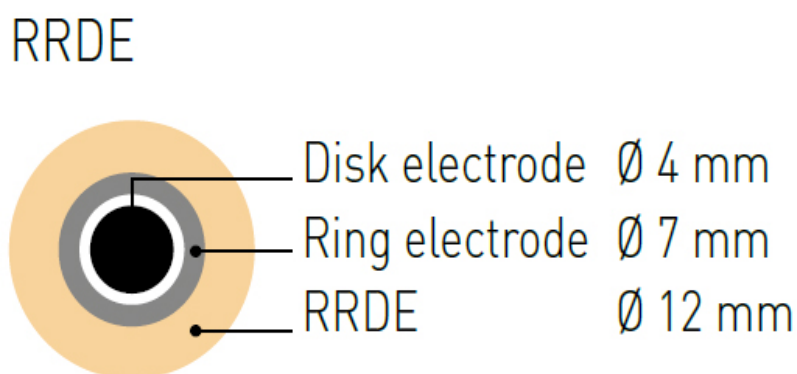


Figure 5.3: Scheme of GC/Pt electrode (left) [65].



Figure 5.4: Successful (left) and failed (right) preparation of the paste for GC/Pt electrode.

5.3.2 Electrochemical measurements

All electrochemical measurements were carried out in a RRDE apparatus (RRDE-3A) with a CHI760D bipotentiostat at room temperature and the graphs analyzed with *CH Instruments, Inc.* software. A three electrodes configuration was used, with working, reference and counter electrodes. The working electrode, described in the previous paragraph, has a *disk*, where the semi-reaction of reduction takes place and a *ring*, that it is used to oxidize peroxide ions. As the reference electrode, that has a defined and stable equilibrium potential, an Ag/AgCl electrode was chosen and as counter electrode (in order to close the electrical circuit) a Pt wire. The electrolyte was a N₂- or a O₂-saturated 0.1 M KOH in aqueous solution (Figure 5.5). In order to have a rapid comparison with the literature, the potentials, that were measured with respect to reference electrode, were referred to reversible hydrogen electrode (RHE), using the *Nernst* equation (5.1):

$$E_{RHE} = E_{Ag/AgCl} + E_{Ag/AgCl}^0 + 0.059pH \quad (5.1)$$

where E_{RHE} is the potential measured with respect to the reference electrode, $E_{Ag/AgCl}$ is the potential measured with respect to Ag/AgCl electrode, $E_{Ag/AgCl}^0$ is the standard potential of Ag/AgCl electrode, that is equal to 0.197 V at 25°C, 0.059 is the *Nernst* number and pH is equal to 13 for 0.1 M KOH solution.

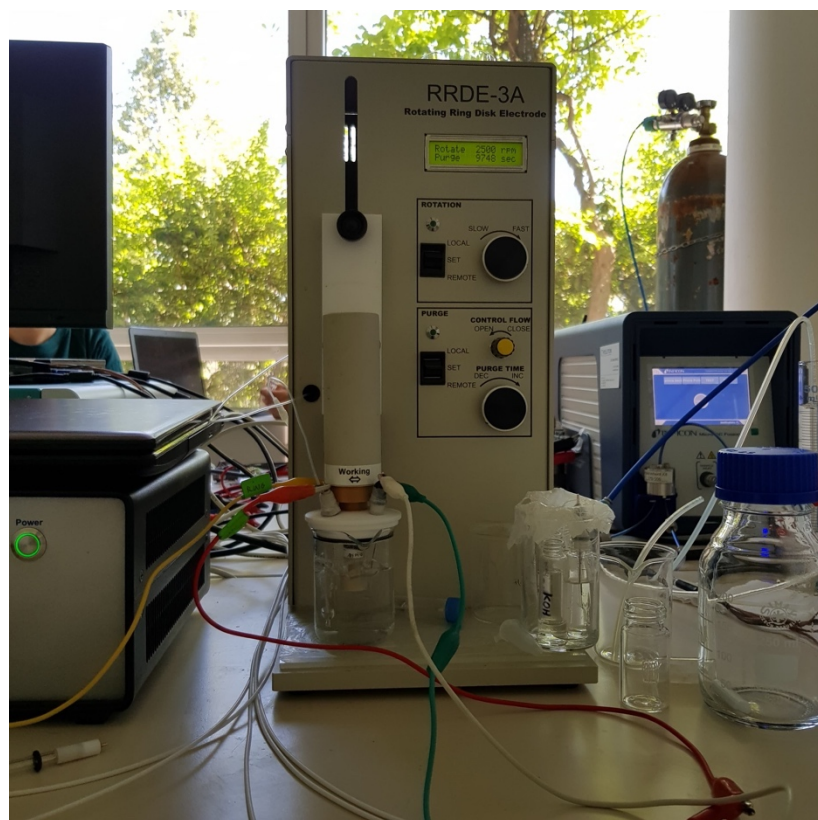


Figure 5.5: RRDE-3A.

The first test that was carried out is *cyclic voltammetry* (CV). CV was carried out first in N₂-saturated 0.1 M KOH solution and then, with a continuous flow of oxygen, in O₂-saturated 0.1 M KOH solution. The settings were maintained the same in all cases, with a scan rate of 10

mV/sec in a range of potential between 1.16 V vs. RHE and 0.16 V vs. RHE. CV measurements [66] provide a graph of the resulting current as function of the applied potential, allowing to identify each oxidation-reduction reaction, that occurs in that potential range and in that conditions. Scanning is run going from high potentials to low potentials and then vice versa for a number of cycles such that the sample is stable and, therefore, there are not differences from previous cycle. The graph can show some peaks, that can be upward, representing an oxidation, or downward, representing a reduction.

The area comprised between two branches is function of capacitive property of each sample, while the resulting current depends on their conductivity. As example a sample with a big area and a high current is both capacitive and conductive.

The *linear sweep voltammetry* (LSV) or *rotating disk electrode* (RDE) [67] is an electrochemical measurement, where a fixed potential range is employed. Contrarily to CV, in the LSV the potential moves only in one direction, that is from high potentials to low potentials. The test was performed with a scan rate of 5 mV/sec and with rotating working electrode at different speeds (400, 625, 900, 1225, 1600, 2025 and 2500 rpm) in O₂-saturated solution. As the previous case, a *I-E* graph is obtained. The typical curves are constituted by an about plateau at high potentials. Overlapping the curves at different speeds, it is possible to highlight the onset potential of reduction and, going in the high potential region and fixing a value of it, the current on the plateau area should increase, when speed increases. This type of analysis is important because it represents an indirect measure for the obtainment of number of transferred electrons and, therefore, to understand if the reaction follows four-electron pathway or two-electron pathway. In particular, by fixing a value of potential in the plateau area, that corresponding in an area controlled both by mass and charge transfer and taking the corresponded value of current for each curve, it is possible to elaborate the *Koutecky-Levich* plot. It theoretically provides a number, that moves between 2 and 4. If it is close to 2, it means that the reaction follows the undesired pathway, whereas it is close to 4 (usually higher than 3.5), it follows the four-electron pathway. The plotting is formed according to equation 5.2:

$$\frac{1}{I} = \frac{1}{I_K} + \frac{1}{\beta\omega^{1/2}} \quad (5.2)$$

where *I* (A) is the resulting current, *I_K* (A) is the kinetic current from the electrochemical reactions and corresponds to the intercept of *I⁻¹-ω^{-1/2}* graph with the vertical axis, *ω* is the angular rotation rate of the electrode, expressed in rad/s, and *β* is the most important parameter because it contains the number of transferred electrons (*n*) and, specifically it is given by the equation 5.3:

$$\beta = 0.62nFC_{O_2}D_{O_2}^{2/3}\mu^{-1/6} \quad (5.3)$$

where *C_{O₂}* is the concentration of oxygen (mol/cm³), *D_{O₂}* is the diffusion coefficient of oxygen (cm²/s) and *μ* is the kinetic viscosity (cm²/s). Usually, a material is considered good for the ORR if *n* is greater or equal to 3.5.

The *rotating ring-disk electrode* (RRDE) analysis allows the direct measurement of number of the transferred electrons number. The test was performed with a scan rate of 5 mV/sec, a disk potential range of 0.16-1.16 V vs. RHE, a speed of 2500 rpm and an applied ring potential of

1.16 V vs. RHE in O₂-saturated solution. It provides as output the disk current (I_D) and the ring current (I_R). Given these values, the number of transferred electrons is calculated by the equation 5.4:

$$n = \frac{4I_D}{I_D + \frac{I_R}{N}} \quad (5.4)$$

where N is the collection efficiency of RRDE. In adding, it is possible to calculate the percentage of produced peroxide, according the equation 5.5:

$$\% H_2O_2 = 200 \frac{I_R/N}{I_D + \frac{I_R}{N}} \quad (5.5)$$

The *electrochemical impedance spectroscopy* (EIS) [68] consists on the application of AC voltage to the system and on the obtainment of an AC current as function of the frequency. Contrarily to the other electrochemical measurements, it induces small perturbations from the equilibrium state in order to have a linear response. This test was run in order to gain insight on the material activity towards ORR. In fact, EIS allows to consider separately intrinsic conductivity, electron transfer and diffusion, because they are three phenomena that occur at different frequencies.

In this case, it was performed with an AC signal of 10 mV amplitude and 100 kHz-10 mHz frequency range, a rotating speed of 2500 rpm and a disk potential of 0.66 V vs. RHE in O₂-saturated solution. The signal, that was applied to the system, was (eq. 5.6):

$$E = E_0 \sin(\omega t) \quad (5.6)$$

where E is the applied potential at time t , E_0 is the signal amplitude, ω is the angular frequency. Also, the current response (I) is sinusoidal with the same frequency, but with a different phase φ and amplitude I_0 (eq. 5.7):

$$I = I_0 \sin(\omega t + \varphi) \quad (5.7)$$

At this point, it is possible to define the impedance Z (eq. 5.8):

$$Z = \frac{E}{I} = \frac{E_0 \sin(\omega t)}{I_0 \sin(\omega t + \varphi)} = Z_0 \frac{\sin(\omega t)}{\sin(\omega t + \varphi)} \quad (5.8)$$

Using Euler's equation, the impedance can be also expressed as (eq. 5.9):

$$Z(\omega) = \frac{E}{I} = Z_0 e^{j\varphi} = Z_0 (\cos \varphi + j \sin \varphi) = \text{Re}(Z) + j \text{Im}(Z) \quad (5.9)$$

where j is the imaginary unit. In order to highlight the real and imaginary part. The two contributions can be plotted in the so-called Nyquist plot, i.e. $\text{Re}(Z)$ vs $-\text{Im}(Z)$. In the right area of the graph there are the values calculated at low frequencies, whereas in the left the values calculated at high frequencies.

In addition, the results of EIS analysis were compared to an equivalent circuit, that is an electrical model able to include all different phenomena that take place in the system. Here, it was used the electrical circuit in the Figure 5.6, that is composed by resistances and capacitances. In particular, R_s , that is the internal resistance and is only function as the electrolyte conductivity and the electrical contact of the material. R_t and C_t are the resistance and the capacitance linked to electronic transport, respectively. They are in parallel and are relative to intrinsic behavior of the material. Also, R_{ct} and C_{dl} are in parallel and they represent the resistance related to the charge transfer and the capacitance related to the double layer, respectively. The effect of this second parallel can be seen to lower frequency than the first one, because it is linked to ORR reactions that is intrinsically slower than the electronic transfer.

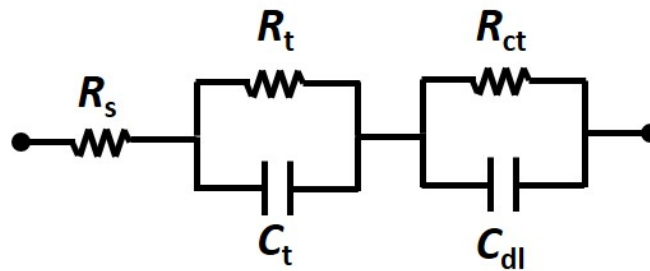


Figure 5.6: Electrical equivalent circuit.

With *chronoamperometry* (CA) measures the variation of the working electrode current, as function of time at fixed applied potential, is used in order to verify the catalyst stability with long-life cycling. The test was performed with a disk potential of 0.66 V vs. RHE, a rotation speed of 2500 rpm and for 15,000 seconds.

5.4 CO₂RR characterization

Among the synthesized samples, only that one, that shown a satisfactory catalytic activity, were tested like: NG2, NG2_S, NG2_SMn, NG2_SFe. In addition, also NG2_Mn, NG2_Cu and NG2_Co were tested. After electrode and cell preparation, electrochemical tests were carried out, consisting in CA and analysis of gaseous and liquid products through chromatography.

Also, in this case, in order to have a rapid comparison with the literature, the potentials, that were measured with respect to reference electrode, were referred to reversible hydrogen electrode (RHE), using the *Nernst* equation (5.10):

$$E_{RHE} = E_{Ag/AgCl} + E_{Ag/AgCl}^0 + 0.059pH \quad (5.10)$$

where E_{RHE} is the potential measured with respect to the reference electrode, $E_{Ag/AgCl}$ is the potential measured with respect to Ag/AgCl electrode, $E_{Ag/AgCl}^0$ is the standard potential of Ag/AgCl electrode, that is equal to 0.197 V at 25°C, 0.059 is the *Nernst* number and pH is equal to 6.8 for CO₂-saturated 0.1 M KHCO₃ solution.

5.4.1 Electrode preparation

As for the preparation of the electrodes for ORR, also in this case the procedure relied on the preparation of a paste and its deposition on a substrate. The paste was similar to previous one: in fact, 2 mg sample (Figure 5.7) were immersed in 180 μl Nafion perfluorinated ion-exchange resin (5% wt.) and 420 μl isopropanol. Also, in this case, the paste was stirred for about 30 minutes in order to have a uniform dispersion.

The substrate was a carbon paper (GDL 28 BC, Sigracet), with dimension of was 1x1.5 cm^2 . For each sample, two electrodes were prepared with a loading equal to 0.66 mg/cm^2 . After deposition on substrate surface, the electrodes were left to dry overnight (Figure 5.7).

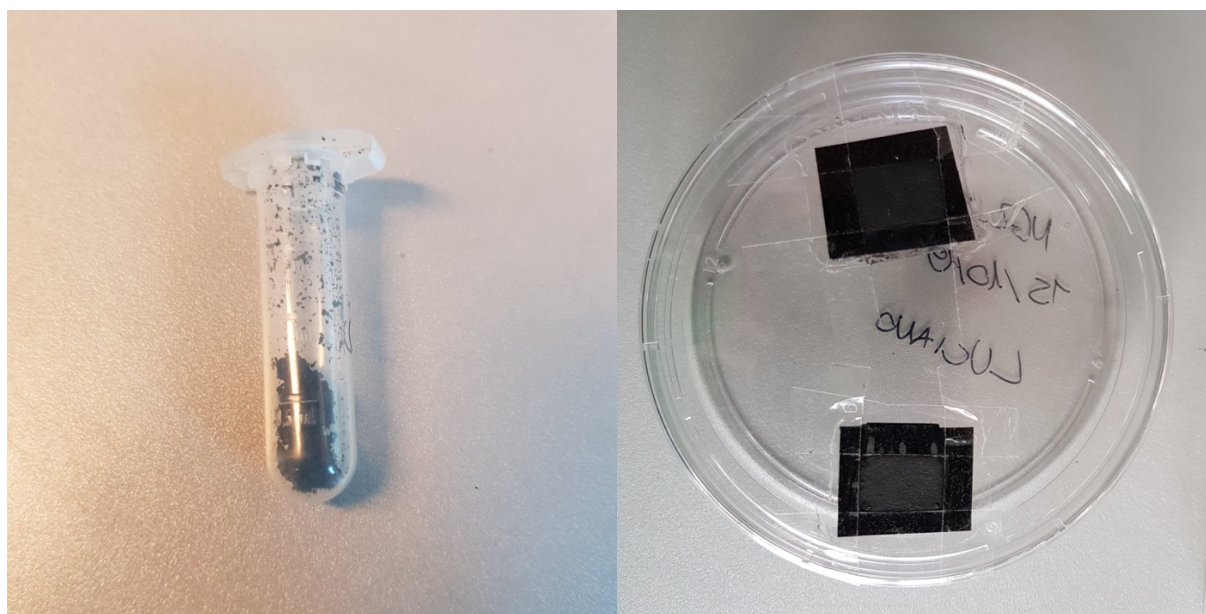


Figure 5.7: 2 mg sample before the mixing with Nafion and IPA (left) and electrodes with deposited ink (right).

5.4.2 Cell preparation

The reactor cell was constituted by a series of layers comprised between a metal rear and front plate (Figure 5.8). Inside the cell, cathode and anode chambers were separated by a proton exchange membrane (Nafion Membrane N117, Sigma-Aldrich).

The electrode with the sample represents the cathode of the cell. In particular, it was fixed on a T support, acting as current collector (Figure 5.8). The anode was constituted by a Pt foil. In addition, a special frame allowed to incorporate the Ag/AgCl reference electrode to the system. The cathode and anode sides were filled with a CO_2 -saturated 0.1 M KHCO_3 aqueous solution, that acted as electrolyte. In particular, at cathode 7 ml of solution was inserted, whereas at the anode 10 ml.

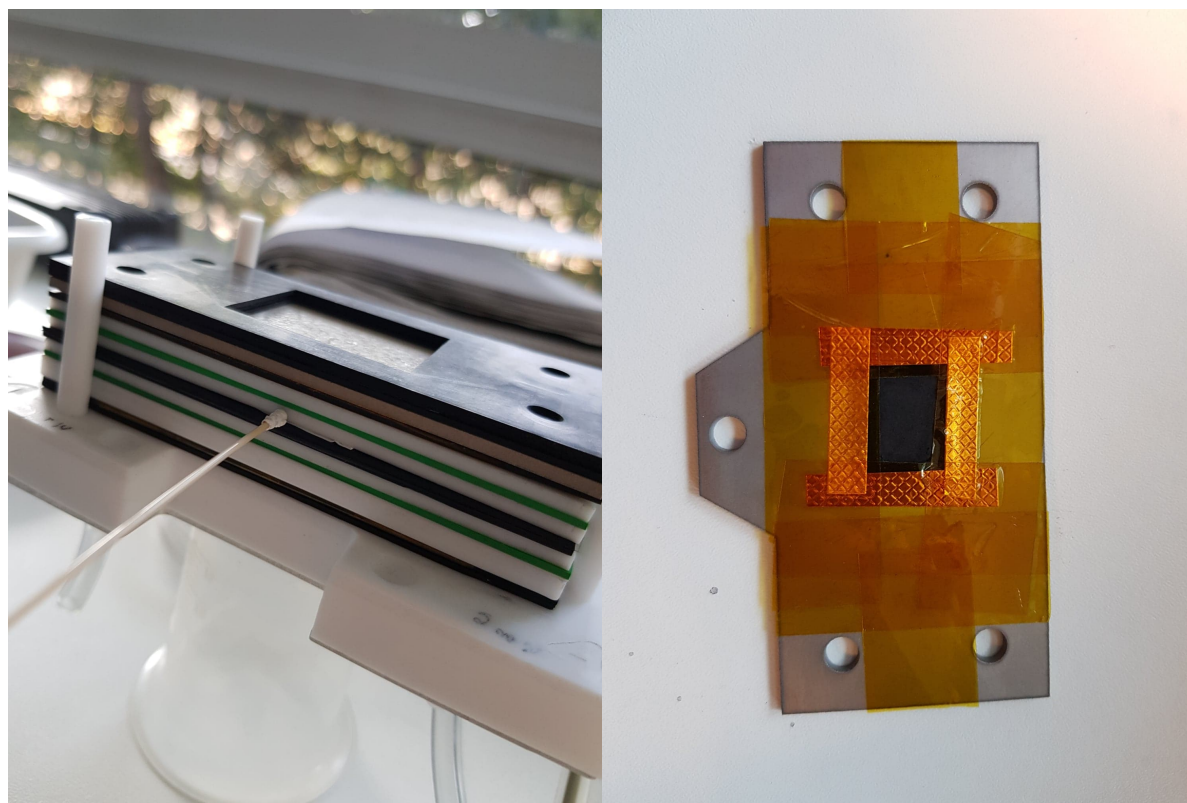


Figure 5.8: Flow cell with the series of frame and gaskets (left) and electrode supported on current collector (right).

5.4.3 Chronoamperometry

As described in the paragraph 5.3.2, the chronoamperometry allowed to measure the electroactivity and the catalyst stability. In this case, the cell was linked to the bipotentiostat CHI760D and the CA was performed for 1 hour with variable potentials (-0.79 V vs. RHE, -0.89 V vs. RHE), with a compensation of the ohmic potential drop.

Typical I-t curves are characterized by an initial sharp rise due to reduction of the material and the reaching of a plateau. Higher absolute values of current indicate a higher electroactivity.

5.4.4 Gas Chromatography

The characterization of gaseous products was carried out through gas chromatograph [69] (GC Fusion, Inficon) (Figure 5.9). It is constituted by a column containing the solid stationary phase. Gases interact with it through a physical adsorption and they are separated as function of retention time, that it is typical of each species. The gaseous products are carried to column through carrier gases (Ar and He), that do not react with the system and represent the mobile phase. It was also equipped by micro thermal conductivity detectors (micro-TCD) and a Genie filter to remove humidity.

Before each day of experiment, it was made a bake-out process to clean the column from eventual residual of previous tests. During the CA, the cell was also linked to two mass flow controllers, that let pass a constant flux of CO₂ through the anode and cathode, respectively. The CO₂ reduction occurred only in the cathode site, but the gas was fluxed in both sides to

avoid differences in pH among the two chambers. The gas flow was fixed to 15 ml/min at the cathode (except for the case of NG2_SMn, that was lowered to 8 ml/min at -0.89 V vs. RHE due to the instability of the resulting graph) and to 3 ml/min at the anode. Every three minutes for an hour, the gas chromatograph withdrew the gases produced inside the cathode side of the cell and recorded the concentration of each species as function of the retention time in order to monitor the evolution of gases.

Finally, the results were compared through Faradaic efficiency, that is the ratio between the current density for a specific reaction and the total current density (eq. 5.11):

$$FE_X = \frac{\dot{V}_{CO_2} C_x n F}{10^6 V_m I 60} \quad (5.11)$$

where FE_X is the Faradaic efficiency for a determined species (H or CO in this case), \dot{V}_{CO_2} is the flux of the gas through the cell in ml/min, C_x is the concentration of the formed species (H or CO) in ppm, n is the number of transferred electron (that is 2 for the reaction involved the formation of H or CO), F is the Faraday constant (96485.3365 C/mol), V_m is the molar volume (22.4 ml/ mmol) and I (mA) is the resulting current from CA test. The values C_x and t were calculated as the average of the last measurements during CA and CG process.



Figure 5.9: Gas Cromatograph GC Fusion, Inficon.

5.5.5 High performance liquid chromatography (HPLC)

The characterization of liquid products from CO₂RR reduction was run through high performance liquid chromatography (HPLC) [70].

The HPLC allows to separate liquid substances, that are present in a solvent, as function of the affinity between a stationary phase and a mobile phase, that flows through it. The stationary phase is composed by small particles of octadecyl silane chemically bonded to porous or non-porous silica or ceramic microparticles, with a diameter of the order of μm or less, inside a column. The sample is injected at the beginning of the column and is pumped through the stationary phase with a pressure in the order of tens of Mpa. If the substance has a higher affinity with the stationary phase than the mobile one, employs more time to pass through the column or vice versa. So, it has a higher or a lower retention time, respectively. At the end of the column, a detector (UV-VIS) measures constantly the exiting species, also allowing to identify them through the sample's adsorption light at different wavelengths (Figure 5.10). So, it carried out both a quantitative and a qualitative analysis. In fact, the result is a chromatogram, that plots the absorbance as function of retention time.

The test was carried out using a Shimadzu Prominence HPLC. The column was a ThermoScientific Dionex, whereas software to elaborate the data was Chromeleon Chromatography Data System. The analysis was run for 15 minutes with a wavelength of 210 nm.

As the formic acid was the only liquid product detected, the Faradaic efficiency for it was calculated, according to equation 5.12:

$$FE_{HCOOH} = \frac{C_{HCOOH} \cdot V \cdot d_{HCOOH} \cdot n \cdot F}{PM_{HCOOH} \cdot I \cdot t} \quad (5.12)$$

where C_{HCOOH} is the concentration of the formic acid (in ppm), d_{HCOOH} is formic acid density (that is equal to 1.22 g/ml), V is the volume of the catholyte (in l), n is the number of electrons (that is equal to 2 in this case), F is the Faraday constant (in C/mol), PM_{HCOOH} is the formic acid molar mass (that is equal to 46.03g/mol), I is the current (in mA) and t is the time of chronoamperometry (in seconds).

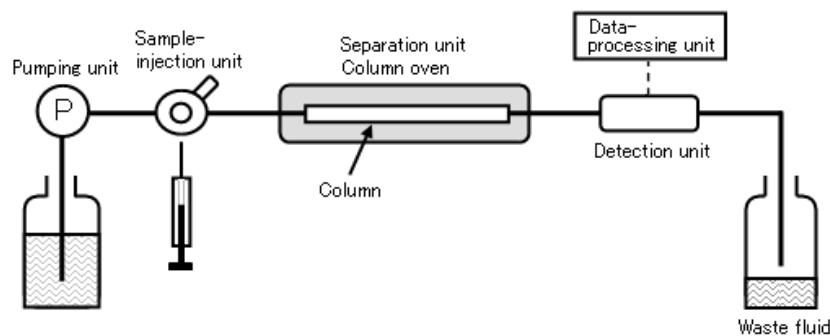


Figure 5.10: Scheme of a HPLC system [71]

6 Results and discussion

6.1 Physical, morphological and chemical characterization

6.1.1 Field Emission Scanning Electron Microscopy (FESEM)

In the figure 6.1 a FESEM image of NG2 sample is reported as a model, due to the fact that this magnification did not allowed to accurately investigate the effect of dopant elements on the rGO structure and only by means of TEM and XPS will be build a complete picture. In any case, it was useful to understand that rGO flakes did not undergo any damage after the reduction process, confirming the MW-assisted process is effective in fabricate graphene-based catalyst.

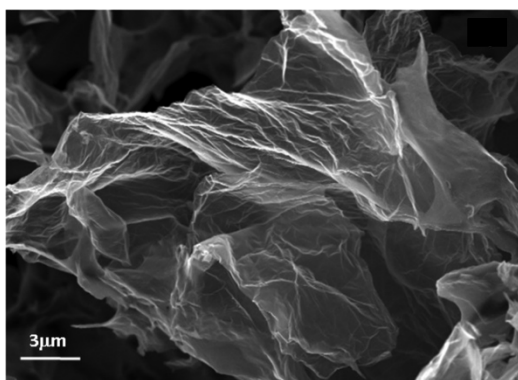


Figure 6.1: FESEM micrograph of NG2.

6.1.2 Transmission electron microscopy (TEM)

In TEM images at different magnifications, shown in Figure 6.2, rGO presents the typical curled structure, that was originated from the distortion of reduction process and the presence of dopant atoms. Nevertheless, the material appears uniform with no evident nanostructure present, meaning that the dopants were effectively incorporated in the structure. The only exception is constituted by NG2_SFe (Figure 6.2 i-j), which shows flakes completely decorated by nanocrystals and flakes with any crystals, such crystals have identified as hematite ($\alpha\text{-Fe}_2\text{O}_3$) from the Fast Fourier Transform (FTT) (Figure 6.3).

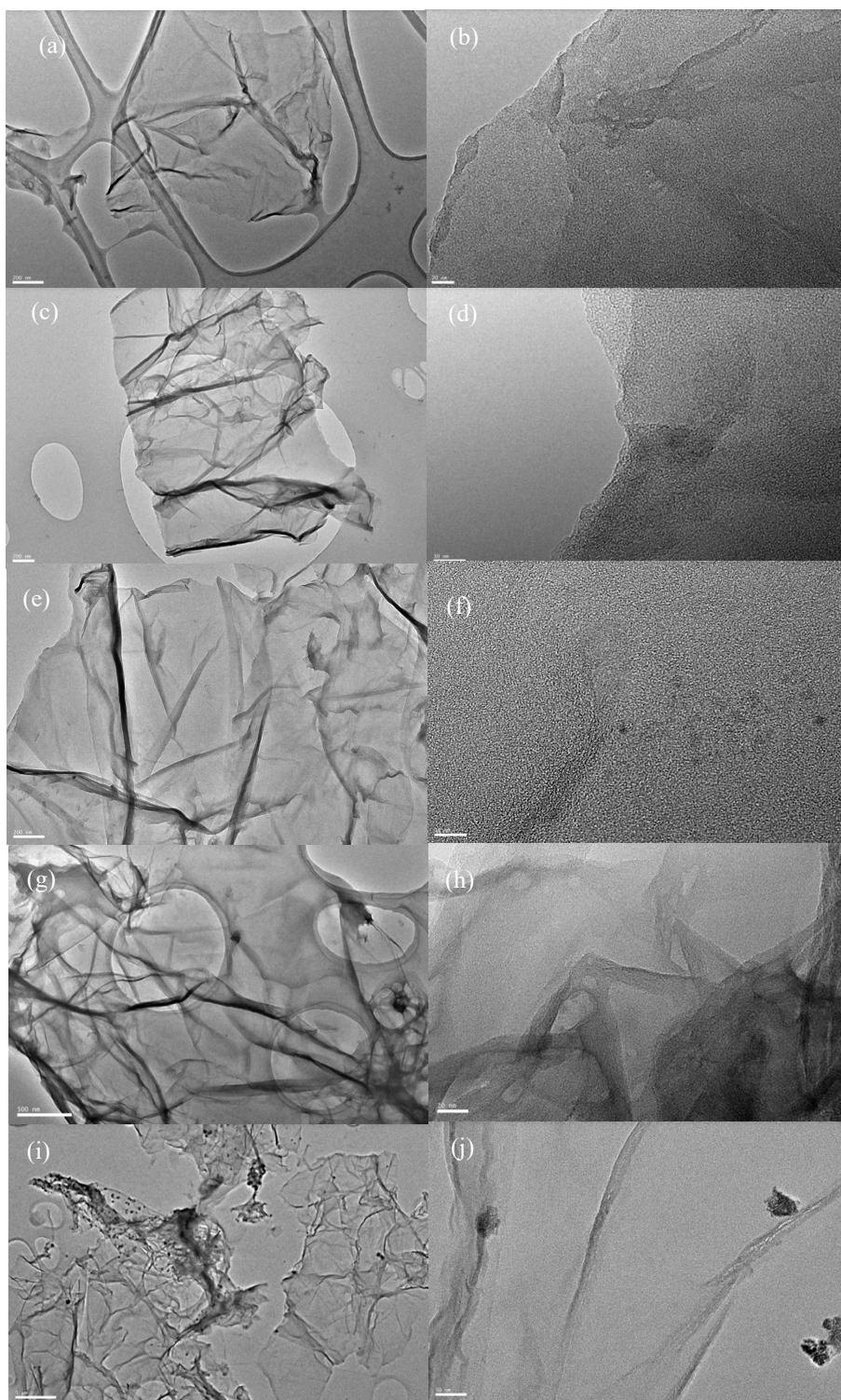


Figure 6.2: TEM images of NG2_S (a- scale: 200 nm, b-scale: 20 nm), NG2_Ni (c-scale: 200 nm, d-scale: 10 nm), NG2_SNi (e-scale: 500 nm, f-scale 20 nm), NG2_SMn (g-scale: 200 nm, h-scale:10 nm) and NG2_SFe (i-scale: 1 μ m, j-scale: 50 nm).

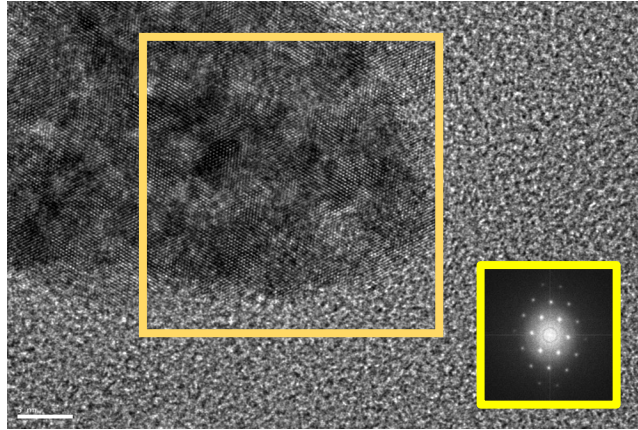


Figure 6.3: Fast Fourier Transform for NG2_SFe (scale: 9 nm).

The EDX spectrums, reported in Figure 6.4, confirm the presence of dopant element for all samples. Beyond the expected peaks, there are peaks related to C, Cu, Fe and Co, that are due the holey carbon copper grid (C, Cu) and to electromagnetic lenses (Co, Fe). In addition, in NG2_S (Figure 6.4a) other contaminants are present such as Na and Ca, whereas in NG2_SFe (Figure 6.4e) the presence of Fe into the material is confirmed by the more elevated height of the relative peak than the other samples.

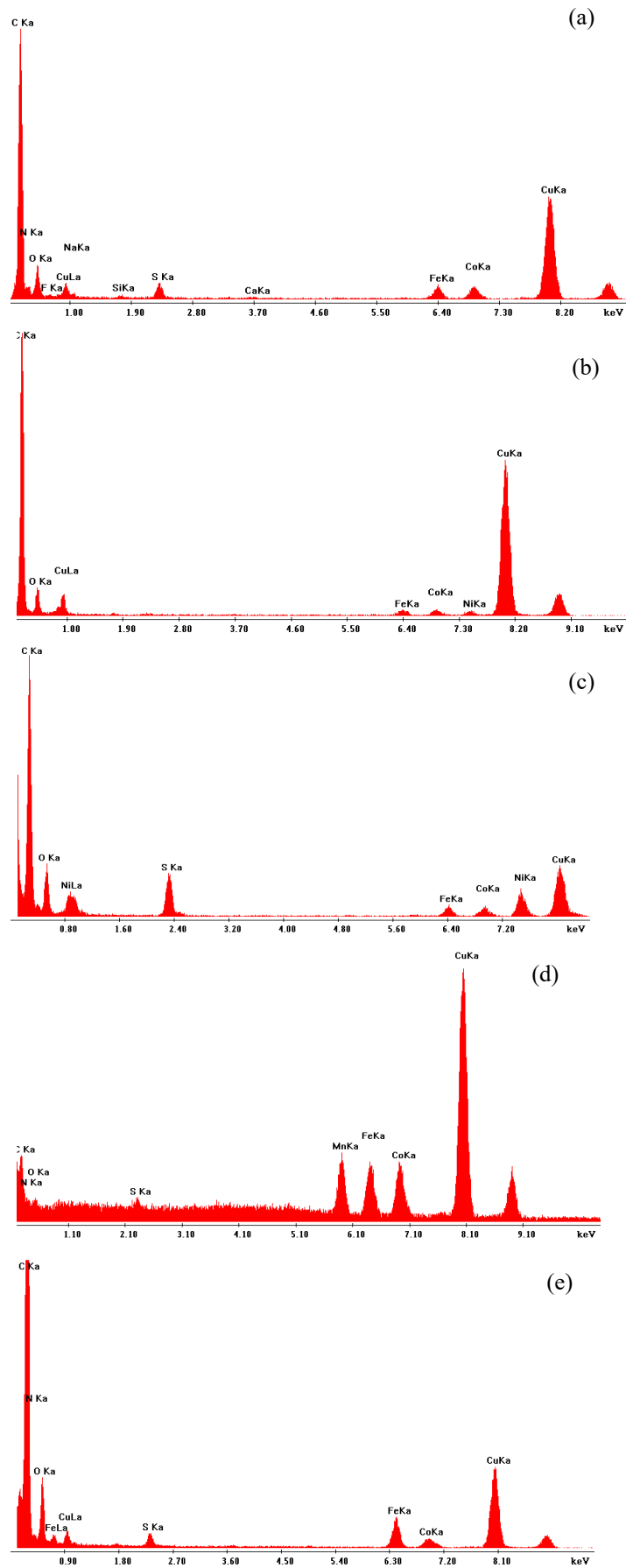


Figure 6.4: EDX for NG2_S (a), NG2_Ni (b), NG2_SNi (c), NG2_SMn (d), NG2_SFe (e).

6.1.3 X-ray Photoelectron Spectroscopy (XPS)

In order to deeply analyze the chemical composition of samples, also XPS was run and here the results are presented.

The results related to sample NG2 are not reported, since they can be found in [72].

As anticipated from TEM, survey spectra relative to each sample (Figure 6.5) showed that all elements that are incorporated in the rGO structure, are present. The only exception is the presence of sulfur (0.7 at. %) in NG2_Ni sample, probably due to contamination, given its low amount. In particular, from Table 6.1, where atomic concentrations of each element have been evaluated from high resolution spectra and listed, it was possible to calculate C/O ratio, that can be used to determine the effectiveness of the GO reduction. As it was stated in the theoretical part of this work (see section 2.3.5), the reduction of GO can be considered satisfactory if C/O ratio is not less than 4 [35]. Samples showed a ratio of about 4 or a slight larger. This means that the reduction of GO effectively took place, however the fraction of oxygen, that remained in the structure, is not negligible.

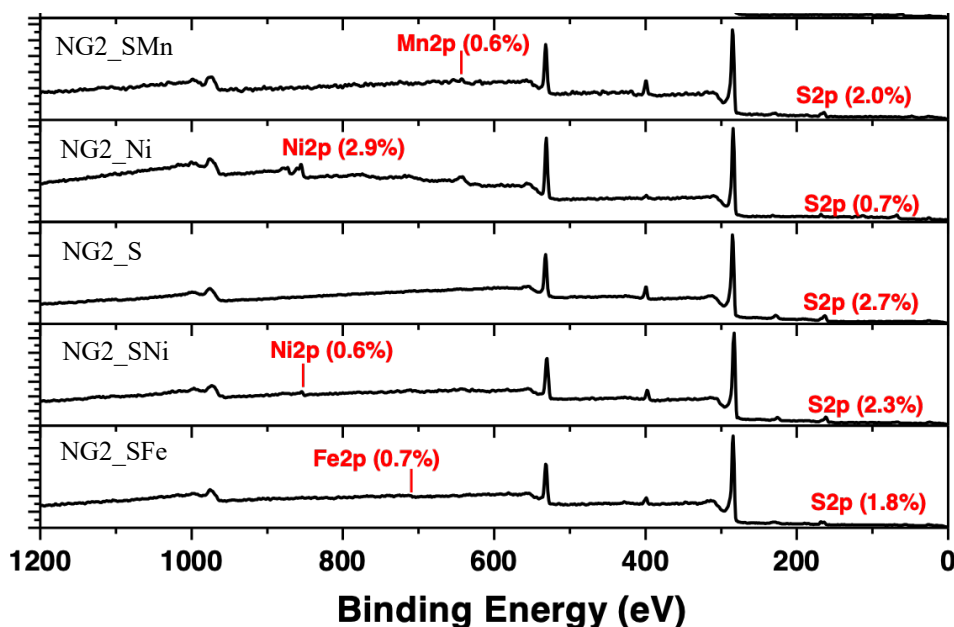


Figure 6.5: XPS spectra for all samples (survey).

Table 6.1: Atomic concentration of each element and C/O ratio from HR spectra.

Sample	Atomic concentration (at. %)					
	C1s	O1s	N1s	S2p	Others	C/O
NG2_Ni	75.0	19.3	2.1	0.7	Ni: 2.9	3.9
NG2_S	74.2	17.0	6.1	2.7	-	4.4
NG2_SNi	75.8	15.5	5.8	2.3	Ni: 0.6	4.9
NG2_SMn	73.4	17.2	6.8	2.0	Mn:0.6	4.3
NG2_SFe	76.3	16.8	4.5	1.8	Fe: 0.7	4.5

The analysis of the deconvolution spectra was reported in order to understand the oxidation state and the type of species that the same elements form in catalyst structure.

All the samples exhibit a similar C1s peak (Figure 6.6a), for this reason its deconvoluted spectrum was reported only for NG2_SFe because for other samples they can be considered similar to it (Figure 6.6b). In particular, the chemical shifts have been assigned to C-(C, H) at 284.52 eV, that was also the component with the highest percentage (55.36 %), C-(O, N, S) at 285.51 eV, C=O at 287.07, O-C=O and O-C-O at 288.63, and, finally, $\pi - \pi^*$ transition at 290.76 eV [72, 73]. In addition, *Garino et al.* [72] confirmed the same peaks also in NG2.

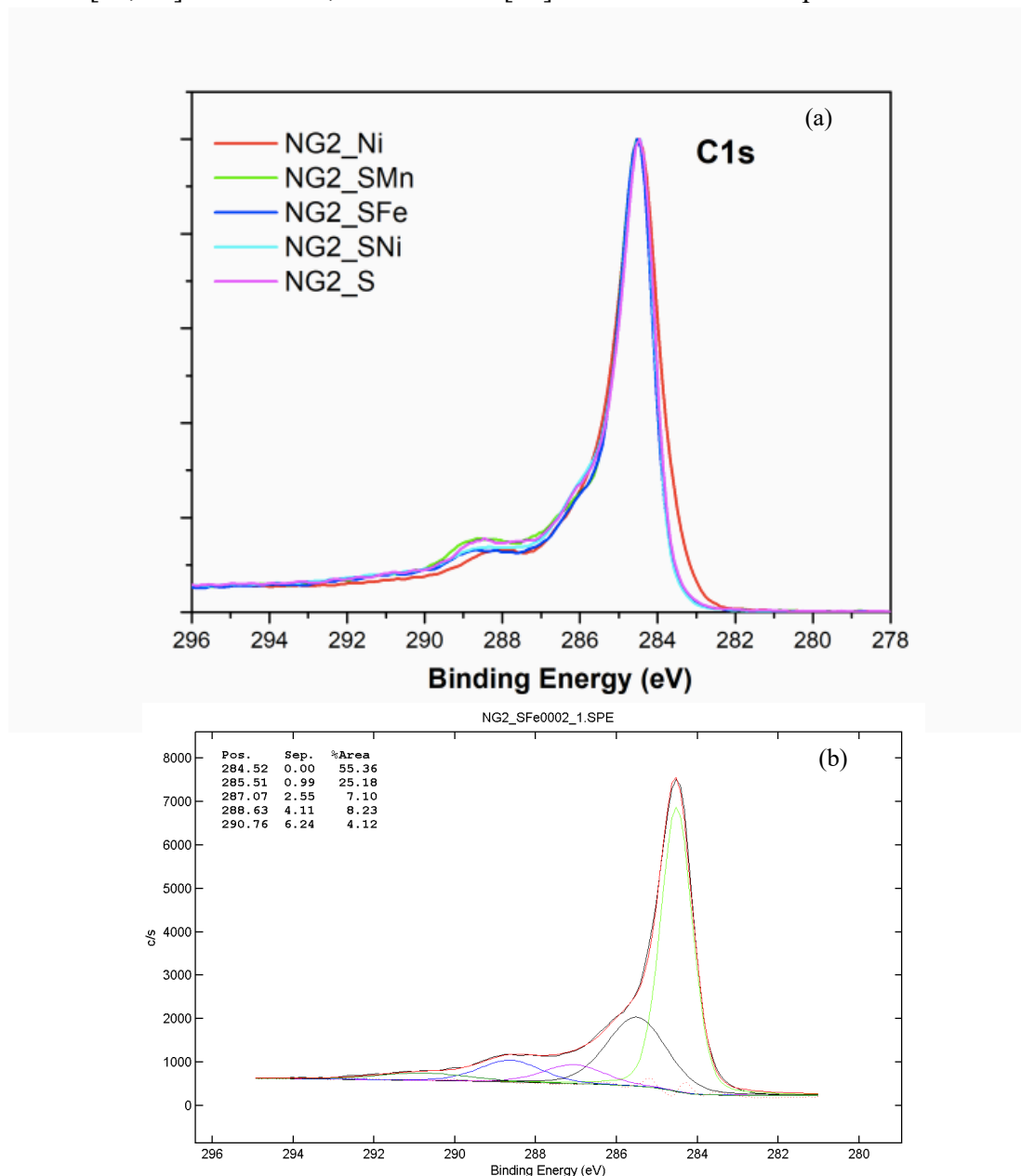


Figure 6.6: C1s peaks for the samples (a), C1s deconvolution spectra for NG2_SFe (b).

The N1s deconvolution spectra showed two peculiar peaks at 399 eV and 401 eV, that are assigned to pyrrolic-like nitrogen and graphitic-like nitrogen, respectively for all samples, including NG2 [72, 73]. In the Figure 6.7 was reported the N1s deconvolution spectra for NG2_SFe as example. Moreover, for NG2_SNi a third peak at 398.12 eV was detected and assigned to pyridinic-like nitrogen [74]. Analyzing the percentage of each component (Table 6.2), pyrrolic-like nitrogen was the component present with the higher concentration. In

particular, it was very high for NG2_SMn, in fact graphitic-like nitrogen was just 3.03 %. As graphitic-like nitrogen allows to improve ORR activity [11, 53], it is reasonable that for this sample it will be lower than the other ones. As opposite, it was remarkably higher for NG2_SFe and NG2_Ni (22.62 % and 30.05 %, respectively). In addition, the percentage of pyrrolic-like nitrogen decreased below 70 % for Ni-containing samples. The presence of pyridinic-like nitrogen in NG2_SNi is important because it make easier the adsorption of oxygen and the capture of electrons from current collector [11, 53].

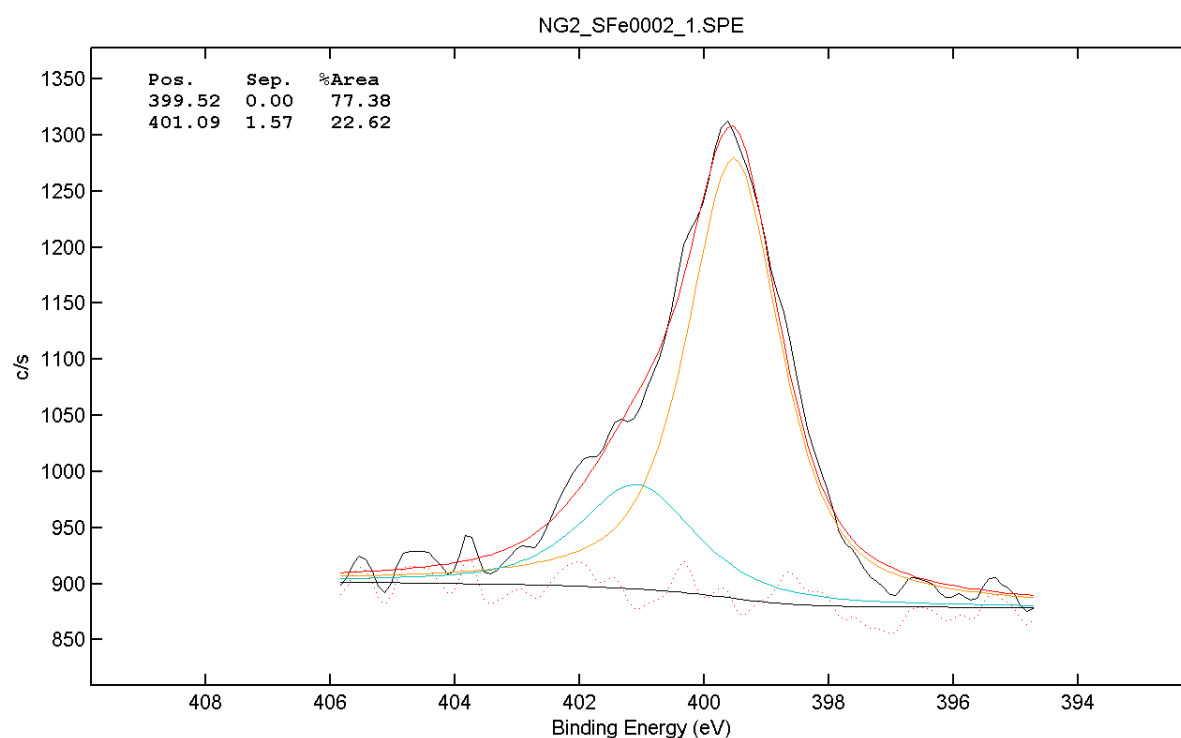


Figure 6.7: The N1s deconvolution spectrum for NG2_SFe.

Table 6.2: Percentage of nitrogen species for all samples.

Sample	Pyrrolic-like nitrogen (%)	Graphitic-like nitrogen (%)	Pyridinic-like nitrogen (%)
NG2_Ni	69.95	30.05	-
NG2_S	88.08	11.92	-
NG2_SNi	66.00	16.67	17.34
NG2_SMn	96.97	3.03	-
NG2_SFe	77.38	22.62	-

The S2p deconvolution spectra showed a variable number of peaks, that, in summary, can be assigned to sulfide, R-SH or sulphate. In particular, NG2_S and NG2_SNi (Figure 6.8) presented six peaks: the first two comprised between 161 eV and 163 eV are relative to sulfide, the two peaks comprised between 163 eV and 165 eV are relative to R-SH and, finally, the last two peaks comprised between 168 eV and 169 eV are relative to SO_x [75]. As the percentage

of the components for this two samples were very similar (Table 6.3), Ni atoms may not be coupled with the sulfur, but only with nitrogen. As regard NG2_SMn and NG2_SFe, only four peaks were detected: two comprised between 163 eV and 165 eV, that are relative to sulfide, and the other two comprised between 168 eV and 169 eV are relative to sulphate [75]. Analyzing the percentage of each component, it results that total presence of sulphate was remarkably higher in NG2_SMn and NG2_SFe (Table 6.3). However, sulfur, when is not linked with the oxygen, is able to active carbon atoms, but at the same time catalyzes the two-electron pathway for ORR, so, if the percentage of sulphate is low, also the efficiency probably will be low [55].

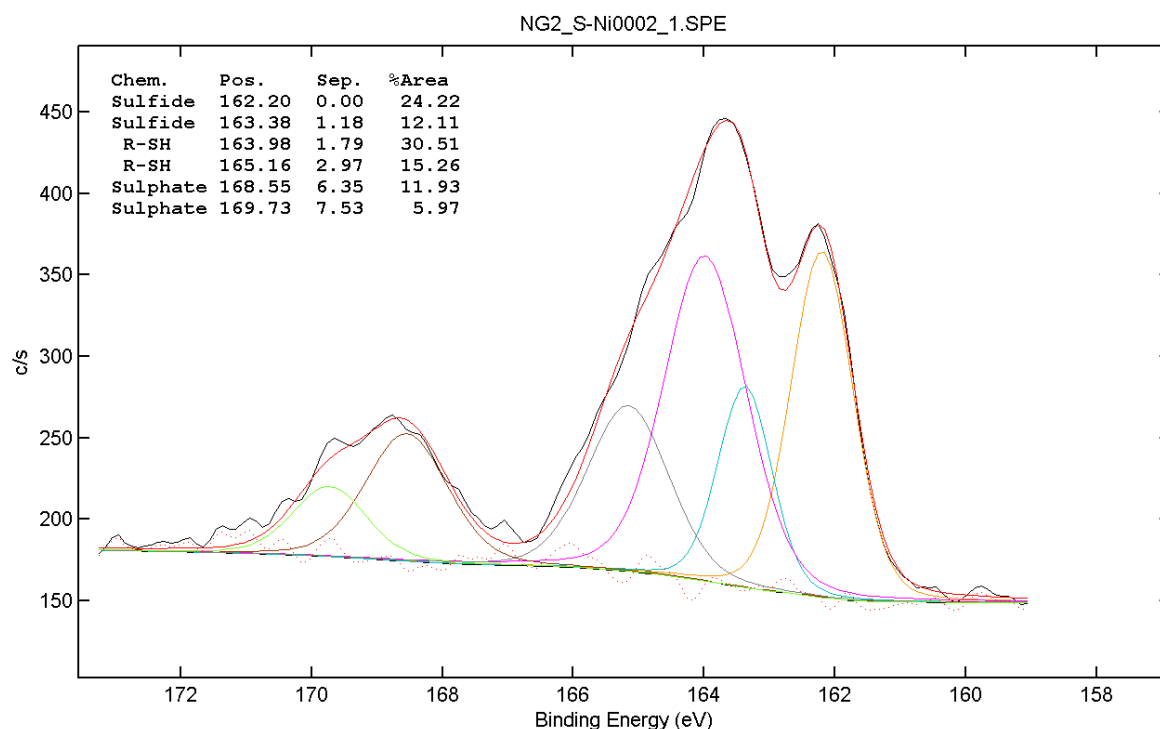


Figure 6.8: The S2p deconvolution spectrum for NG2_SNi

Table 6.3: Summary of the percentages of sulfur components.

Sample	Sulfide (%)	Total sulfide (%)	R-SH (%)	Total R-SH (%)	Sulphate (%)	Total sulphate (%)
NG2_S	22.20	33.3	30.79	46.18	13.68	19.92
	11.10		15.39		6.24	
NG2_SNi	24.22	36.33	30.51	45.77	11.93	17.90
	12.11		15.26		5.97	
NG2_SMn	42.26	63.39	-	-	24.41	36.61
	21.13		-		12.20	
NG2_SFe	33.72	50.58	-	-	32.95	49.42
	16.86		-		16.47	

The Ni2p deconvolution spectrum for NG2_Ni put in evidence peak and satellite features that are relative to Ni²⁺, however, this ions could form the oxide (NiO) or the hydroxide (Ni(OH)₂), so only a deeper refining can state it (Figure 6.9) [76]. However, it is worth noting that TEM analysis revealed the absence of any oxide crystalline structures [77].

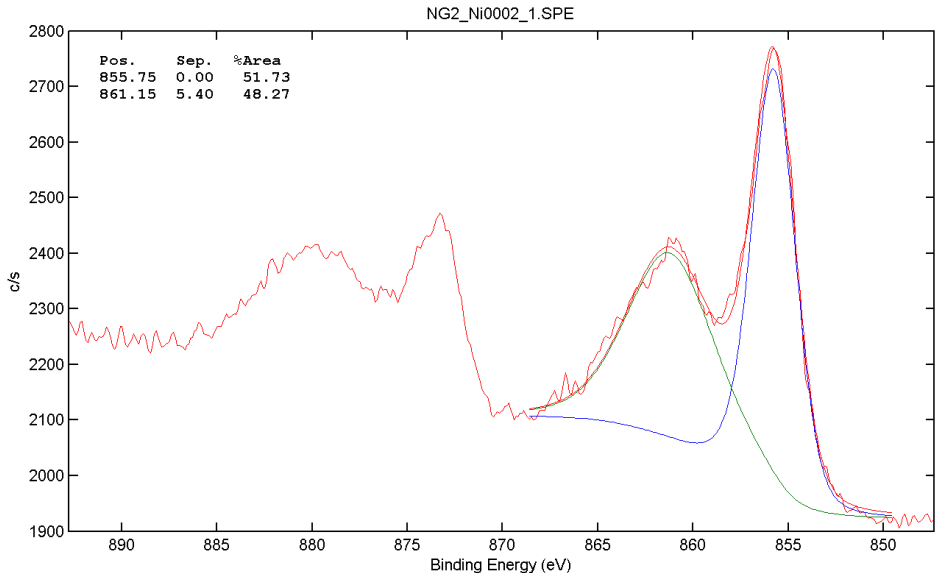


Figure 6.9: The Ni2p spectrum for NG2_Ni.

The Ni LMM deconvolution spectrum for NG2_Ni can be compared to several species, but, as the presence of sulfur contamination, it is reasonable that it is relative to NiSO₄•6H₂O (Figure 6.10 a-b) [78].

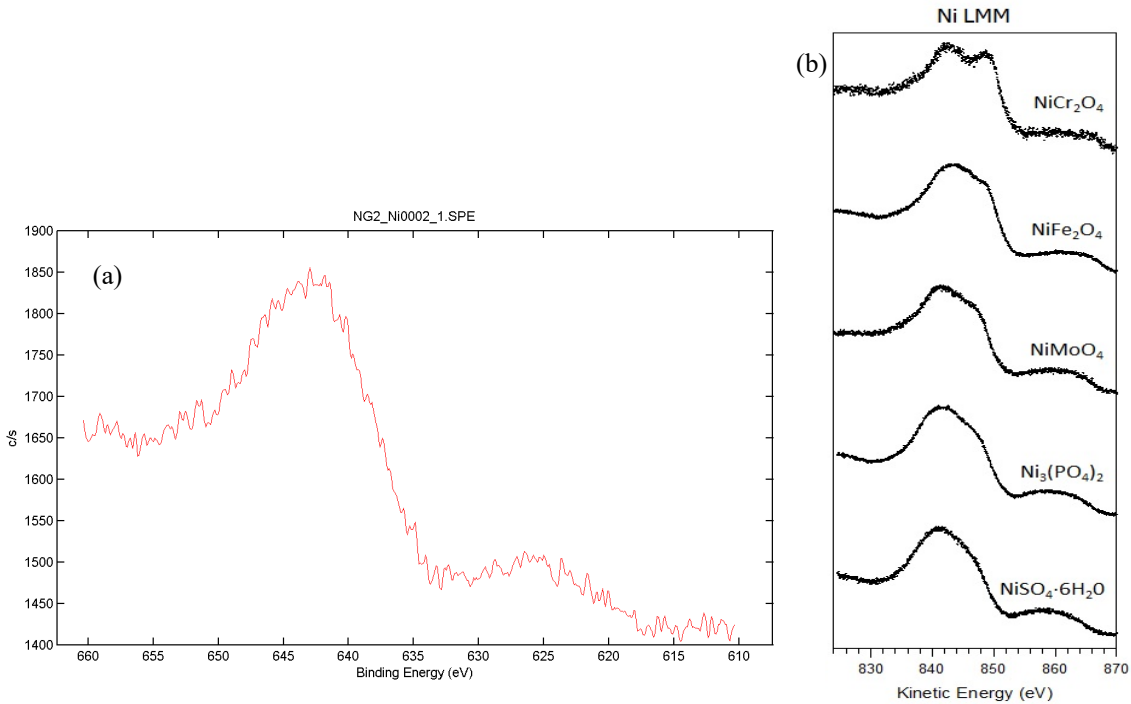


Figure 6.10: The Ni LMM spectrum for NG2_Ni (a) and Ni LMM typical species (b) [78].

Equal results were detected from the Ni2p deconvolution spectrum and the Ni LMM spectrum of NG2_SNi than NG2_Ni, so the graph was not reported.

Mn was investigated through two doublets: Mn2p and Mn3s, the relative deconvolution spectra are in Figure 6.11 a-b. In particular, for Mn3s doublet the average oxidation state was calculated and revealed that ΔE , i.e. the peak splitting, was comprised between 5.7 eV and 6.2 eV [79]. This ΔE corresponds to +2 as oxidation state, so, since oxidized species was not detected from TEM, Mn^{2+} is present as metal ion into the matrix or on the surface. A further refining is needed to confirm the hypothesis.

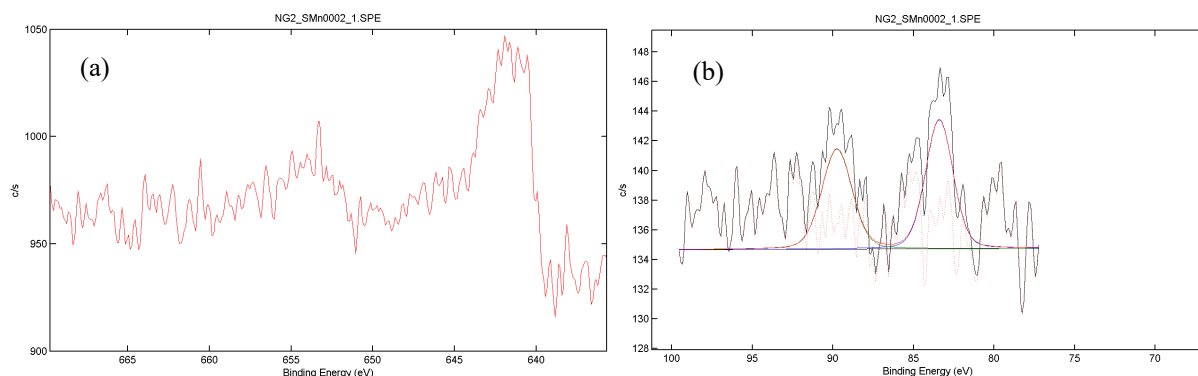


Figure 6.11: The Mn2p (a) and Mn3s (b) spectra of NG2_SMn.

Finally, despite the noisy signal of the Fe2p deconvolution spectrum, the peak relative to Fe_2O_3 can be clearly distinguished around 710 eV (Figure 6.12), as it was seen with TEM. This also confirmed by the presence of Fe_2O_3 oxide phases.

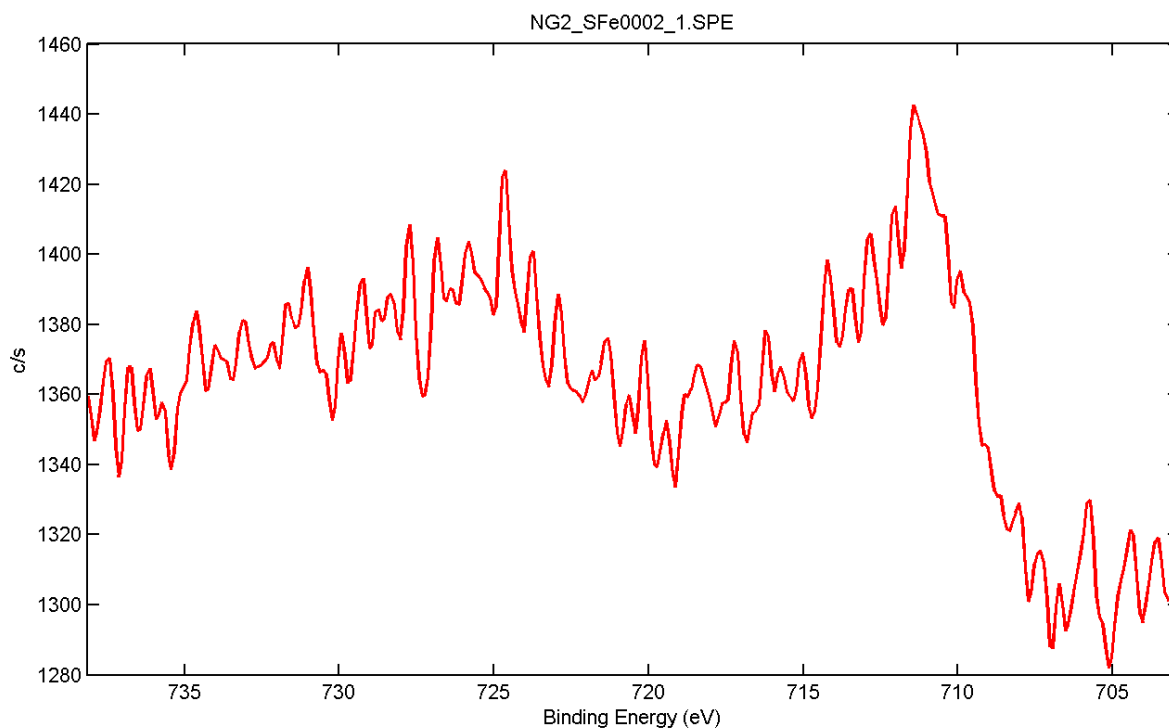


Figure 6.12: The Fe2p deconvolution spectrum for NG2_SFe.

6.2 Electrochemical properties for ORR

In this chapter the results of electrochemical test are reported, making a comparison of catalytic properties of the all as prepared materials. In the last part, each sample will be analyzed in the detail and compared with carbon-supported Pt nanoparticles (Pt-C) sample, assumed as reference.

6.2.1 Cyclic voltammetry

CV measurements showed that all samples tested in N_2 -saturated 0.1 M KOH solution did not present redox peaks in the potential range between 0.16 and 1.16 V vs. RHE. On the contrary, the same samples tested in O_2 -saturated 0.1 M KOH solution presented a reduction peak, confirming the ORR activity. As regard the anodic peak, it is less evident due to the high capacitive behavior of the sample. In particular, the reduction peak was clear in the case of NG2 at 0.76 V vs. RHE (Figure 6.13), whereas in the other materials was sometimes just hinted (Figure 6.14). Then, some evaluations can be carried on the onset potential. In NG2_S, NG2_Ni and NG2_SFe, it was around 0.76 V vs. RHE, but in NG2_SNi and NG2_SMn, it was beyond 0.56 V vs. RHE.

In addition, from the graph it is possible to see the difference in capacitance, that is linked to conductivity, and the presence of electrocatalytic sites, though the area comprised inside each curve. As expected, increasing the number of different elements into rGO structure decreased the capacitance. That is maximum for NG2 because nitrogen was the only dopant element, whereas it was significantly lower for samples like NG2_SNi or NG2_SMn, since they were doped with nitrogen, sulfur and a metal, increasing the probability to close the voids. The variations in capacitance depended also on the size of the specific atoms and the species, that they formed, and, in this context, it is particular the case of NG2_SNi, that showed a very narrow curve with value of current near to zero. Among these materials, NG2_SFe was different because it had a larger capacitance and a reduction peak at lower potential than other two samples.

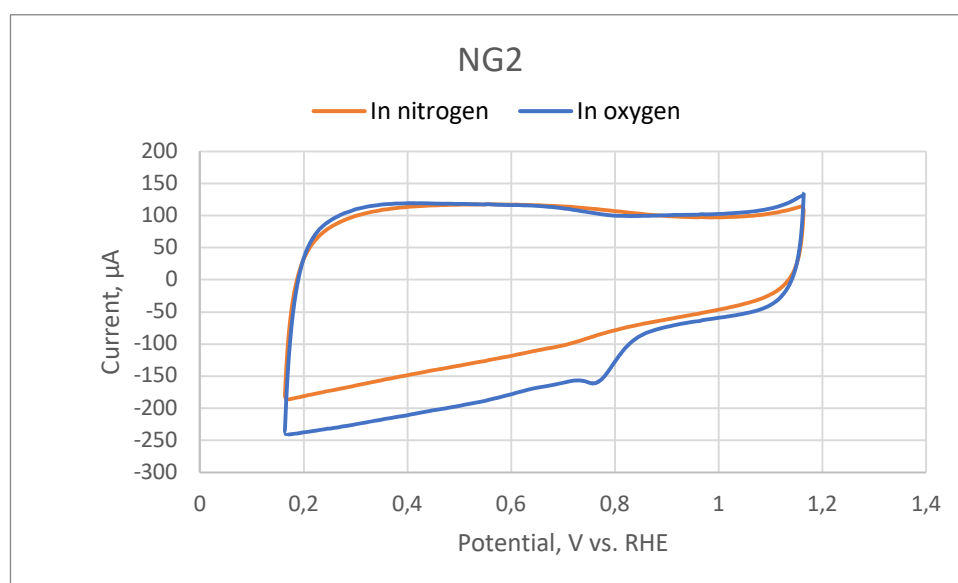


Figure 6.13: Cyclic voltammetry (CV) of NG2 in N_2 - and O_2 -saturated 0.1 M KOH solution.

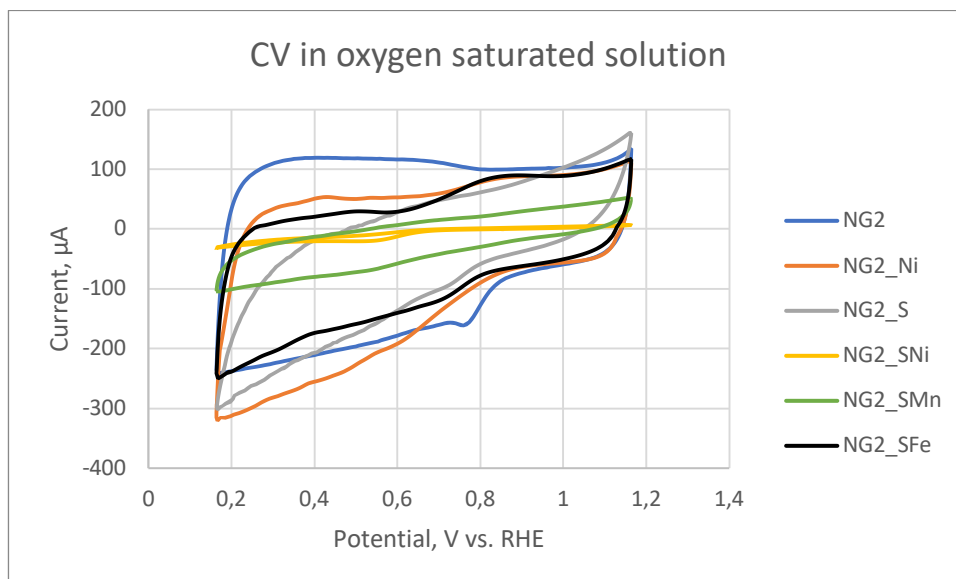


Figure 6.14: Cyclic voltammetry (CV) of NG2, NG2_Ni, NG2_S, NG2_SNi, NG2_SMn in O₂-saturated 0.1 M KOH solution.

6.2.2 Rotating disk electrode

The efficiency of dopants was calculated by RDE measurements, rotating the working electrode at different speeds in a potential range between 0.16 V vs. RHE and 1.16 V vs. RHE in O₂-saturated 0.1 M KOH solution. The number of transferred electrons (n) was calculated by Koutecky-Levich equation, fixing a value of potential. However, in most of tested samples the resulting n was invalid because the relative error was too big at the considered potential window, as reported by Vidal-Iglesias et al. [82]. For the NG2_S (Figure 6.15) and NG2_SMn (Figure 6.16), the resulting n was 3.22 and 3.08 at 0.26 V vs. RHE, respectively. Such values would show the concurrence of four-electron and two-electron reactions, determining a low efficiency for the purpose, but probably these results were underestimated by the reasons mentioned before.

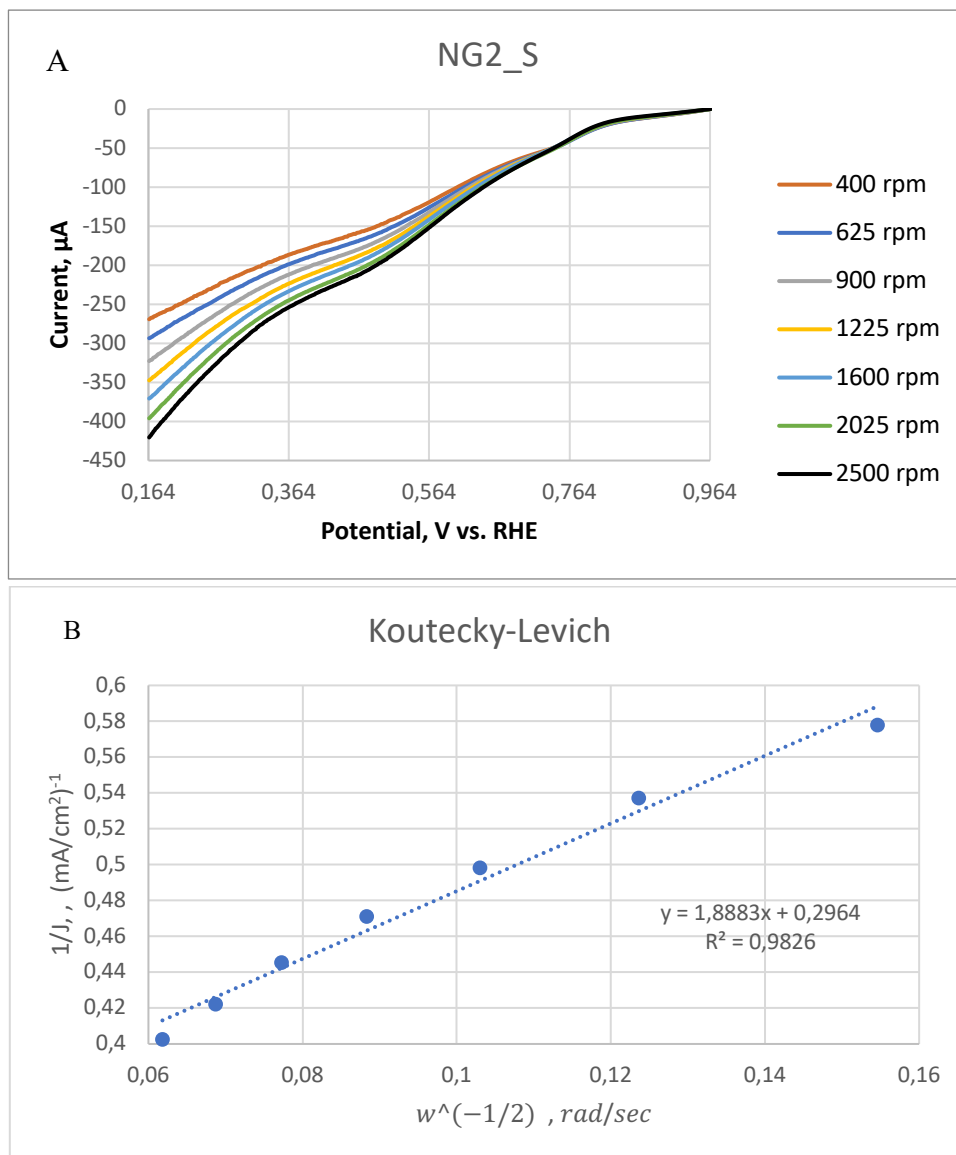


Figure 6.15: a) Rotating disk electrode (RDE) voltammograms of NG2_S in O₂-saturated 0.1 M KOH solution at different rotation speeds, b) Koutecky-Levich plot of J^{-1} vs $w^{-1/2}$ at 0.26 V vs. RHE.

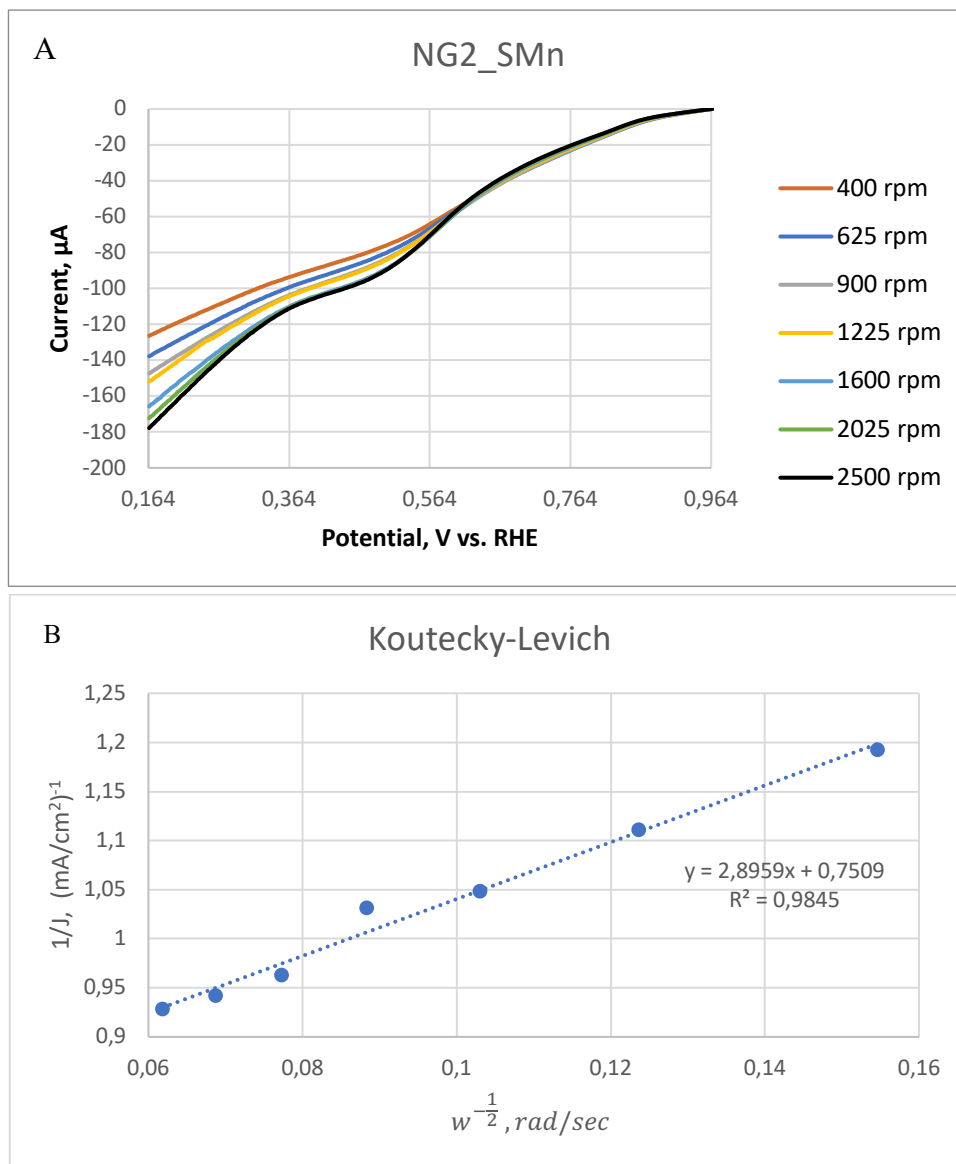


Figure 6.16: a) Rotating disk electrode (RDE) voltammograms of NG2_SMn in O_2 -saturated 0.1 M KOH solution at different rotation speeds, b) Koutecky-Levich plot of J^{-1} vs $w^{-1/2}$ at 0.26 V vs. RHE.

In the figure 6.17, the RDE graph was compared at constant speed of 1600 rpm for each sample in order to establish the onset potential (E_0) for the reduction reaction. This was done, calculating the intersection between the linear fitting of the curve for current values close to zero and the linear fit of the curve in the range, where the current increased constantly. The results, that were listed in the table 6.4, showed that E_0 is around 0.86 V vs. RHE for all samples, except for NG2_SNi and NG2_S because it was a bit higher (0.78 and 0.81 V vs. RHE, respectively) and for NG2_SMn because it was a bit lower (0.90 V vs. RHE).

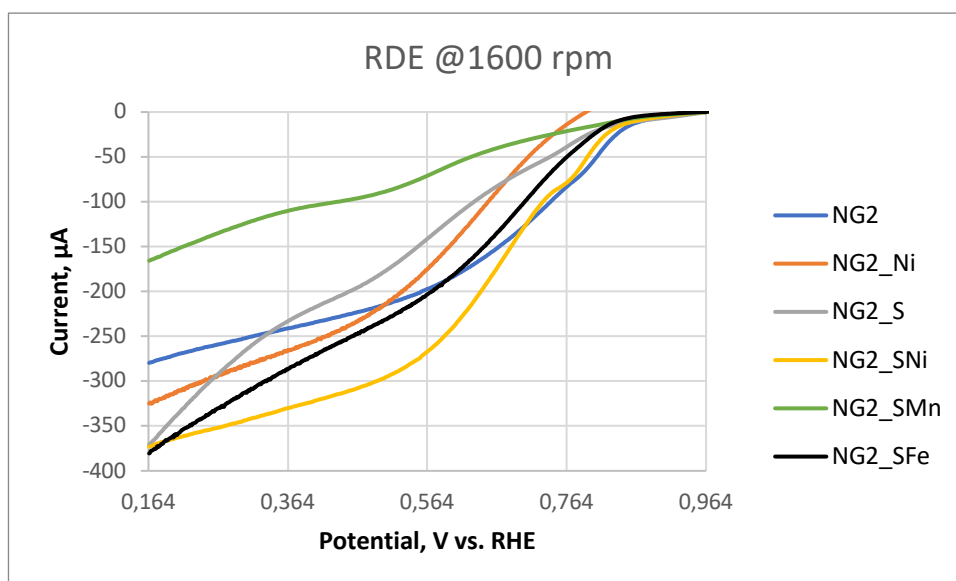


Figure 6.17: RDE measurements at 1600 rpm.

Table 6.4: List of onset potentials (E_0) for all samples.

Sample	E_0 (V vs. RHE)
NG2	0.866
NG2_Ni	0.859
NG2_S	0.813
NG2_SNi	0.786
NG2_SMn	0.898
NG2_SFe	0.848

6.2.3 Rotating ring disk electrode

RRDE measurements defined the catalytical behavior of samples in a better way by means of disk and ring currents, the number of transferred electrons and the percentage of produced hydrogen peroxide. An efficient material will be defined by a high disk current and a low ring current, a number of transferred electron higher than 3.5 and as close as possible to 4, so with a minimum production of hydrogen peroxide. For a best understanding of the catalyst efficiency of the materials, the results were compared to commercial Pt-C.

The disk currents showed similar trends for all samples as function of potential, except for NG2_SMn, that was characterized by a lower disk current than the others (Figure 6.18). The comparison with Pt-C clarified that it maintained the highest electrocatalytic activity, but some samples as NG2_Ni, NG2_SNi and NG2_SFe were not too far, especially at earlier potentials. A list of the resulting current at 0.36 V vs. RHE is present in the Table 6.5.

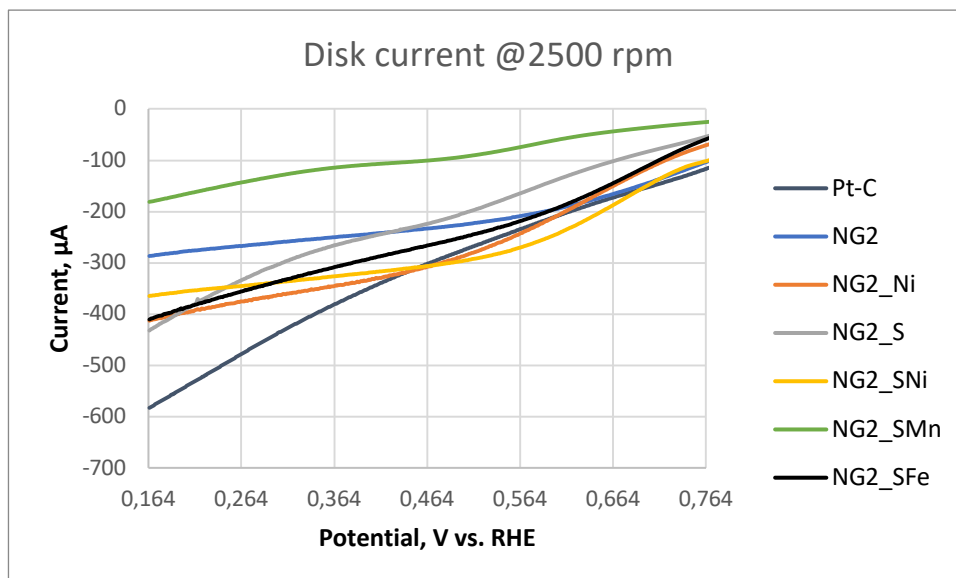


Figure 6.18: Disk current vs potential plot for NG2, NG2_Ni, NG2_S, NG2_SNi, NG2_SMn, NG2_SFe in O₂-saturated 0.1 M KOH solution.

Table 6.5: Disk current for NG2, NG2_Ni, NG2_S, NG2_SNi, NG2_SMn, NG2_SFe at 0.36 V vs. RHE.

Sample	I _D (µA)
Pt-C	-381
NG2	-250
NG2_Ni	-345
NG2_S	-266
NG2_SNi	-326
NG2_SMn	-114
NG2_SFe	-308

The ring current was enough low for NG2_S, NG2_SMn, in fact, it is a little higher than Pt-C. But it is for NG2_SFe, that was reported the best result because the ring current was also lower than the reference. In addition, it showed a constant trend, varying the potential. On the other hand, ring current was quite higher for NG2 and much higher for NG2_Ni and NG2_SNi (Figure 6.19). Also, in this case, ring current was listed at 0.36 V vs. RHE for each sample in Table 6.6.

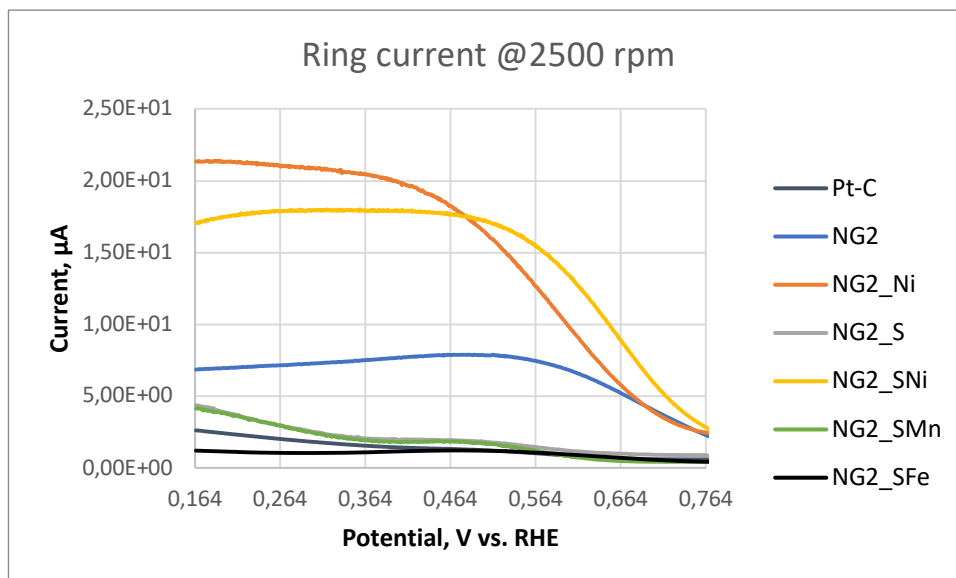


Figure 6.19: Ring current vs potential plot for NG2, NG2_Ni, NG2_S, NG2_SNi, NG2_SMn, NG2_SFe in O₂-saturated 0.1 M KOH solution.

Table 6.6: Ring current for NG2, NG2_Ni, NG2_S, NG2_SNi, NG2_SMn, NG2_SFe at 0.36 V vs. RHE.

Sample	I_r (μA)
Pt-C	1.54
NG2	7.49
NG2_Ni	20.5
NG2_S	2.07
NG2_SNi	18.0
NG2_SMn	1.92
NG2_SFe	1.08

Given the values of disk and ring current, it was possible to calculate the number of transferred electrons and the percentage of peroxide. Looking at transferred electrons, the plot reported in Figure 6.20 clearly shows the exact behavior of each sample. In fact, the base material (NG2), whose performance was enough high as starting point, was lower only respect to NG2_SFe, NG2_S, NG2_SMn samples, that shown 3.97, 3.92 and 3.84 electrons, respectively, as listed in Table 6.7. The efficiency of Pt-C (3.95 electrons) was practically equal to NG2_SFe and, beyond it, can be compared only with NG2_SFe and NG2_S. The other two samples (NG2_Ni and NG2_SNi) showed a lower efficiency, due to the fact that their number of transferred electrons was in the order of 3.50, that is the lowest limit to the occurrence of four-electron pathway. In addition, it was noticed a mismatch of values between RRDE and RDE for NG2_S and NG2_SMn, confirming the inaccuracy of Koutechy-Levich equation.

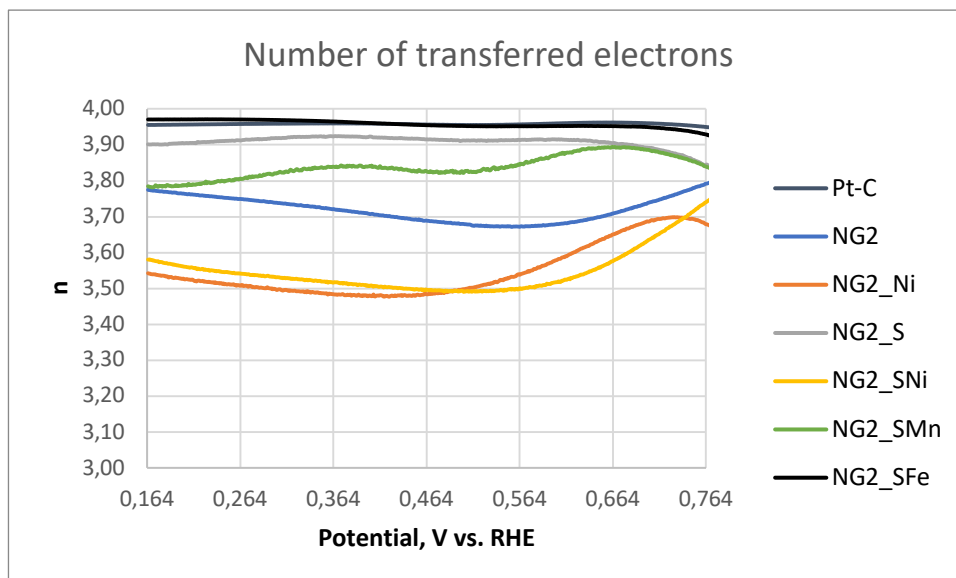


Figure 6.20: Number of transferred electrons vs potential plot for NG2, NG2_Ni, NG2_S, NG2_SNi, NG2_SMn, NG2_SFe in O₂-saturated 0.1 M KOH solution.

Table 6.7: Number of transferred electrons for NG2, NG2_Ni, NG2_S, NG2_SNi, NG2_SMn, NG2_SFe at 0.36 V vs. RHE.

Sample	n
Pt-C	3.96
NG2	3.72
NG2_Ni	3.48
NG2_S	3.92
NG2_SNi	3.52
NG2_SMn	3.84
NG2_SFe	3.97

The results for the calculation of hydrogen peroxide percentage confirmed the catalytic trend of the number of transferred electrons. Also, in this case, NG2 showed a behavior comprised between the group of the efficient samples (NG2_SFe, NG2_S and NG2_SMn) and the group of inefficient samples (NG2_Ni and NG2_SNi) (Figure 6.21). In fact, as in the previous case, the best sample was NG2_SFe at 1.7 % and, then, NG2_S at 3.8 % and NG2_SMn at 8.0 %, while for the other samples the percentage is higher than 10 %, as listed in the Table 6.8. The same considerations can be also made for Pt-C, whose hydrogen peroxide percentage was limited to 2%.

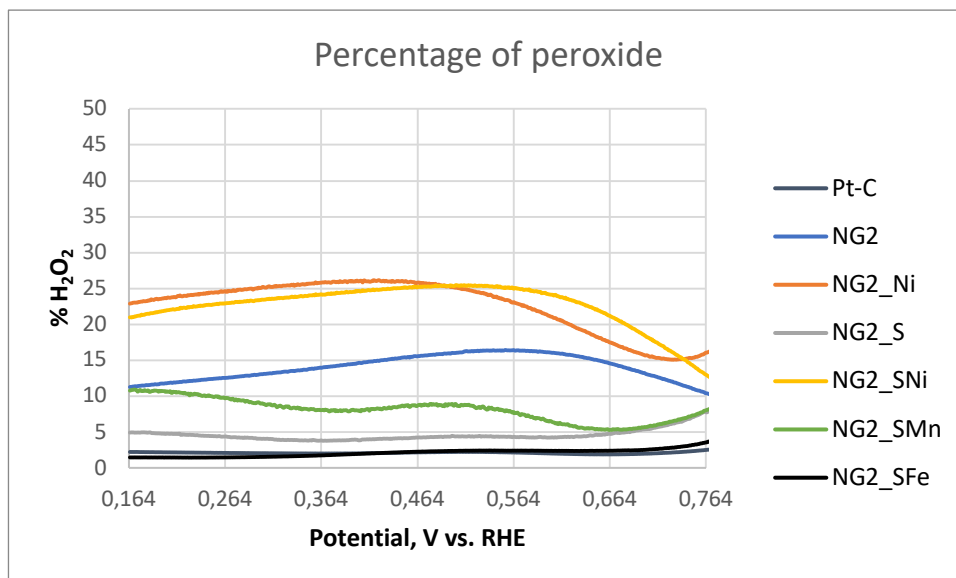


Figure 6.21: Percentage of peroxide vs potential plot for NG2, NG2_Ni, NG2_S, NG2_SNi, NG2_SMn, NG2_SFe in O₂-saturated 0.1 M KOH solution.

Table 6.8: Percentage of peroxide for NG2, NG2_Ni, NG2_S, NG2_SNi, NG2_SMn, NG2_SFe at 0.36 V vs. RHE.

Sample	H ₂ O ₂ (%)
Pt-C	2
NG2	13.9
NG2_Ni	25.8
NG2_S	3.8
NG2_SNi	24.2
NG2_SMn	8.0
NG2_SFe	1.7

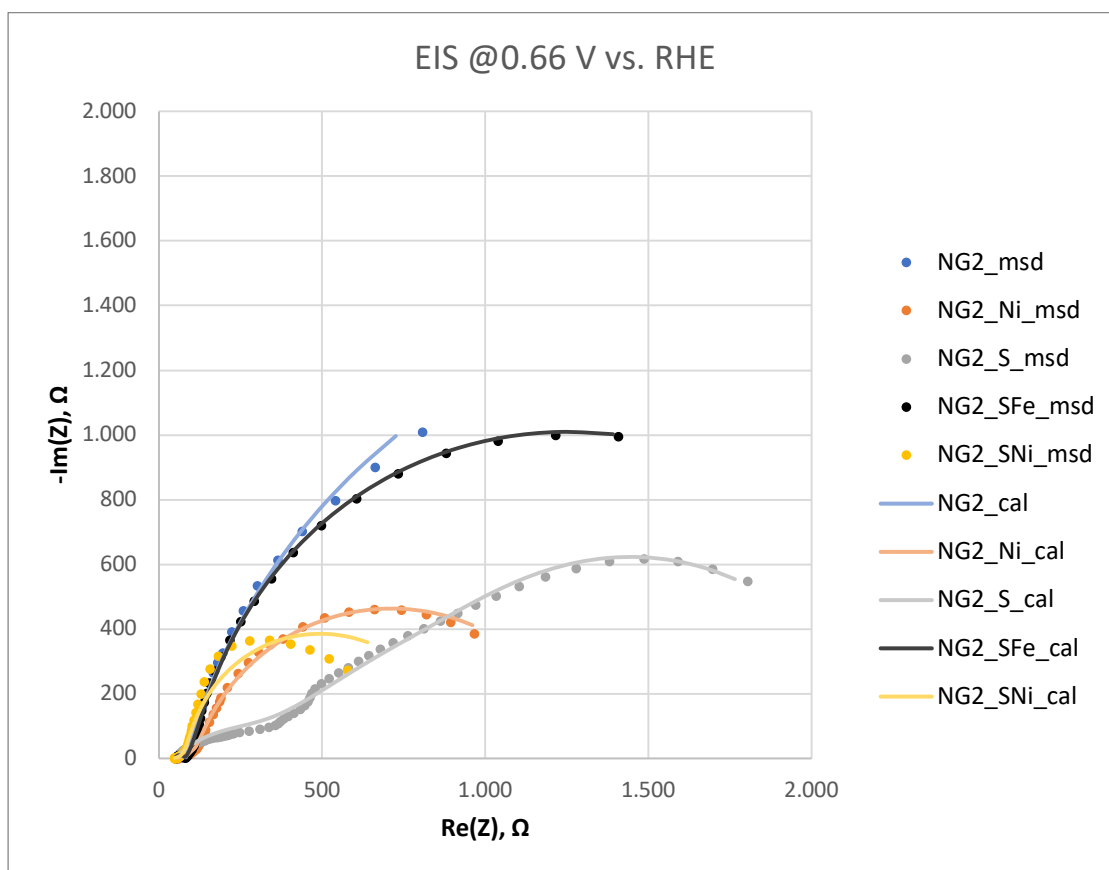
6.2.4 Electrochemical impedance spectroscopy

The EIS was carried out to analyze the results obtained from the other tests, separating the contributions of conductivity, electron transfer and diffusion. The graphs, shown in the figure 6.22 and 6.23, are referred to the equivalent circuit and, so, present the calculated values for each electrochemical component (cal). In addition, they compare them with experimental results (msd), showing a good overlapping. This was confirmed by the chi-squared errors values, listed in the table 6.9, that maintained quite low levels. At 0.66 V vs. RHE NG2_SMn reached impedance values enough higher than the other samples, for this reason was shown separately.

In the table 6.9, also C_t and C_{dl} were shown.

Table 6.9: Chi-squared errors, C_t and C_{dl} values.

Sample	Chi-squared errors	C_t (μF)	C_{dl} (μF)
NG2	0,00143	1.3	14800
NG2_Ni	0,0006685	1.4	10600
NG2_S	0,003236	2.3	7000
NG2_SFe	0,0005201	1.4	2630
NG2_SMn	0,0008233	3.0	3390
NG2_SNi	0,002764	3.5	19700

**Figure 6.22:** The EIS graphs at 0.66 V vs. RHE in O_2 -saturated 0.1 M KOH.

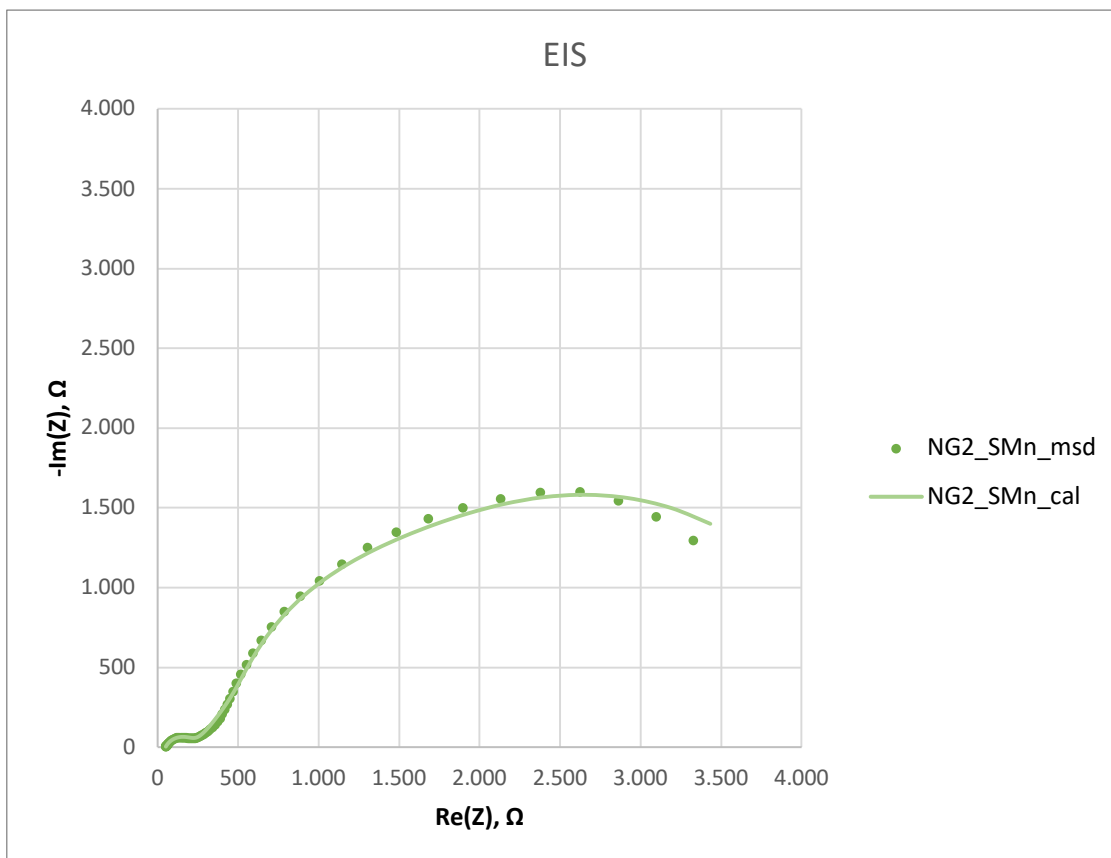


Figure 6.23: The EIS graph at 0.66 V vs. RHE for NG2_SMn in O₂-saturated 0.1 M KOH.

Analyzing in the details the graphs presents above, it is possible to focus on the left part of them, which is that at high frequencies (Figure 6.24). The real contribution starts from around 50 Ω for all samples, as expected, and it is linked to the series resistance by referring to the equivalent circuit in the Figure 5.5.

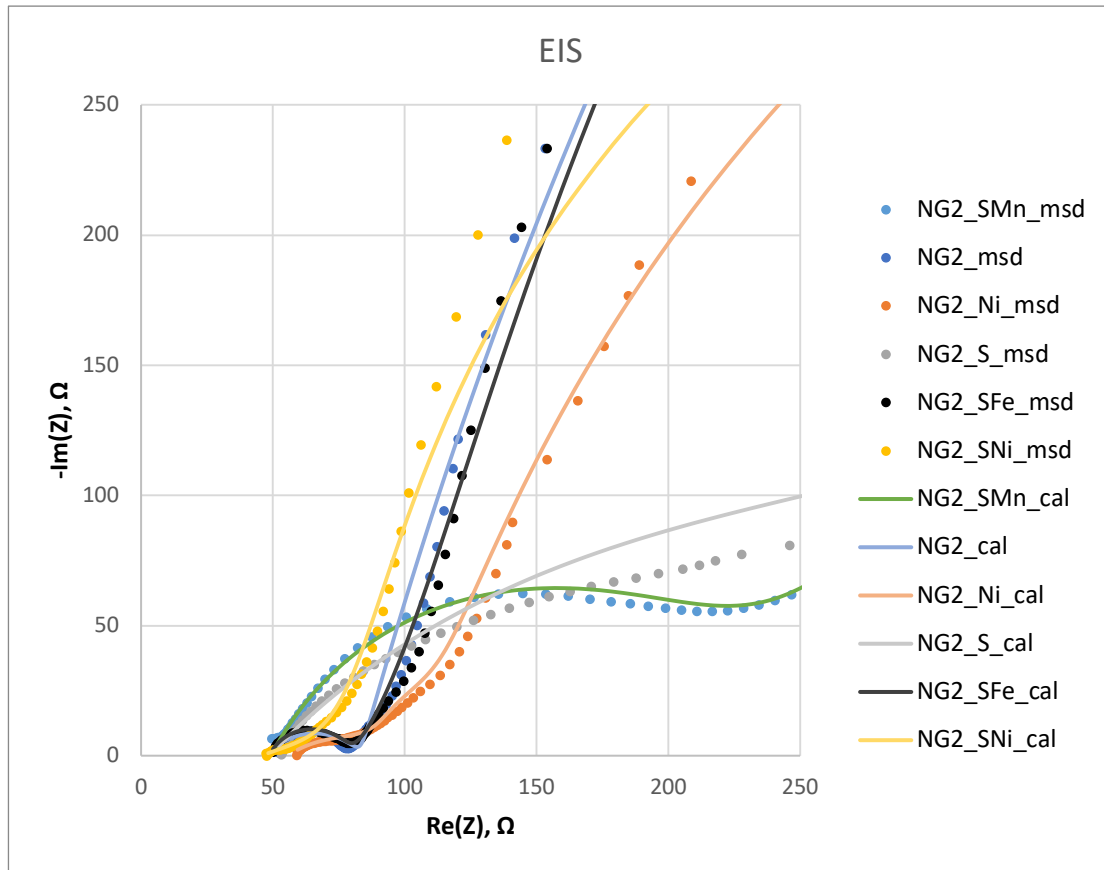


Figure 6.24: Focus of the EIS graphs at high frequencies.

The first part of the graph is relative to the intrinsic behavior of material and to the parallel between R_t and C_t , e.g. the resistance and the capacitance linked to the electronic transfer. Accounting the R_t values (Figure 6.25), NG2_SMn was confirmed as the more resistive material with 219.3 Ω , while NG2, NG2_Ni and especially NG2_SFe were the more conductive with 31.9 Ω , 32.9 Ω and 29.7 Ω , respectively. The electron transport for NG2_S and NG2_SNi was intermediate, being 95.3 Ω and 65.4 Ω , respectively. So, the effect of doping was not able to enhance the conductivity of material.

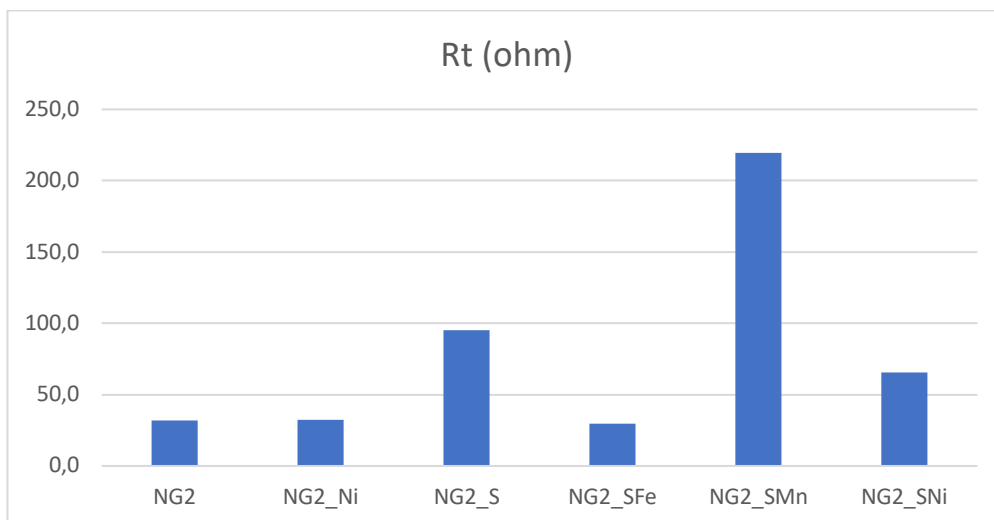


Figure 6.25: Transfer electron resistance for all samples.

The second parallel of the equivalent circuit is composed by R_{ct} and C_{dl} , e.g. charge transfer resistance and double layer capacitance. They are characterized by lower frequencies than the first parallel, that means slower process and for this reason they describe the phenomena that takes place during the reaction.

In particular, the R_{ct} is the limiting resistance because it is the highest than the others. Overlooking the case of NG2_SMn, that was confirmed the more resistive material (2594 Ω), the base material NG2 showed 1909 Ω . The effect of doping allowed to decrease the resistance and made the sample more active towards the ORR. In fact, NG2_Ni and NG2_S, that had a similar resistance, were 1205 Ω and 1216 Ω . The simultaneous addition of both S and Ni allowed to decrease further the resistance until 654 Ω . In the case of NG2_SFe, the trend was different because it is less active than NG2_S with 1722 Ω . All values were listed in the figure 6.26.

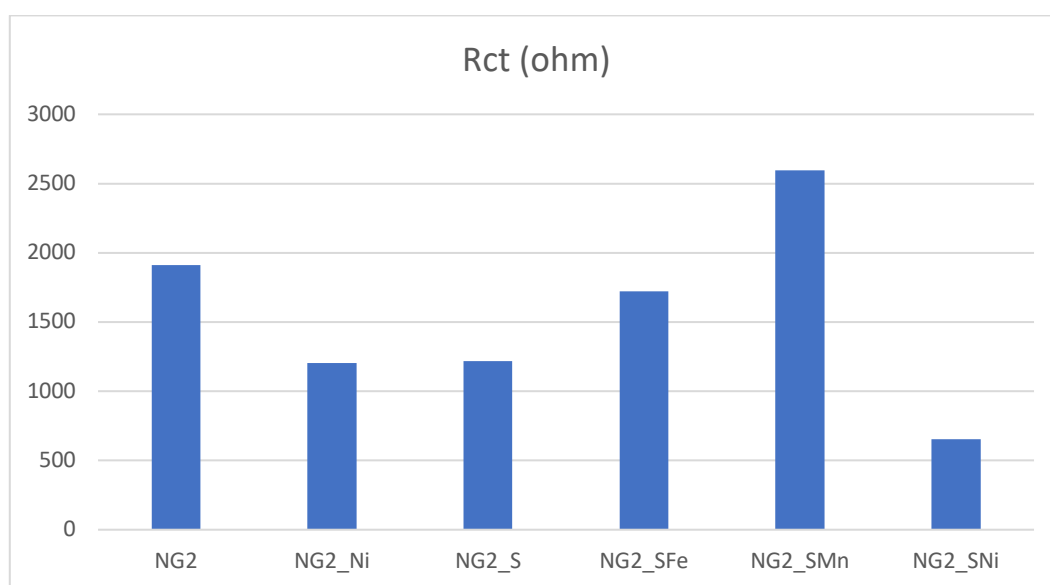


Figure 6.26: Charge transfer resistance for all samples.

Finally, by multiplying R_{ct} and C_{dl} , it is possible to know the ability of each material to transfer the charge through the employed time (Figure 6.27). As expected, the addition of dopant elements helped to increase the speed of process. In fact, for NG2 the transfer employed 28.3 s, whereas the only addition of a metal (as the case of the nickel) or the sulfur reduced significantly the time, 12.7 s and 8.5 s, respectively. The best efficiency was reached combining the sulfur with metal particles, as for NG2_SMn (8.8 s) and NG2_SFe (4.5 s). The exception was NG2_SNi because the time went up to 12.9 s.

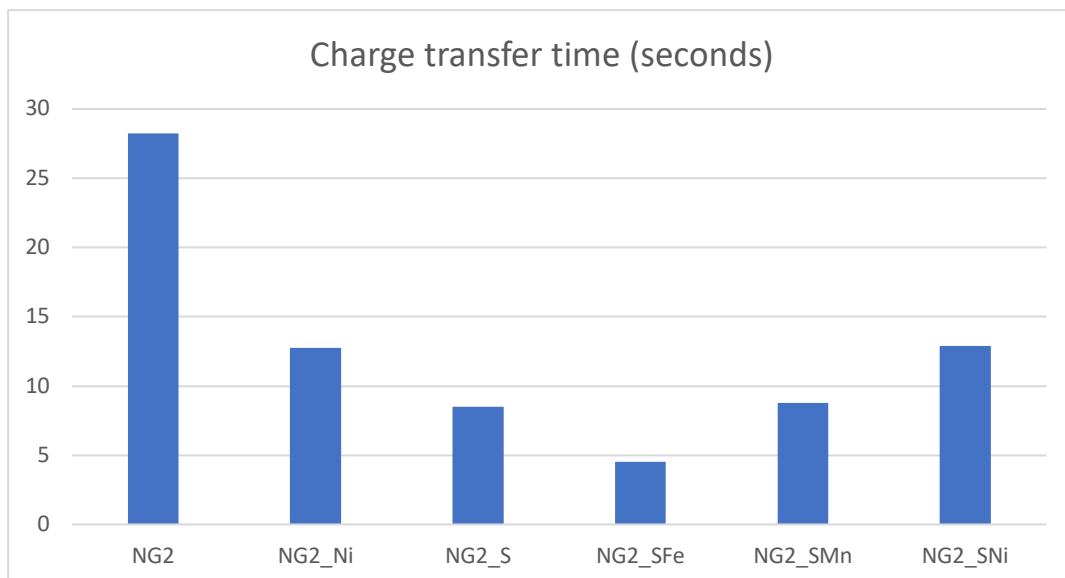


Figure 6.27: Charge transfer time for all samples.

6.2.5 Chronoamperometry

The chronoamperometry was carried out for 15,000 seconds, applying a potential of 0,66 V vs. RHE and maintaining the working electrode with a rotation speed of 2,500 rpm.

The resulting graphs (Figure 6.28) were reliable only for NG2_Ni, NG2_S and NG2_SFe. Unfortunately, due the problematic oxygen flux variations during the test it was not possible to perform accurate measurements for the other samples.

The current values as function of the time were normalized to the initial current value for each sample in order to highlight the drop of current during the test.

The three tested samples were showed a good stability, limiting the current drop at 15%, 29% and 18% for NG2_Ni, NG2_S and NG2_SFe, respectively, as listed in the Table 6.10. In fact, these results are competitive with the economical Pt-C, that are treated in literature [83, 84].

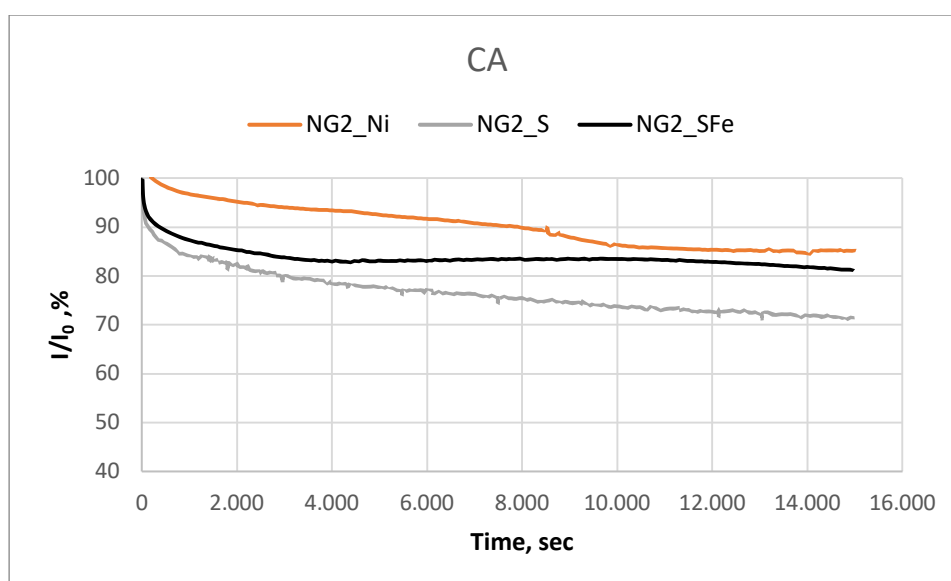


Figure 6.28: Chronoamperometry graph, showing the normalized current as function of time for NG2_Ni, NG2_S and NG2_SFe.

Table 6.10: List of the current drop for NG2_Ni, NG2_S and NG2_SFe.

Sample	Current drop (%)
NG2_Ni	15.0
NG2_S	28.7
NG2_SFe	18.8

6.2.6 Discussion of results

After a comparison between all the results obtained with all the electrochemical tests carried out, it is possible to define the efficiency for ORR of each sample. An overview is presented on the table 6.11.

The starting material was NG2, consistent in the N-doped rGO. The electrochemical tests showed that it is a promising material due to the high conductivity showed in CV plot, confirmed by R_t , and electrocatalytic activity was inferior than that of commercial Pt-C catalyst, but anyway good. At the same time, the efficiency, although maintaining respectable values, was inferior to the reference sample, both for the number of transferred electrons and, especially, for the production of peroxide.

In spite of favorable results, we tried to add other dopant atoms beyond nitrogen. Initially, two ways were followed: first the addition of a metal and second the addition of a new heteroatom. The former resulted on NG2_Ni, i.e. the Ni/N-doped rGO. The resistivity of this sample was comparable to previous one, as it can be seen by CV graphs, whereas its electrocatalytic activity was better, as suggested by disk current and R_{ct} , but the efficiency dramatically dropped with a number of transferred electrons below the conventional threshold values of 3.50 and a percentage of produced peroxide, resulting in the highest among all tested catalysts. As compared with NG2, the charge transfer time was more than halved and, in addition, it showed optimal long-life stability.

The latter resulted on NG2_S, i.e. the S/N-doped rGO. In this case, CV graph presented a material with a conductivity that was distinctly lower than NG2 and NG2_Ni, as also confirmed by R_t , that is three time greater than the previous ones. Simultaneously, a modest electrochemical activity goes with an optimal efficiency. In fact, the results of n and H_2O_2 were comparable with Pt-C. The charge transfer time was further lowered and stability as function of time was still good.

At this point, it was considered reasonable to join the last two attempts to further improve the electrochemical performances. However, NG2_SNi, i.e. the S/N/Ni-doped rGO, did not confirmed the expectation because it resulted enough similar to NG2_Ni. Furthermore, the onset potential, to which the reduction took place, was quite lower than that of NG2 and the other tested materials, leading to an undesirable increase of energy necessary to carry out the process.

Then, two other attempts were proved in order to further improve the optimal performance of NG2_S. The first one consisted on the use of Mn in NG2_SMn, i.e. the S/N/Mn-doped rGO. As in the previous case, the onset potential for the reduction peak occurred at lower potential and the resistivity was extraordinary elevated, more than seven times than NG2, to make a

comparison. As reported, the disk current was the lowest and R_{ct} was twice than NG2_S, resulting in a very poor electrochemical conductivity. Nevertheless, the ring current was lower than NG2_S, while the number of transferred electrons, the percentage of produced peroxide and charge transfer time were similar, making the performance of this sample not negligible. The second and the last attempt was NG2_SFe, i.e. S/N/Fe rGO, that can be regarded as the best material among tested ones. NG2_SFe showed a CV graph in O₂-saturated 0.1 M KOH solution similar to NG2, therefore similar capacitance and conductivity, confirmed by the lowest value of R_t . The disk current reached the highest value, as consequence the electrochemical activity level was remarkable. The ring current was only comparable with Pt-C, assuming very low values. Follow that n resulted maximized and H₂O₂ minimized. Also, charge transfer time was about half of NG2_S and durability was excellent. Finally, tested materials, if they are compared to commercial Pt-C, show equal or lower electrochemical activity, whereas the performance of only some materials can be confronted, including NG2_S, NG2_SMn and, especially, NG2_SFe, that was the best from all point of view.

Table 6.11: Summary of the electrochemical tests.

Sample	I_D (μ A)	I_R (μ A)	n	H ₂ O ₂ (%)	R_t (Ω)	R_{ct} (Ω)	Charge transfer time (s)	I/I_0 (%)
Pt-C	-381	1.5	3.96	2.0	-	-	-	-
NG2	-250	7.5	3.72	13.9	31.9	1909	28.3	-
NG2_Ni	-345	20.5	3.48	25.8	32.2	1205	12.7	15
NG2_S	-266	2.1	3.92	3.8	95.3	1216	8.5	28.6
NG2_SNi	-326	18.0	3.52	24.2	65.4	654	12.9	-
NG2_SMn	-114	1.9	3.84	8.0	219.3	2594	8.8	-
NG2_SFe	-308	1.1	3.97	1.7	29.7	1722	4.5	18.8

6.3 CO₂RR characterization

In the following section, the results of chronoamperometry and gas and liquid chromatography will be shown for all samples at different potentials in order to understand the electrochemical activity and the concentration of CO, HCOOH or H₂, that was produced during the reduction reaction.

6.3.1 NG2

For NG2, the analysis at -0.79 V vs. RHE showed stable values of current, that moved around 2.06 mA and the production of 914 ppm of hydrogen, whereas no traces of CO were detected (Figure 6.29). As regard liquid products, formic acid was seen in the order of 17 ppm.

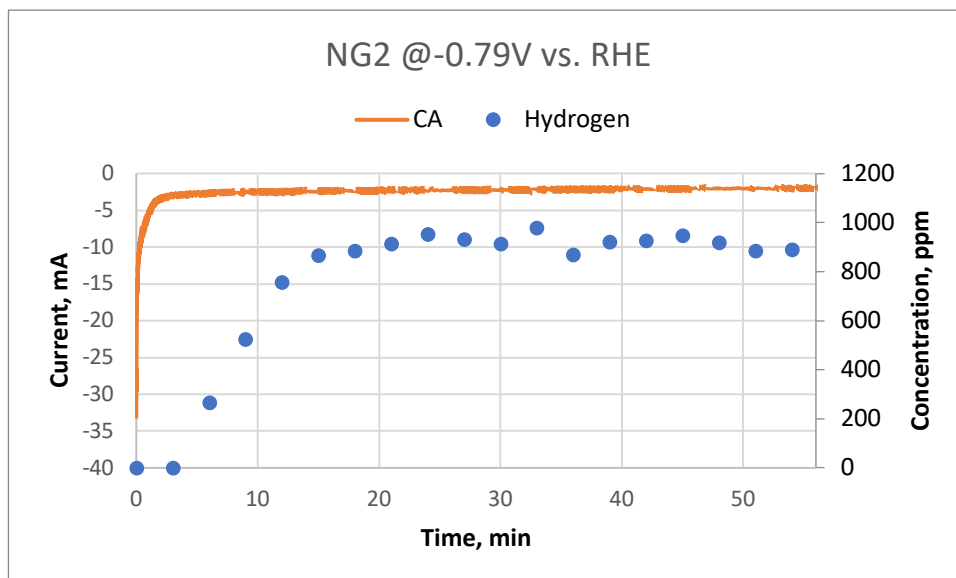


Figure 6.29: Current and product concentration of NG2 at -0.79 V vs. RHE.

The analysis at -0.89 V vs. RHE showed a current, that moved around higher values than the measurement at lower potential (2.66 mA) and the more elevated activity led to higher production of hydrogen (1139 ppm). Also, CO was detected (35 ppm), as it can see in the Figure 6.30. As regard liquid products, formic acid was lower (7 ppm).

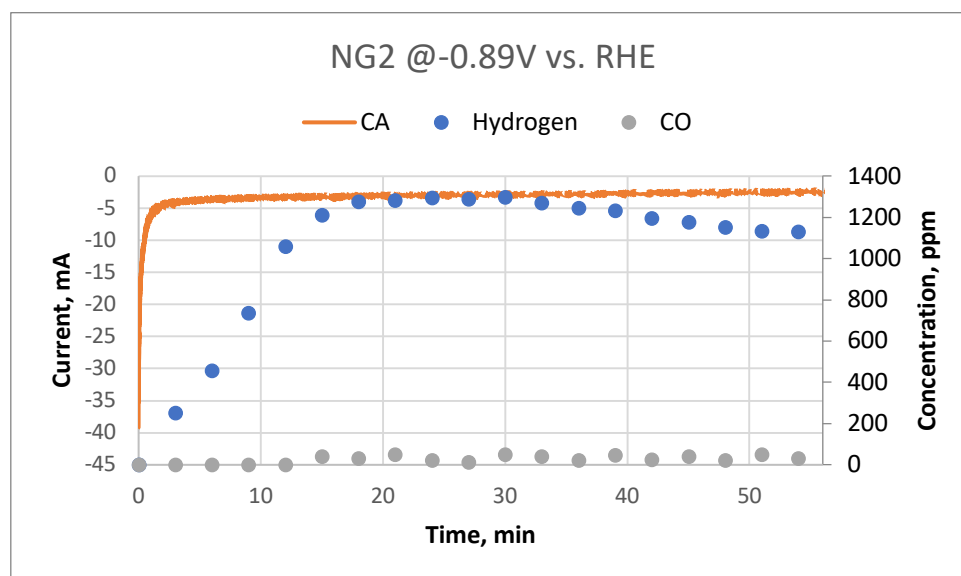


Figure 6.30: Current and product concentration of NG2 at -0.89 V vs. RHE.

The calculation of the Faradaic efficiency showed a similar value for formic acid in the case of both potentials, 2.3 % and 2.1 %, respectively. For CO, it was 2.9 % at -0.89 V vs. RHE, whereas HER was the prominent reaction, being the efficiency 97.7% and 95 %, respectively (Figure 6.31).

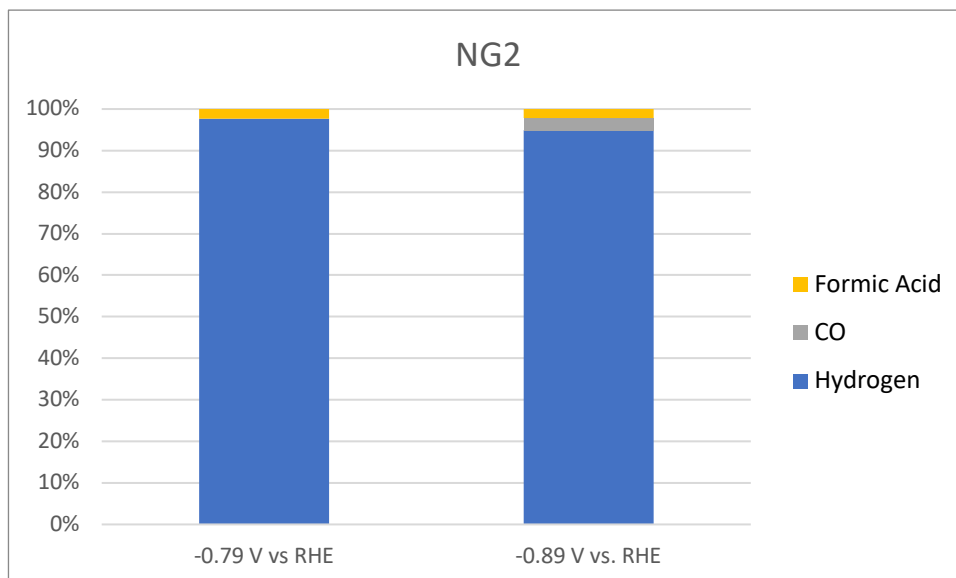


Figure 6.31: The Faradaic efficiencies for NG2 at -0.79 V vs. RHE and -0.89 V vs. RHE.

6.3.2 NG2_S

For NG2_S, the analysis at -0.79 V vs. RHE showed stable values of current, that moved around 1.39 mA and the production of 535 ppm of hydrogen and 14 ppm of CO (Figure 6.32).

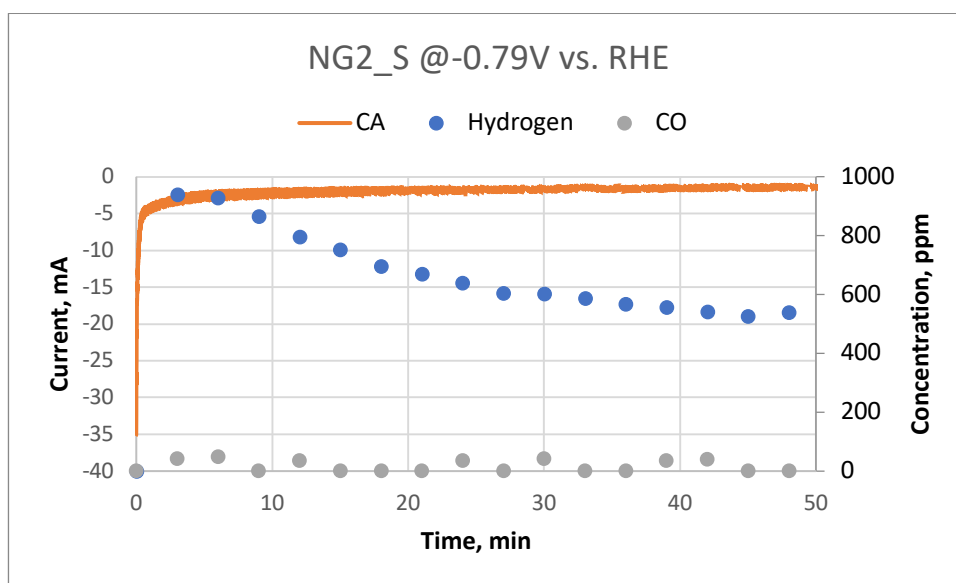


Figure 6.32: Current and product concentration of NG2_S at -0.79 V vs. RHE.

The analysis at -0.89 V vs. RHE showed a current, that moved around higher values than the measurement at lower potential (1.86 mA) and the more elevated activity led to higher production of hydrogen (741 ppm). Also, CO was detected (23 ppm), as it can see in the Figure 6.33. No liquid products were detected.

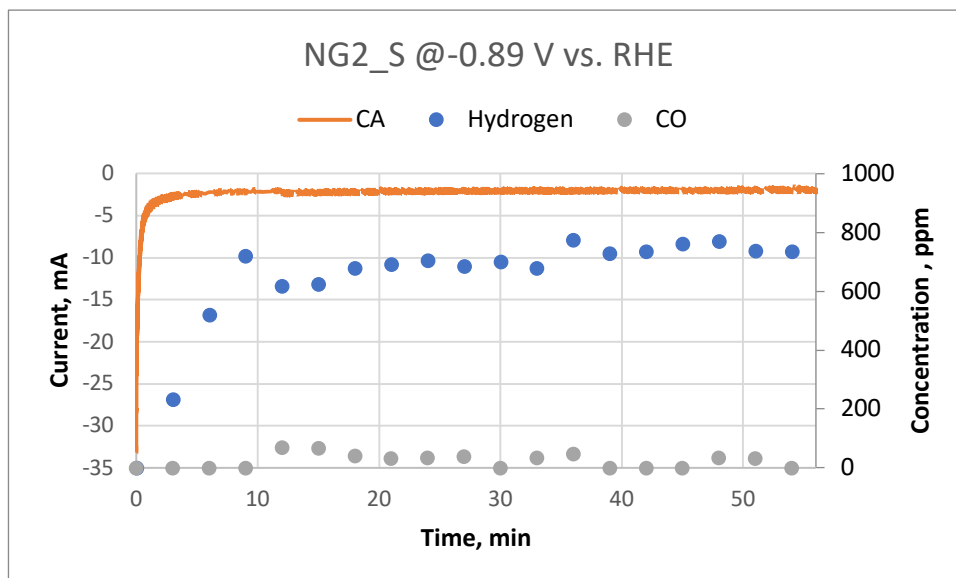


Figure 6.33: Current and product concentration of NG2_S at -0.89 V vs. RHE.

The calculation of the Faradaic efficiency showed that efficiency related to CO was limited to 2.5 and 3 %, respectively at 0.79 and 0.89 V vs. RHE (Figure 6.34).

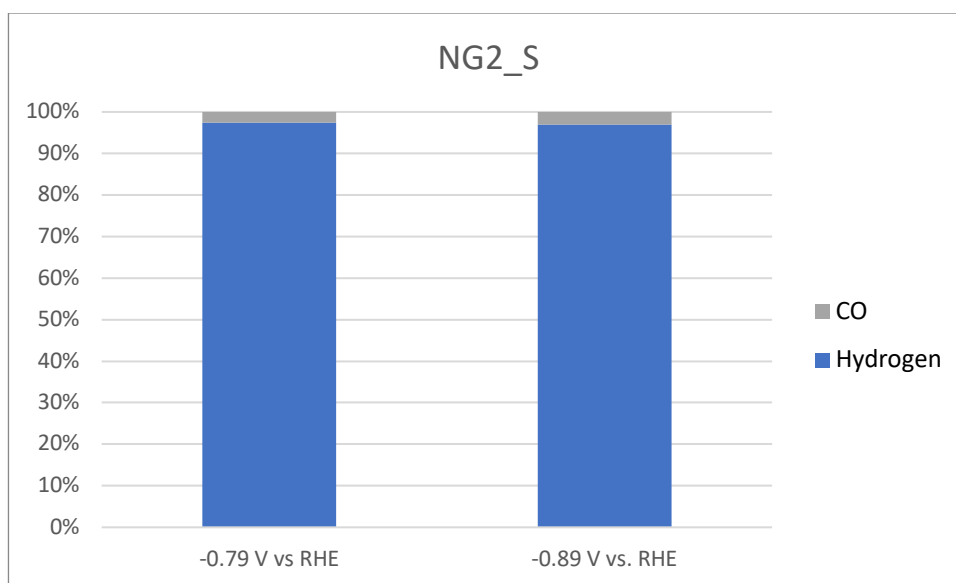


Figure 6.34: The Faradaic efficiencies for NG2_S at -0.79 V vs. RHE.

6.3.3 NG2_SMn

For NG2_SMn, the analysis at -0.79 V vs. RHE showed stable values of current, that moved around 1.01 mA and the production of 366 ppm of hydrogen, whereas no CO was detected (Figure 6.35).

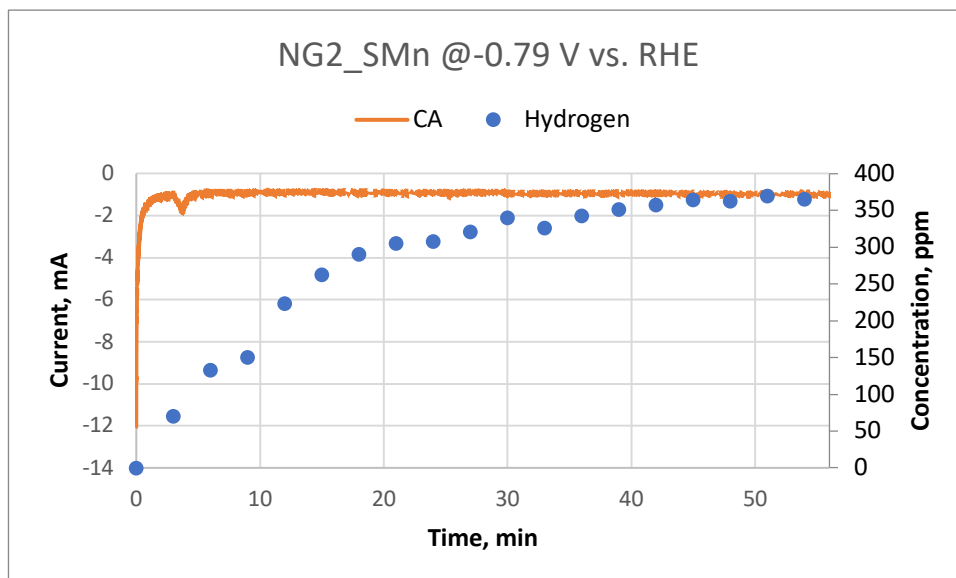


Figure 6.35: Current and product concentration of NG2_SMn at -0.79 V vs. RHE.

Also, the analysis at -0.89 V vs. RHE showed stable values of current, that moved around 1.41 mA and the production of 1011 ppm of hydrogen and 14 ppm of CO (Figure 6.36). As regard liquid products, formic acid was not found.

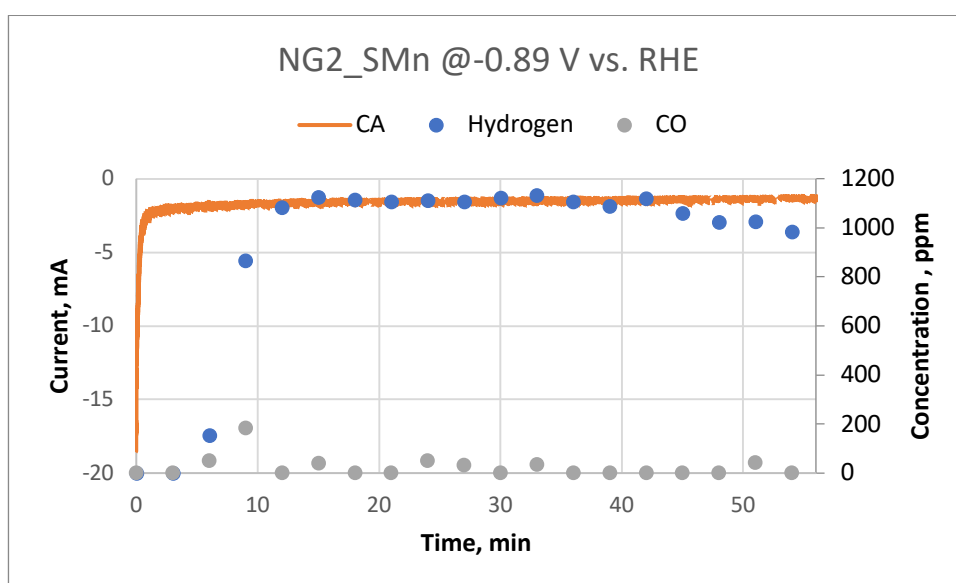


Figure 6.36: Current and product concentration of NG2_SMn at -0.89 V vs. RHE.

The calculation of the Faradaic efficiency at 0.89 V vs. RHE showed that it was very limited for CO (1.4 %), whereas for HER was fixed to 98.6 % (Figure 6.37), while at 0.79 V vs. RHE the graph was not reported, given the only production of hydrogen.

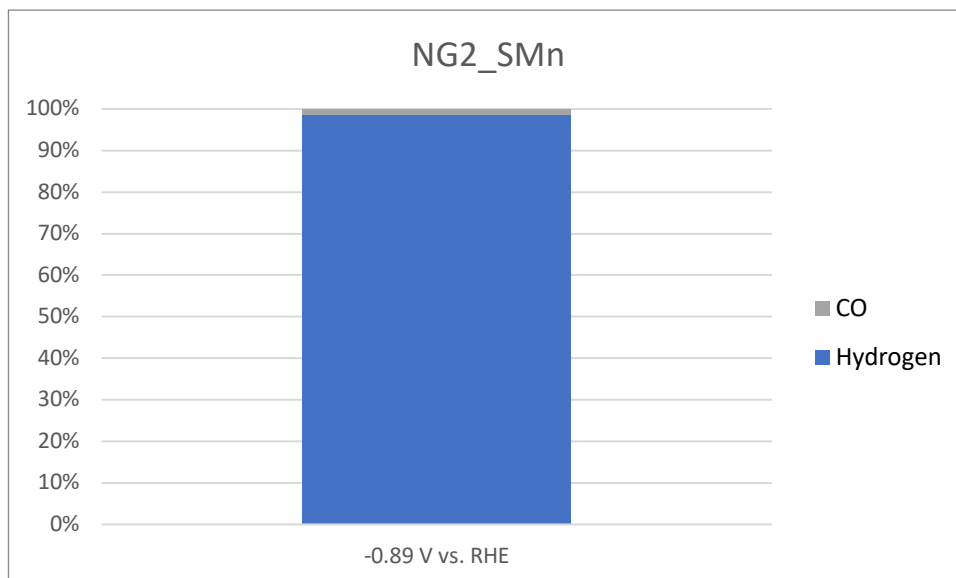


Figure 6.37: The Faradaic efficiencies for NG2_SMn at -0.89 V vs. RHE.

6.3.4 NG2_SFe

For NG2_SFe, the analysis at -0.79 V vs. RHE showed stable values of current, that moved around 5.59 mA and the production of 2628 ppm of hydrogen, whereas CO was not detected (Figure 6.38). As regard liquid products, also formic acid was not found.

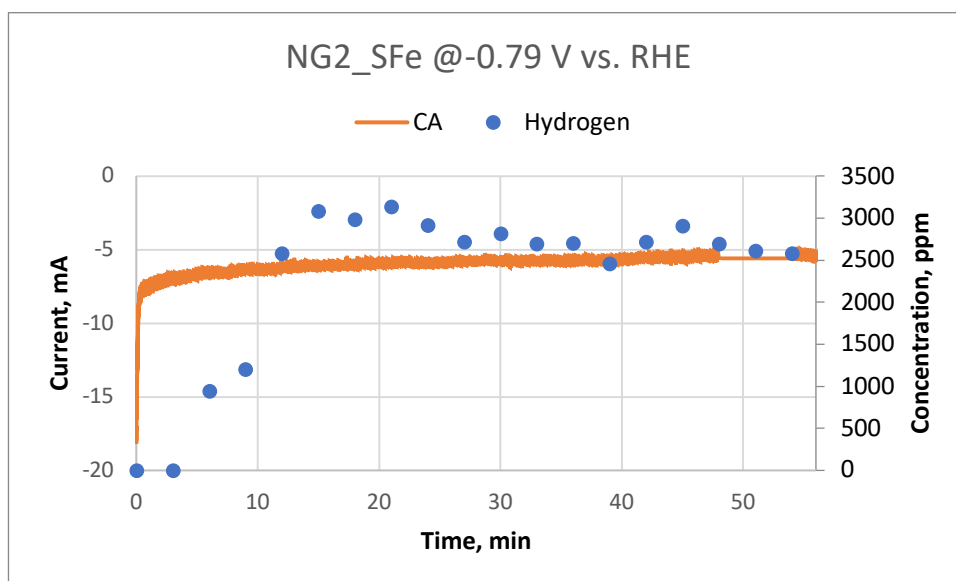


Figure 6.38: Current and product concentration of NG2_SFe at -0.79 V vs. RHE.

The analysis at -0.89 V vs. RHE showed a current, that moved around higher values than the measurement at lower potential (6.37 mA) and the more elevated activity led to higher production of hydrogen (2913 ppm) (Figure 6.39). As in the previous case, CO and HCOOH were not detected. So, the graphs relative to Faradaic efficiency were not reported because it was equal to 100 %, being hydrogen the only product.

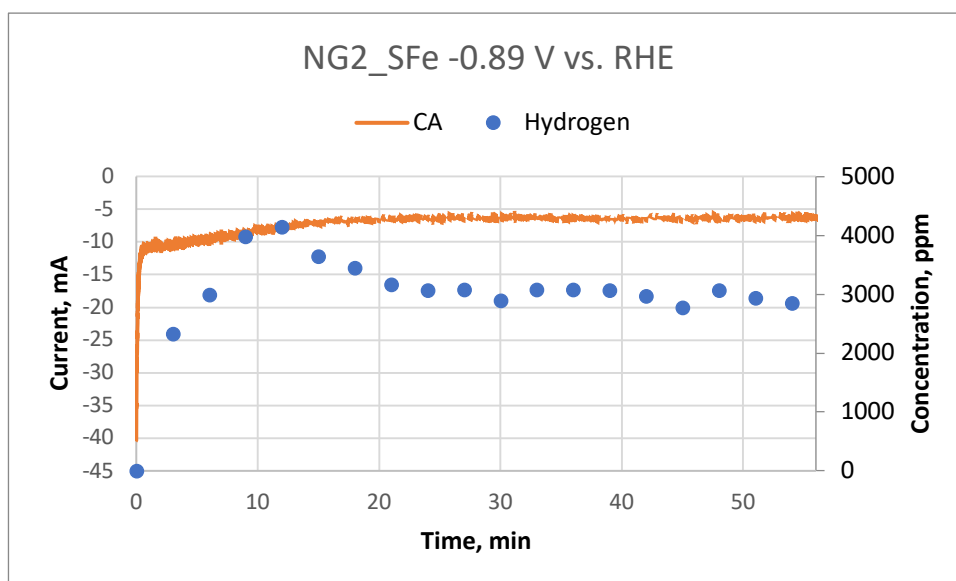


Figure 6.39: Current and product concentration of NG2_SFe at -0.89 V vs. RHE.

6.3.5 NG2_Mn

For NG2_Mn, the analysis at -0.79 V vs. RHE showed stable values of current, that moved around 1.23 mA and the production of 507 ppm of hydrogen, whereas CO was not detected (Figure 6.40). As regard liquid products, also formic acid was not found.

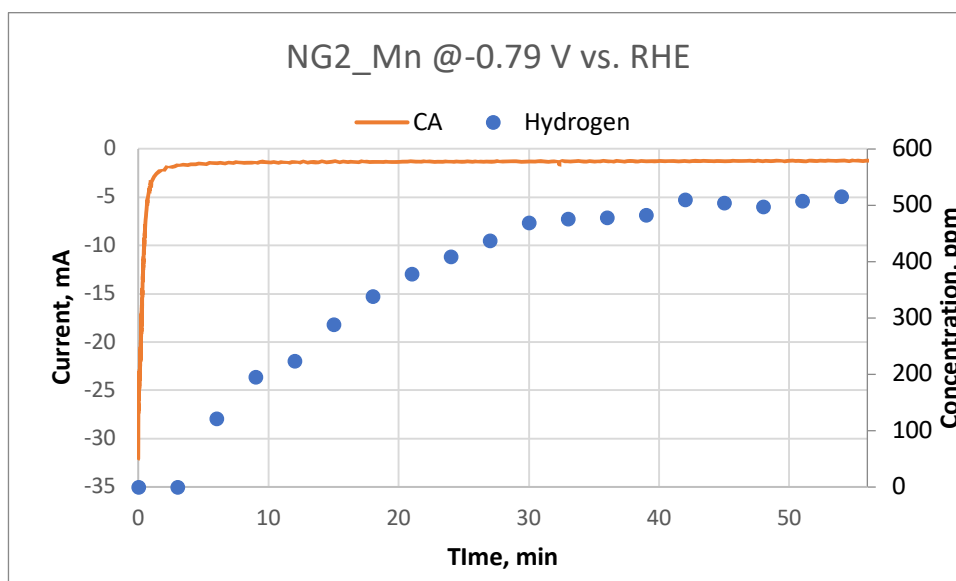


Figure 6.40: Current and product concentration of NG2_Mn at -0.79 V vs. RHE.

The analysis at -0.89 V vs. RHE showed a current, that moved around higher values than the measurement at lower potential (2.15 mA) and the more elevated activity led to higher production of hydrogen (914 ppm), while CO was not detected (Figure 6.41). As regard liquid products, formic acid was detected on the contrary of the previous case and it was equal to 2 ppm.

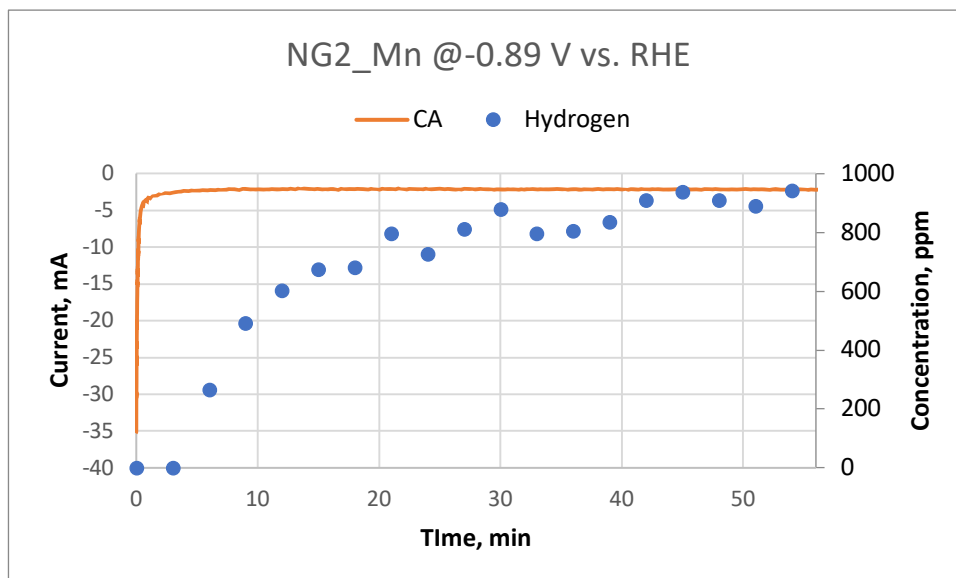


Figure 6.41: Current and product concentration of NG2_Mn at -0.89 V vs. RHE.

The calculation of the Faradaic efficiency showed that for NG2_Mn at -0.89 V vs. RHE formic acid had a very low efficiency, around 0,8 %. For the same sample at -0.79 V vs. RHE the graph was reported only as a comparison, being hydrogen the only product (Figure 6.42).

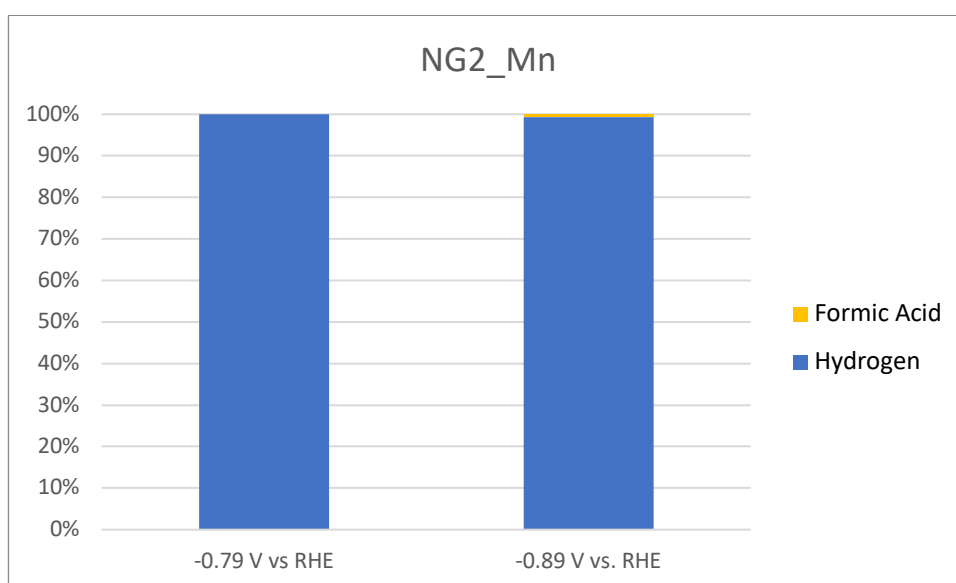


Figure 6.42: The Faradaic efficiencies for NG2_Mn at -0.79 V vs. RHE and -0.89 V vs. RHE.

6.3.6 NG2_Cu

For NG2_Cu, the analysis at -0.79 V vs. RHE showed stable values of current, that moved around 4.18 mA and the production of 1825 ppm of hydrogen, whereas CO was not detected (Figure 6.43). As regard liquid products, formic acid was around to 7 ppm.

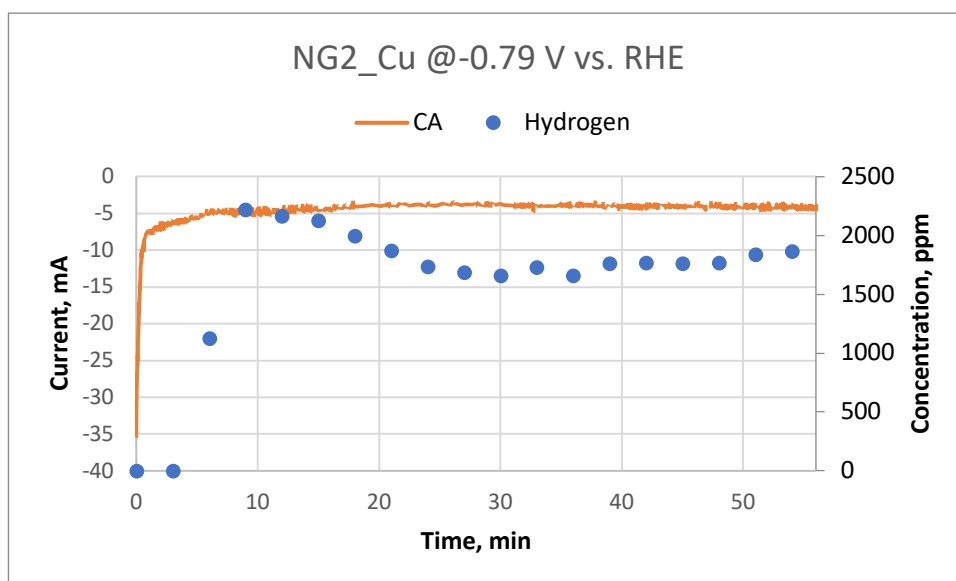


Figure 6.43: Current and product concentration of NG2_Cu at -0.79 V vs. RHE.

The analysis at -0.89 V vs. RHE showed a current that moved around higher values than the measurement at lower potential (6.67 mA) and the more elevated activity led to higher production of hydrogen (2779 ppm), while CO was not detected (Figure 6.44). As regard liquid products, formic acid was detected and, also for it, the production is more elevated, reaching 48 ppm.

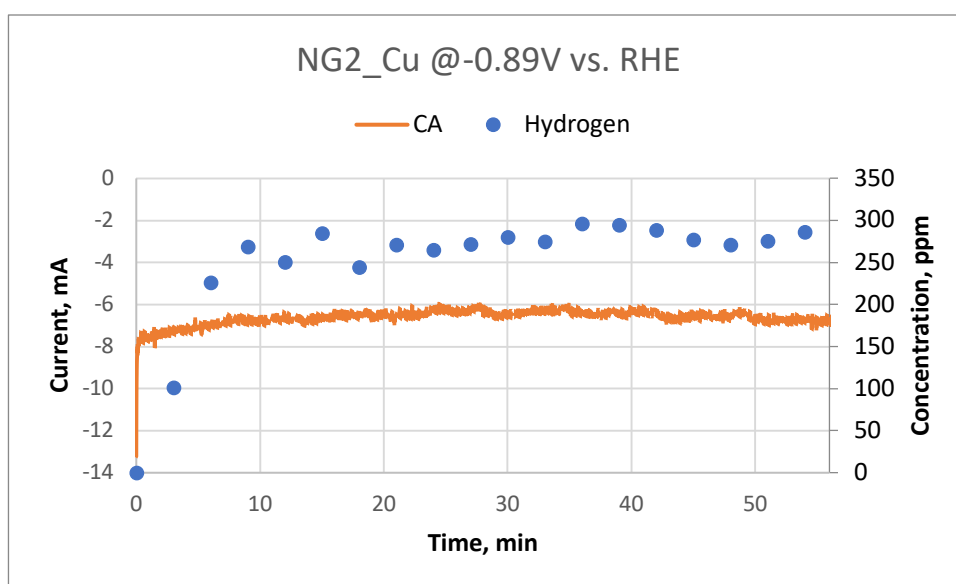


Figure 6.44: Current and product concentration of NG2_Cu at -0.89 V vs. RHE.

The calculation of the Faradaic efficiency showed that the efficiency of formic acid is significant, especially at -0.89 V vs. RHE, because it reached 6.8 %, whereas at -0.79 V vs. RHE it quite lower (1.2 %). HER kept being the prevalent reaction (Figure 6.45).

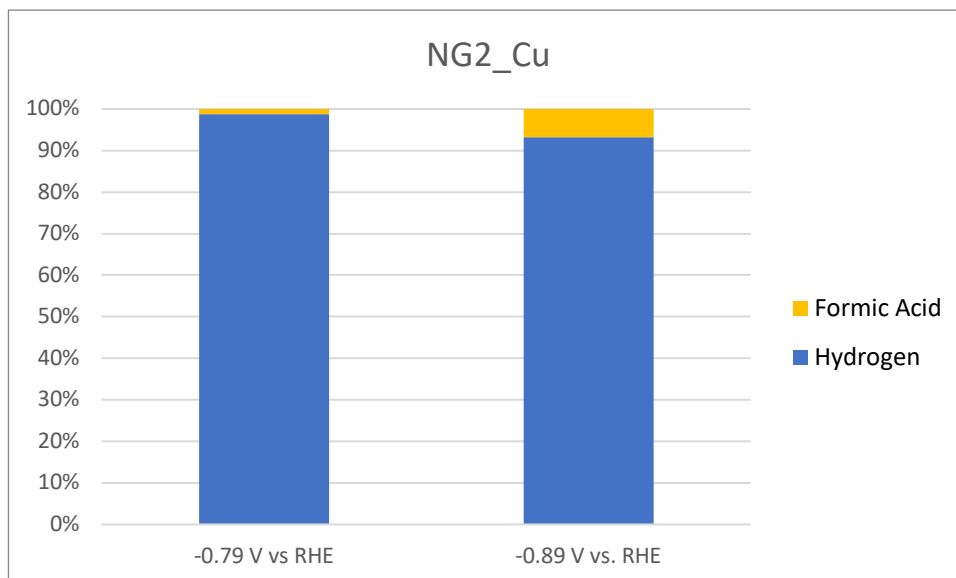


Figure 6.45: The Faradaic efficiencies for NG2_Cu at -0.79 V vs. RHE and -0.89 V vs. RHE.

6.3.7 NG2_Co

For NG2_Co, the analysis at -0.79 V vs. RHE showed stable values of current, that moved around 3.03 mA and the production of 1030 ppm of hydrogen and 243 ppm of CO (Figure 6.46). As regard liquid products, formic acid was not detected.

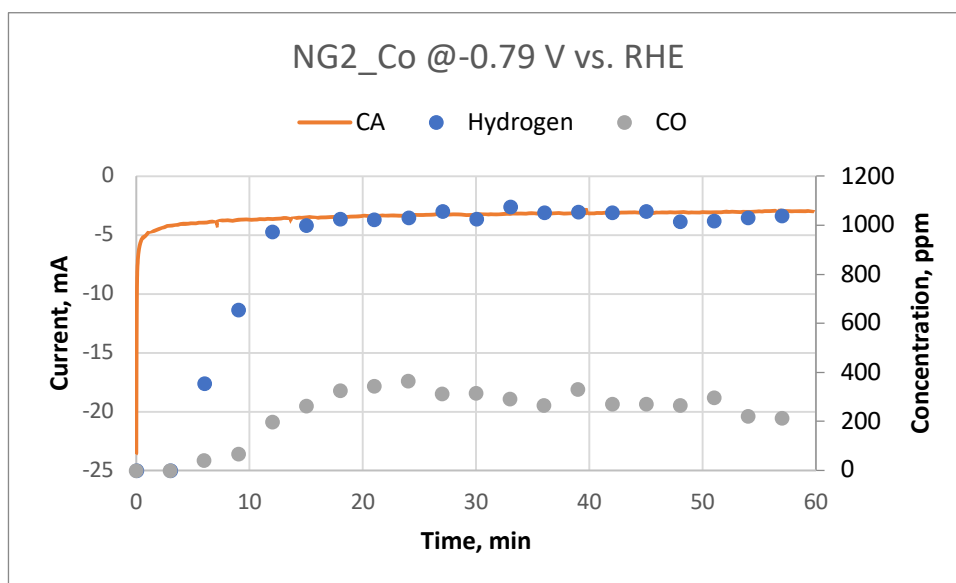


Figure 6.46: Current and product concentration of NG2_Co at -0.79 V vs. RHE.

The analysis at -0.89 V vs. RHE showed a current, that moved around higher values than the measurement at lower potential (3.17 mA) and the more elevated activity led to higher production of hydrogen (1268 ppm), but a lower production of CO (129 ppm) (Figure 6.47). As regard liquid products, formic acid was not detected also in this case.

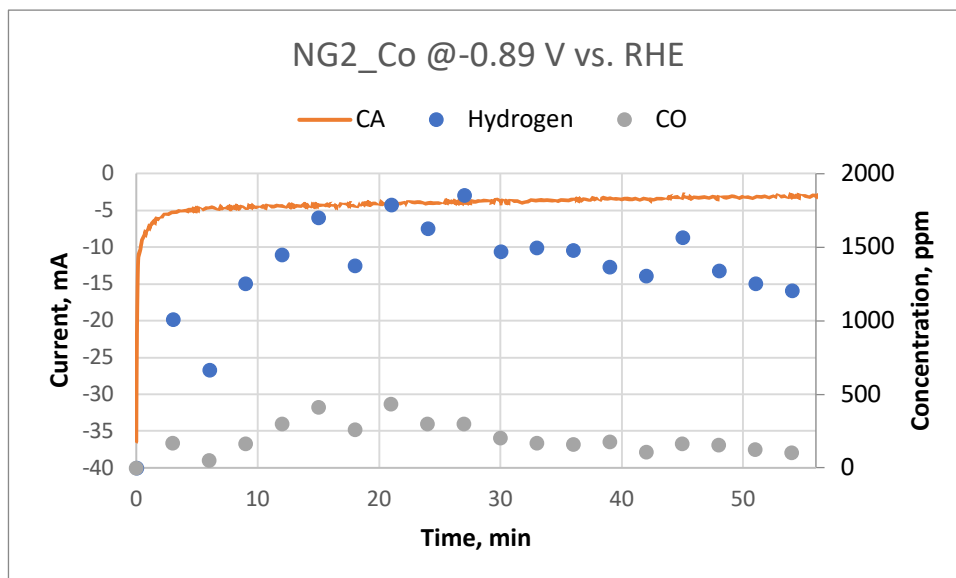


Figure 6.47: Current and product concentration of NG2_Co at -0.89 V vs. RHE.

The calculation of the Faradaic efficiency showed that it was remarkable for CO in both cases, reaching 19.1 % and 9.2 %, respectively. However, increasing the potential decreased the efficiency (Figure 6.48). For this reason, it is reasonable that testing this material at lower potentials it may be further maximized.

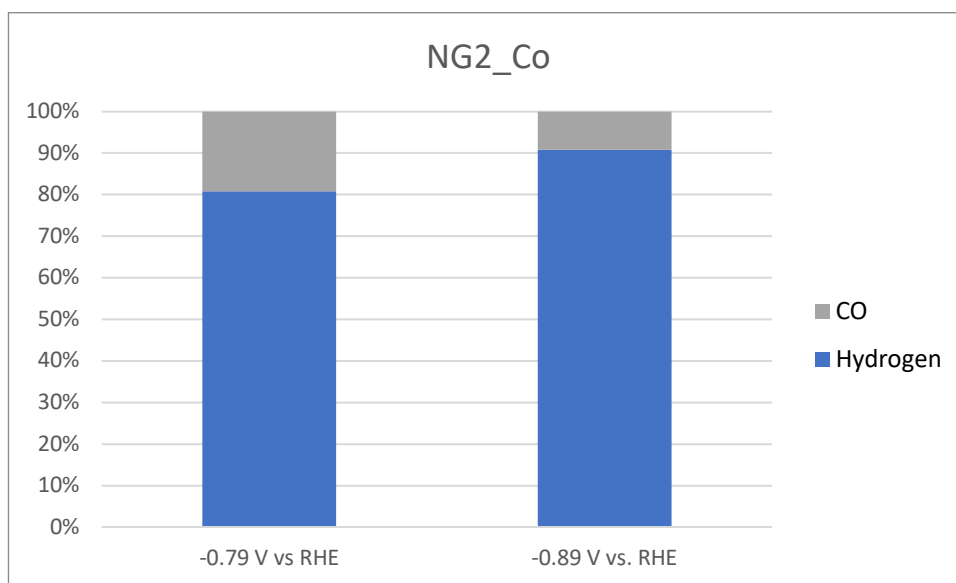


Figure 6.48: The Faradaic efficiencies for NG2_Co at -0.79 V vs. RHE and -0.89 V vs. RHE.

Then, NG2_Co was tested at 0.69 V vs. RHE and at 0.59 V vs. RHE. In the first case, the current values decreased, as expected, fixing to 1.02 mA. The same trend was confirmed to amount of hydrogen and CO, that were 280 ppm and 46 ppm, respectively (Figure 6.49).

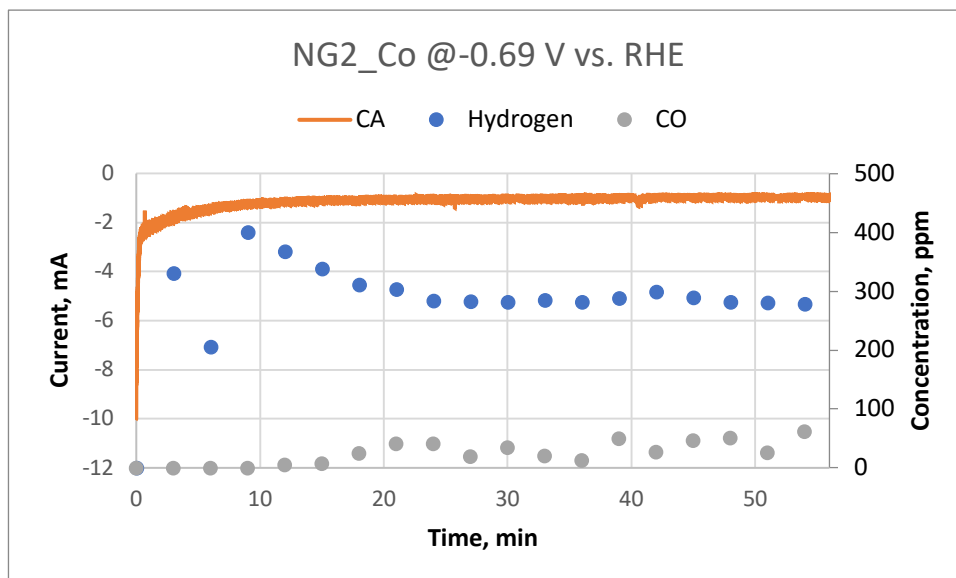


Figure 6.49: Current and product concentration of NG2_Co at -0.69 V vs. RHE.

In the second case, the current decreased further, reaching 0.76 mA, hydrogen was 210 ppm and CO was not detected (Figure 6.50).

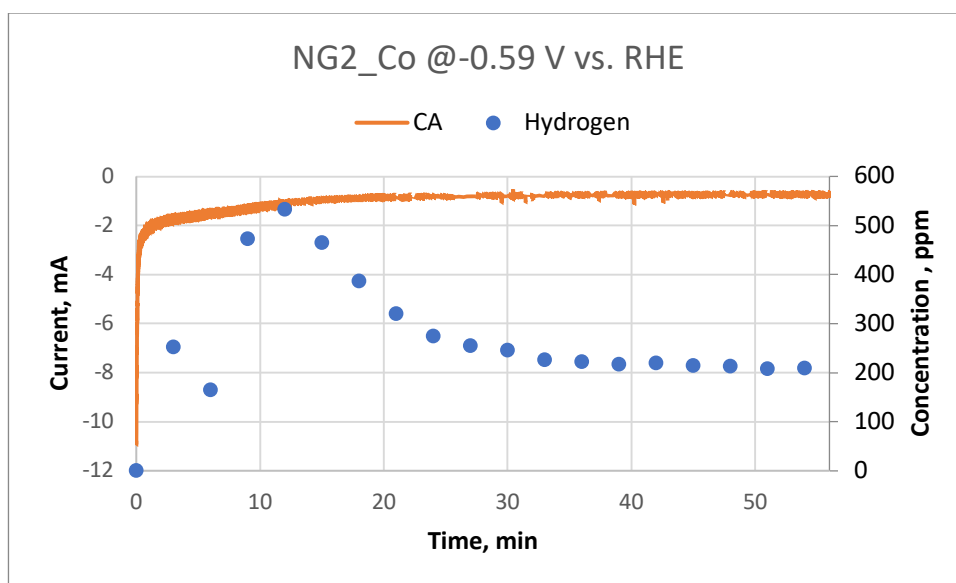


Figure 6.50: Current and product concentration of NG2_Co at -0.59 V vs. RHE.

The calculation of the Faradaic efficiency showed that for CO it decreased to 14.1 % at 0.69 V vs. RHE, not confirming the trend previous seen (Figure 6.51), whereas at 0.59 V vs. RHE the graph was not reported, given the only production of hydrogen.

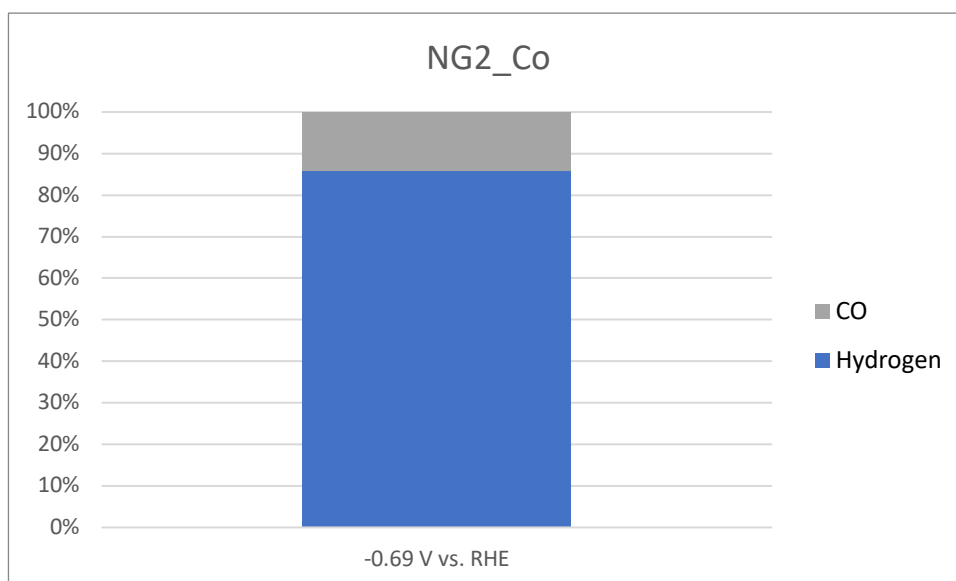


Figure 7.51: The Faradaic efficiencies for NG2_Co at -0.69 V vs. RHE.

6.3.8 Comparison of results

By comparing the results of chronoamperometry and chromatography, it was possible to better understand the performance and the efficiency of each catalyst. The discussion will be focused on the comparison of the resulting current, that is linked to electrochemical activity, and on the ratio between CO₂RR and HER through the measure of the Faradaic efficiency, relative to each product of reduction reaction.

For the first point, Figure 6.52 showed clearly that the increasing of the potential led to raise the current, as expected, also if it was quite pronounced for some samples as NG2_Cu, whereas it was limited for other samples like NG2_Co between 0.79 and 0.89 V vs. RHE, but a remarkable gap was formed when the potential was further lowered, due to Tafel law, that links overpotential and current in exponential way.

Chronoamperometry exhibited current values enough stable as function of time, however the levels that were reached were different among various materials. In particular, NG2_SFe and NG2_Cu showed a significant electrochemical activity, while for NG2_Co the current was sharply lower but despite this it maintained a good activity level. So, it was reasonable expecting a large formation of chemical species as a result of CO₂ reduction reaction for these samples.

Regarding the other materials, since the current can be considered modest for NG2 and NG2_S, it is certainly low for NG2_Mn and NG2_SMn. So, also in the eventuality that efficiency should be high, the production would be limited. In addition, it was noticed that the addition of sulfur to NG2_Mn had not the desired effect because the current further decreased.

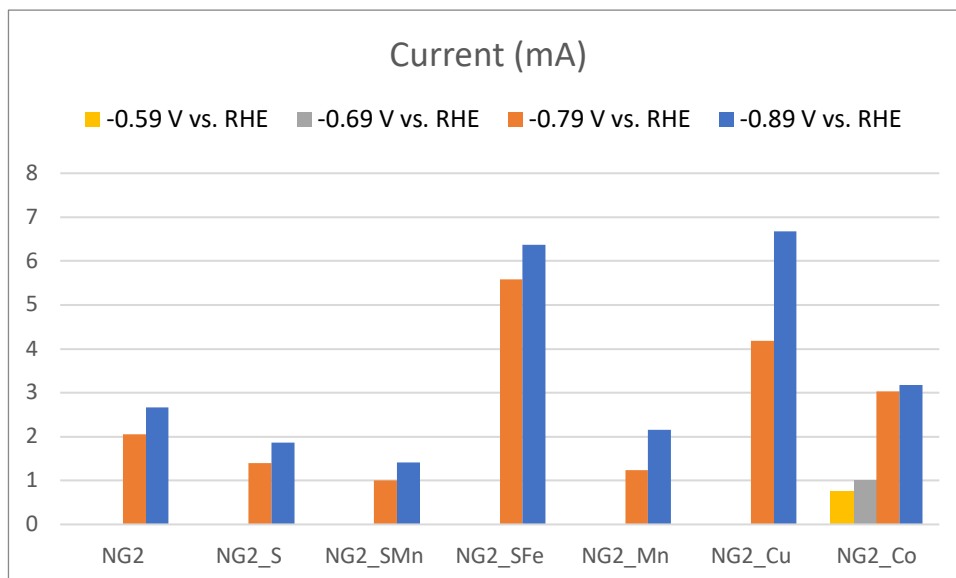


Figure 7.52: Comparison of current for all samples at different potentials.

From GC and HPLC, it was possible to characterize the products formed during the reduction reaction. Only CO was detected among possible gaseous products and only formic acid among possible liquid ones. However, the main part of samples had seen the formation of one or the other (rarely both), but more importantly the Faradaic efficiency relative to these products was quite low if it is compared to HER, that it was the prominent reaction in all cases (see Table 6.12).

Considering in the detail the behavior of samples, that were showed a good electrochemical activity, they had totally different results.

NG2_SFe led to the only formation of hydrogen. No CO and no HCOOH was detected. So, despite of its high electrochemical activity, it has to be ruled out or converted for other applications.

NG2_Cu was distinct from the others because of the formation of HCOOH, especially at -0.89 V vs. RHE. In fact, it reached 6.8 % of the Faradaic efficiency, that is the most elevated.

NG2_Co was the material with the lowest Faradaic efficiency relative to H₂. In fact, FE_{CO} reached 19.1 %, making this sample interesting for a deepening study. In particular, follow the trend of FE_{CO}, it was tested at low potential. At 0.69 V vs. RHE FE_{CO} decreased, maintaining a higher level than the other samples in any way, but at 0.59 V vs. RHE CO was not detected.

In conclusion, the results of CO₂RR tests had not a surprising outcome because of the prevalence of HER. However, some samples showed a good electrochemical activity (NG2_SFe, NG2_Cu and NG2_Co) and among these NG2_Cu has to be mentioned for the formation of formic acid and, especially, NG2_Co for carbon monoxide.

Table 6.12: Summary of CO₂RR tests.

Sample	Potential (V vs. RHE)	Current (mA)	H ₂ (ppm)	CO (ppm)	HCOOH (ppm)	FE_{H_2} (%)	FE_{CO} (%)	FE_{HCOOH} (%)
NG2	-0.79	2.06	914	-	17	97.7	-	2.3
	-0.89	2.66	1139	35	7	95	2.9	2.1
NG2_S	-0.79	1.39	535	14	-	97.5	2.5	-
	-0.89	1.86	741	23	-	97	3	-
NG2_SMn	-0.79	1.01	366	-	-	100	-	-
	-0.89	1.41	1011	14	-	98.6	1.4	-
NG2_SFe	-0.79	5.59	2628	-	-	100	-	-
	-0.89	6.37	2913	-	-	100	-	-
NG2_Mn	-0.79	1.23	507	-	-	100	-	-
	-0.89	2.15	914	-	2	99.2	-	0.8
NG2_Cu	-0.79	4.18	1825	-	7	98.8	-	1.2
	-0.89	6.67	2779	-	48	93.2	-	6.8
NG2_Co	-0.59	0.76	210	-	-	100	-	-
	-0.69	1.02	280	46	-	85.9	14.1	-
	-0.79	3.03	1030	243	-	80.9	19.1	-
	-0.89	3.17	1268	129	-	90.8	9.2	-

7. Conclusion

In this work, doped rGO was studied as possible efficient catalyst for the reduction reaction of oxygen and carbon dioxide to replace the traditional metal catalysts (Pt, Cu, ecc.). In fact, its particular structure contains several active sites on the surface, that differentiate it from pure graphene and allowed to anchored metal particles or to promote the reactions.

The synthesis of samples started from GO powders, that were reduced and doped through microwave irradiation due to its high efficiency, limited energy consumption and short time needed. FESEM and XPS confirmed the goodness of MW-assisted process, due to the lack of any damage on rGO flakes and the reaching of a sufficient C/O ratio. As dopants, heteroatoms (like N and S) and/or metal ions (like Ni, Mn or Fe ones) are used. They were introduced into the matrix in different combinations by means of precursors like urea, thiourea and relative sulphates for metals. TEM and XPS showed that dopants were effectively incorporated into the structure of samples because no crystalline structures were seen, excepting NG2_SFe that presented a decorated structure with several nanocrystals, that were identified as hematite (α Fe₂O₃).

The electrochemical tests to investigate the behavior of catalysts for ORR revealed that NG2_SFe was the best performing sample because it presented a good electrochemical activity and high efficiency, as confirmed by RRDE measurements and EIS, and a good stability as function of the time, as reported by CA. Indeed, also NG2_SMn and NG2_S showed high efficiencies, but the first was characterized by a poor electrochemical activity and high resistivity and the second presented an average behavior that was inferior to NG2_SFe. The anomalous performance of NG2_SMn was explained by means of XPS. In fact, it showed a limited graphitic-like nitrogen percentage, that is responsible of ORR activity, into its structure. XPS allowed also to understand because NG2_S and, especially, NG2_SNi failed, despite of their good electrochemical activity: in fact, the percentages of sulphate, that is the only sulfur species that catalyzes the four-electron reaction, were low for this samples. In any case, for all samples the addition of dopants was not effective to minimize the overpotential than the starting material (NG2), as reported by CV graphs.

The tests to investigate the behavior of catalysts for CO₂RR revealed that the prominent reaction was HER for all samples. In fact, despite of CA reported high levels of electrochemical activity for NG2_SFe and, especially, NG2_Cu and NG2_Co, GC and HPLC detected a poor concentration of valuable products. In particular, the calculation of faradaic efficiency showed that only NG2_Cu had a no-negligible percentage of HCOOH, whereas NG2_Co had an interesting percentage of CO. However, even the variation of potential did not allow to minimize the HER, also for this last sample.

In conclusion, NG2_SFe can represent a valid alternative to commercial Pt-C catalyst for ORR because it showed a similar behavior but would allow to overcome its typical limitations. However, the same catalyst cannot be used for CO₂RR because of the absence of formation of valid products. While NG2_Cu and NG2_Co can be the subject of further studies, given their ability to form HCOOH and CO from CO₂ reduction, respectively.

Bibliography

1. Luis Pérez-Lombard, José Ortiz, Christine Pout, A review on buildings energy consumption information, *Energy and Buildings*, Volume 40, Issue 3, Pages 394-398, 2008
2. <https://www.informazioneambiente.it/combustibili-fossili/>
3. Dai Liming, Xue Yuhua, Qu Liangti, Choi Hyun-Jung and Baek Jong-Beom, Metal-Free Catalysts for Oxygen Reduction Reaction, *Chemical Reviews*, Volume 115, pages 4823-4892, 2015
4. Qi Lu and Feng Jiao, Electrochemical CO₂ reduction: Electrocatalyst, reaction mechanism, and process engineering, *Nano Energy*, Volume 29, Pages 439-456, 2016
5. <https://www.britannica.com/science/catalyst>
6. Vijay Gayakhe, Shatrughn Bhilare, Afsana Yashmeen, Ian J.S. Fairlamb, Anant R. Kapdi, Chapter 6 - Transition-Metal Catalyzed Modification of Nucleosides, Palladium-Catalyzed Modification of Nucleosides, Nucleotides and Oligonucleotides, Elsevier, 2018, Pages 167-195
7. Jiang, L., Sheng, L. & Fan, Z. *Sci. China Mater.* (2018) 61: 133
8. Carbocatalysis by Graphene-Based Materials, Sergio Navalon, Amarajothi Dhakshinamoorthy, Mercedes Alvaro, and Hermenegildo Garcia, *Chemical Reviews* 2014 114 (12)
9. Yanan Tang, Zongxian Yang, Xianqi Dai, Noble metals induced magnetic properties of graphene, *Journal of Magnetism and Magnetic Materials*, Volume 323, Issue 20, 2011, Pages 2441-2447
10. <https://phys.org/news/2018-08-high-graphene-based-catalysts.html>
11. Huang, Cancan & Li, Chun & Shi, Gaoquan. (2012). Graphene-Based Catalysts. *Energy Environ. Sci.*
12. Das, Dr. Vijay & Shifrina, Z & Bronstein, Lyudmila. (2017). Graphene and graphene-like based materials in biomass conversion: Paving the way to the future. *Journal of Materials Chemistry*
13. Stankovich Sasha, Dikin Dmitriy A., Dommett Geoffrey H. B., Kohlhaas Kevin M., Zimney Eric J., Stach Eric A., Piner Richard D., Nguyen SonBinh T. and Ruoff Rodney S., Graphene-based composite materials, *Nature*, Volume 442, 2006
14. McAllister Michael J., Li Je-Luen, Adamson Douglas H., Schniepp Hannes C., Abdala Ahmed A., Liu Jun, Herrera-Alonso Margarita, Milius David L., Car Roberto, Prud'homme Robert K. and Aksay Ilhan A., Single Sheet Functionalized Graphene by Oxidation and Thermal Expansion of Graphite, *Chemistry of Materials*, Vol. 19, pp. 4396-4404, 2007
15. Zhu Ying-Jie and Chen Feng, Microwave-Assisted Preparation of Inorganic Nanostructures in Liquid Phase, *Chemical Reviews*, Vol. 114, pp. 6462-6555, 2014
16. B. C. Brodie, *Philos. Trans. R. Soc. London*, 1859, 149, 249–259
17. Roksana Muzyka, Monika Kwoka, Łukasz Smędowski, Noel Díez, Grażyna Gryglewicz, Oxidation of graphite by different modified Hummers methods, *New Carbon Materials*, Volume 32, Issue 1, 2017, Pages 15-20

18. D. W. Lee, L. De Los Santos V., J. W. Seo, L. Leon Felix, A. Bustamante D., J. M. Cole, and C. H. W. Barnes, *The Journal of Physical Chemistry B*, 2010
19. L. Staudenmaier, *Ber. Dtsch. Chem. Ges.*, 1989, 31, 1481–1487
20. W. S. Hummers and R. E. Offeman, *J. Am. Chem. Soc.*, 1958, 80, 1339
21. Pei Songfeng, Wei Qinwei, Huang Kun, Cheng Hui-Ming, Ren Wencai, Green synthesis of graphene oxide by seconds timescale water electrolytic oxidation, *Nature Communications*, Vol. 9, 2018
22. U. Hofmann and R. Holst, *Ber. Dtsch. Chem. Ges.*, 1939, 72, 754–771
23. G. Ruess, *Monatsh. Chem.*, 1946, 76, 381–417
24. M. Mermoux, Y. Chabre and A. Rousseau, *Carbon*, 1991, 29, 469–474
25. W. Scholz and H. P. Boehm, *Z. Anorg. Allg. Chem.*, 1969, 369, 327–340
26. T. Nakajima, A. Mabuchi and R. Hagiwara, *Carbon*, 1988, 26, 357–361
27. T. Nakajima and Y. Matsuo, *Carbon*, 1994, 32, 469–475
28. Dreyer, Daniel R. and Park, Sungjin and Bielawski, Christopher W. and Ruoff, Rodney S., The chemistry of graphene oxide, *Chem. Soc. Rev.*, Vol. 39, pp. 228–240, 2010
29. H. He, T. Riedl, A. Lerf and J. Klinowski, *J. Phys. Chem.*, 1996, 100, 19954–19958
30. Lerf, H. He, M. Forster and J. Klinowski, *J. Phys. Chem.*, 1998, 102, 4477–4482
31. A. Lerf, H. He, T. Riedl, M. Forster and J. Klinowski, *Solid State Ionics*, 1997, 101–103, 857–862
32. T. Szabo, O. Berkesi, P. Forgo, K. Josepovits, Y. Sanakis, D. Petridis and I. Dekany, *Chem. Mater.*, 2006, 18, 2740–2749
33. Qi Lu, Feng Jiao, Electrochemical CO₂ reduction: Electrocatalyst, reaction mechanism, and process engineering, *Nano Energy*, Volume 29, Pages 439–456, 2016
34. A. V. Talyzin, B. Sundqvist, T. Szabo, and V. Dmitriev, *J. Phys. Chem. Lett.*, 2011, 2, 309–313
35. Pei, Songfeng & Cheng, Hui-Ming, The reduction of graphene oxide, *Carbon* 50, 2012
36. Yanwu Zhu, Shanthi Murali, Meryl D. Stoller, Aruna Velamakanni, Richard D. Piner, Rodney S. Ruoff, Microwave assisted exfoliation and reduction of graphite oxide for ultracapacitors, *Carbon*, Volume 48, Issue 7, Pages 2118–2122, 2010
37. Tong Hao, Zhu Jijia, Chen Jianhui, Han Yongqin, Yang Sudong, Ding Bing & Zhang Xiaogang, Electrochemical reduction of graphene oxide and its electrochemical capacitive performance, *Journal of Solid State Electrochemistry*, 2013
38. <https://www.lifegate.it/persona/stile-di-vita/cose-la-fuel-cell-la-cella-combustibile>
39. <https://www.newsauto.it/notizie/batterie-zinco-aria-per-auto-elettrica-2018-176817/>
40. Lee, J. , Tai Kim, S. , Cao, R. , Choi, N. , Liu, M. , Lee, K. T. and Cho, J., Metal–Air Batteries with High Energy Density: Li–Air versus Zn–Air. *Adv. Energy Mater.*, 2011
41. A. Damjanovic, V. Brusic, Electrode kinetics of oxygen reduction on oxide-free platinum electrodes, *Electrochimica Acta*, Volume 12, Issue 6, Pages 615–628, 1967
42. Halina S. Wroblowa, Yen-Chi-Pan, Gerardo Razumney, Electroreduction of oxygen: A new mechanistic criterion, *Journal of Electroanalytical Chemistry and Interfacial Electrochemistry*, Volume 69, Issue 2, Pages 195–201, 1976
43. Chunyu Du, Yongrong Sun, Tiantian Shen, Geping Yin, Jiujun Zhang, 7 - Applications of RDE and RRDE Methods in Oxygen Reduction Reaction, *Rotating Electrode Methods and Oxygen Reduction Electrocatalysts*, Pages 231–277, Elsevier, 2014

44. Sujit Kumar Ghosh, Hasimur Rahaman, Chapter 16 - Noble Metal–Manganese Oxide Hybrid Nanocatalysts, In Micro and Nano Technologies, Noble Metal-Metal Oxide Hybrid Nanoparticles, Pages 313-340, Woodhead Publishing, 2019
45. Lindiwe Khotseng, Oxygen Reduction Reaction, Electrocatalysts for Fuel Cells and Hydrogen Evolution- Theory to Design, 2018
46. <http://www.rsc.org/suppdata/c6/ra/c6ra23100d/c6ra23100d1.pdf>
47. Gomez-Marín, Ana & Rizo, R & Feliu, J.M., Some reflections on the understanding of the oxygen reduction reaction at Pt(111), Beilstein journal of nanotechnology, 2013
48. Gaixia Zhang, Qiliang Wei, Xiaohua Yang, Ana C. Tavares, Shuhui Sun, RRDE experiments on noble-metal and noble-metal-free catalysts: Impact of loading on the activity and selectivity of oxygen reduction reaction in alkaline solution, Applied Catalysis B: Environmental, Volume 206, Pages 115-126, 2017
49. Albo J., Alvarez-Guerra, M., Castaño P., Irabien A., Towards the electrochemical conversion of carbon dioxide into methanol, Green Chemistry, Vol. 17, The Royal Society of Chemistry, 2015
50. Majidi Mir Reza and Ghaderi Seyran, Performance comparison of graphene and graphene oxide-supported palladium nanoparticles as a highly efficient catalyst in oxygen reduction, Iranian Chemical Communication, volume 6, Issue 3, pp. 218-324, pages 242-25, 2018
51. Duan, Xiaoguang, Sun Hongqi and Wang Shaobin, Metal-Free Carbocatalysis in Advanced Oxidation Reactions, Accounts of Chemical Research, volume 51, pages 678-687, 2018
52. Ganesan Pandian, Prabu Moni, Sanetuntikul Jakkid and Shanmugam Sangaraju, Cobalt Sulfide Nanoparticles Grown on Nitrogen and Sulfur Codoped Graphene Oxide: An Efficient Electrocatalyst for Oxygen Reduction and Evolution Reactions, ACS Catalysis, volume 5, pages 3625-3637, 2015
53. Liang Yu, Xiulian Pan, Xiaoming Cao, P. Hu, Xinhe Bao, Oxygen reduction reaction mechanism on nitrogen-doped graphene: A density functional theory study, Journal of Catalysis, Volume 282, Issue 1, Pages 183-190, 2011
54. <http://www.chimdocet-solido.it/file3h.htm>
55. Zhang Lipeng, Jianbing Niu Mingtao Li and Zhenhai Xia, Catalytic Mechanisms of Sulfur-Doped Graphene as Efficient Oxygen Reduction Reaction Catalysts for Fuel Cells, 2014
56. Jian Song, TianFu Liu, Sajjad Ali, Bo Li, DangSheng Su, The synergy effect and reaction pathway in the oxygen reduction reaction on the sulfur and nitrogen dual doped graphene catalyst, Chemical Physics Letters, Volume 677, Pages 65-69, 2017
57. Huanhuan Zhang, Xiangqian Liu, Guangli He, Xiaoxing Zhang, Shujuan Bao, Weihua Hu, Bioinspired synthesis of nitrogen/sulfur co-doped graphene as an efficient electrocatalyst for oxygen reduction reaction, Journal of Power Sources, Volume 279, Pages 252-25, 2015
58. Miguel A. Molina-García, Neil V. Rees, “Metal-free” electrocatalysis: Quaternary-doped graphene and the alkaline oxygen reduction reaction, Applied Catalysis A: General, Volume 553, Pages 107-116, 2018
59. <https://www.quora.com/Why-is-CO2-considered-a-waste-product-of-the-air>

60. Kortlever Ruud, Shen Jing Schouten Klaas Jan P., Calle-Vallejo Federico and Koper Marc T. M., Catalysts and Reaction Pathways for the Electrochemical Reduction of Carbon Dioxide, *The Journal of Physical Chemistry Letters*, volume 6, pages 4073-4082, 2015
61. Wang Zhongxu, Zhao Jingxiang and Cai Qinghai, CO₂ electroreduction performance of a single transition metal atom supported on porphyrin-like graphene: a computational study, *Physical Chemistry Chemical Physics*, Vol. 19, The Royal Society of Chemistry, 2017
62. Bard, Allen J. and Larry R. Faulkner, *Electrochemical methods: fundamentals and applications*, 2nd ed., John Wiley and Sons., 2001
63. Low Jingxiang, Yu Jianguo and Ho Wingkei, Graphene-Based Photocatalysts for CO₂ Reduction to Solar Fuel, *The Journal of Physical Chemistry Letters*, Vol. 6, pages 4244-4251, 2015
64. Shen Haoming, Li Yawei and Sun Qiang, CO₂ Electroreduction Performance of Phthalocyanine Sheet with Mn Dimer: A Theoretical Study, *The Journal of Physical Chemistry C*, volume 121, pages 3963-3969, 2017
65. http://www.neoscience.co.kr/public_html/?module=Goods&action=SiteGoods&sModule=VIEW_FORM&sCurrSortCd=001005&iGoodsCd=117&CurrentPage=&sSearchField=&sSearchValue=&a=1&goods_ord=2
66. Elgrishi Noémie, Rountree Kelley J., McCarthy Brian D., Rountree Eric S., Eisenhart Thomas T. and Dempsey Jillian L., A Practical Beginner's Guide to Cyclic Voltammetry, *Journal of Chemical Education*, volume 95, pages 197-206, 2018
67. <https://www.ceb.cam.ac.uk/research/groups/rg-eme/Edu/linear-sweep-and-cyclic-voltametry-the-principles>
68. Adriano Sacco, Electrochemical impedance spectroscopy: Fundamentals and application in dye-sensitized solar cells, *Renewable and Sustainable Energy Reviews*, Volume 79, Pages 814-829, 2017
69. <https://www.intechopen.com/books/gas-chromatography-derivatization-sample-preparation-application/sample-preparation-techniques-for-gas-chromatography>
70. De Sio, Francesco & Grimaldi, Michele & Loiudice, Roberto, *Introduzione all'HPLC e Metodi analitici per alimenti vegetali*, 1999
71. <https://www.hitachihightech.com/global/products/science/tech/ana/lc/basic/course3.html>
72. N. Garino, A. Sacco, M. Castellino, J. A. Muñoz-Tabares, A. Chiodoni, V. Agostino, V. Margaria, M. Gerosa, G. Massaglia, M. Quaglio, *ACS Appl. Mater. Interfaces* 2016, 8, 4633–4643
73. N. Garino, A. Sacco, M. Castellino, J. A. Muñoz-Tabares, M. Armandi, A. Chiodoni, C. F. Pirri, *ChemistrySelect*, 2016, 1, 3640
74. Wenning Yan, Xuecheng Cao, Jinghua Tian, Chao Jin, Ke Ke, Ruizhi Yang, Nitrogen/sulfur dual-doped 3D reduced graphene oxide networks-supported CoFe₂O₄ with enhanced electrocatalytic activities for oxygen reduction and evolution reactions, *Carbon*, Volume 99, Pages 195-202, 2016
75. <https://xpssimplified.com/elements/sulfur.php>
76. <https://xpssimplified.com/elements/nickel.php>

77. Dean E. Glass, Vicente Galvan, G.K. Surya Prakash, The Effect of Annealing Temperature on Nickel on Reduced Graphene Oxide Catalysts on Urea Electrooxidation, *Electrochimica Acta*, Volume 253, Pages 489-497, 2017
78. <http://www.xpsfitting.com/2012/01/nickel.html>
79. <https://xpssimplified.com/elements/manganese.php>
80. <https://xpssimplified.com/elements/iron.php>
81. <http://www.xpsfitting.com/2012/01/cobalt.html>
82. Francisco J. Vidal-Iglesias, José Solla-Gullón, Vicente Montiel, Antonio Aldaz, Errors in the use of the Koutecky–Levich plots, *Electrochemistry Communications*, Volume 15, Issue 1, Pages 42-45, 2012
83. Liu, R., Wu, D., Feng, X. and Müllen, K., Nitrogen-Doped Ordered Mesoporous Graphitic Arrays with High Electrocatalytic Activity for Oxygen Reduction, *Angewandte Chemie International Edition*, 2010
84. Y. Tan, C. Xu, G. Chen, X. Fang, N. Zheng, Q. Xie, *Adv. Funct. Mater.* 2012, 22, 4584–4591

Acknowledgements

Nevertheless, the difficulty that surely are in a such pathway far from home, it was an amazing experience and full of satisfactions. However, it would have been impossible deal with it, if I did not have the enormous help of my parents for that concern the moral support and, especially, the economic aspect. So, the first and the biggest thanks is for them.

Then, I want to remember my two grandmothers, that were both missed in these years, but I know that they are with me somehow.

I thank all people that I know, both who occupied an important place on my life and who was only passing through this time. In particular, I thank to Leda for her affect, support and, also, for allowing me to live another city.

I thank prof. Cicero, Adriano and Nadia for their availability and clarity, and all IIT staff for having me in the last months.